SPECTROSCOPIC CHARACTERIZATION OF AMINE SORBENTS FOR CO_2 CAPTURE

A Dissertation
Presented to
The Academic Faculty

by

Jason J. Lee

In Partial Fulfillment
of the Requirements for the Degree
Doctor of Philosophy in the
School of Chemical & Biomolecular Engineering

Georgia Institute of Technology
August 2019

SPECTROSCOPIC CHARACTERIZATION OF AMINE SORBENTS FOR CO_2 CAPTURE

Approved by:

Dr. Christopher W. Jones, Advisor
School of Chemical & Biomolecular Engineering
Georgia Institute of Technology

Dr. Ryan P. Lively
School of Chemical & Biomolecular Engineering
Georgia Institute of Technology

Dr. Carsten Sievers, Advisor
School of Chemical & Biomolecular Engineering
Georgia Institute of Technology

Dr. Seung Soon Jang
School of Materials Science and Engineering
Georgia Institute of Technology

Dr. Michael A. Filler
School of Chemical & Biomolecular Engineering
Georgia Institute of Technology

Dr. Sophia E. Hayes
Department of Chemistry
Washington University in St. Louis

Date Approved: [May 23rd, 2019]

ACKNOWLEDGEMENTS

My time spent in graduate school has resulted in tremendous professional and personal growth. This transformation would not have been possible without the continuous support I have had throughout my time at Georgia Tech. I would like to thank my advisors Chris Jones and Carsten Sievers for their guidance, critical feedback, and support throughout the years. I would also like to express gratitude to Jones and Sievers group members, past and present, for their guidance and support throughout the years. I would specifically like to thank Guo Shiou Foo, Steph Didas, Miles Sakwa-Novak, Eric Moschetta, Lalit Darunte, and Chun-Jae Yoo for training me in lab and/or for their invaluable advice. In addition, I would like to thank Sophia Hayes and Chia-Hsin Chen for being effective and friendly collaborators. Finally, I would like to thank my friends and family for their continuous emotional support.

TABLE OF CONTENTS

LIST OF TABLES

LIST OF FIGURES

SUMMARY

The atmospheric CO_2 concentration has increased throughout the past century and has been linked to global climate change. As a temporary solution it has been proposed to capture CO_2 from either the flue gas point source or from the atmosphere and sequester it underground. Supported amine sorbents are promising candidate materials for capturing CO_2 due to their low heat capacities, large CO_2 adsorption capacities, and high CO_2 selectivities at operating conditions. However, the rational design of these types of sorbents remains challenging because it is not well understood how CO_2 interacts with the sorbent on the molecular level. The work in this thesis focuses on the characterization of interactions between solid supported amine materials and CO_2.

In the first study, CO_2-amine interactions of tertiary aminosilane-grafted silica sorbents were elucidated using NMR and *in situ* FTIR spectroscopy (Chapter 2). It was determined that aklylammonium bicarbonates formed on supported tertiary amine sorbents under the presence of CO_2 and H_2O. While alkylammonium bicarbonate formation is known to occur in aqueous amine solutions in the presence of CO_2, there has been conflicting evidence for its formation on solid supported analogues. This study demonstrated that ammonium bicarbonates can exist on solid supported amines. However, the tertiary amine sorbents were found to be poor CO_2 sorbents under dilute CO_2 concentrations with and without the presence of H_2O.

Next, a series of sterically hindered aminosilane grafted silica sorbents were evaluated for CO_2 adsorption (Chapter 3). Sterically hindered amines, amines with an α-carbon that is secondary or tertiary, have been well studied in solution and are utilized

because of their higher amine efficiencies (mol CO_2 adsorbed/mol N) when compared to their unhindered counterparts. In contrast to solution studies, there has been limited research conducted on solid supported sterically hindered amines. Supported sterically hindered amines were found to have similar CO_2 capacities when compared to unhindered analogs upon exposure to 10% CO_2/He under humid conditions. It was determined using *in situ* FTIR spectroscopy that sterically hindered amines formed more ammonium bicarbonates than unhindered amines in the presence of humid CO_2 and that the CO_2-derived species found on the hindered amine sorbents were weakly bound, indicating that hindered amine sorbents may require less energy to regenerate.

In chapter 4, a sterically hindered aminopolymer, poly(2,2-dimethylenimine) (PDMEI) was synthesized and incorporated into the pores of mesoporous silica, SBA-15. The CO_2 adsorption performance of the hindered polymer/silica composite was compared to unhindered aminopolymer/silica composites under dry and humid conditions using *in situ* FTIR spectroscopy and fixed bed breakthrough analysis. The hindered polymer sorbents had poor amine efficiencies when compared to unhindered polymer sorbents under both dry and humid conditions. The addition of poly(ethylene glycol) (PEG) helped alleviate some of the limitations associated with the hindered aminopolymer/silica composites, improving the CO_2 adsorption performance at the conditions studied. The experiments suggest that these hindered polymer sorbents were less effective at CO_2 capture than their unhindered polymer counterparts due to poor molecular mobility and hydrophobicity of the polymer chains.

The results from this dissertation indicate that supported amine materials can adsorb CO_2 as ammonium bicarbonates in the presence of water and dilute concentrations of CO_2. Ammonium bicarbonate formation, however, appears to be less favorable on solid supported amines than in amine solutions under the conditions employed. In addition, this work also suggests that amine type is only one of many factors that must be considered when designing aminopolymer-based materials as practical CO_2 adsorbents.

CHAPTER 1. INTRODUCTION

1.1 Motivation

There is a heavy reliance on energy supplied by fossil fuels in the world today, and future forecasts do not indicate that fossil fuel usage will diminish.[1] Furthermore, the fossil fuels used release large amounts of CO_2 into the atmosphere, which has been linked with global climate change over the past century. As a result, there has been a significant research focus on developing technologies to reduce such emissions.[2–7]

Post-combustion capture and sequestration has been proposed to reduce CO_2 emissions.[8,9] In this approach, CO_2 is removed from the flue gas of power plants (3-15 vol% CO_2) and is sequestered underground. However, it should be noted that large point sources of CO_2 such as power plants only partially account for all annual CO_2 emissions.[10] Furthermore, dispersed sources such as automobiles and planes account for approximately one-third of annual CO_2 emissions. Removal of CO_2 from the atmosphere (400 ppm CO_2), also known as direct air capture (DAC), has been proposed as a way to account for CO_2 emissions regardless of source.[3] Unlike post-combustion capture, DAC is considered a negative emission technology as it can theoretically achieve a net reduction of CO_2 in the atmosphere. Furthermore, it has been suggested that negative emission technologies will be necessary to mitigate the effects of climate change.[11]

The most common technology proposed for post-combustion CO_2 capture is absorption by aqueous amine solutions.[7] Many amine types have been studied for absorption and include unhindered amines, sterically-hindered amines, and cyclic amines

(Figure 1.1).[12–17] While aqueous amine based absorption is technically feasible, it comes at a high processing cost. In particular, the temperature swing-based regeneration step, in which the CO_2 is stripped from the amine solution, is energy intensive and costly.[7] Researchers have been exploring the use of solid adsorbents as a potential replacement for aqueous amine solutions.[2,18–21] Solid sorbents offer the potential advantage of reduced regeneration energy due to their lower heat capacities when compared to aqueous amine absorbents.[18] Many adsorbents have been evaluated for CO_2 capture including zeolites,[22,23] metal-organic frameworks,[24–28] and activated carbons.[22,23,29]

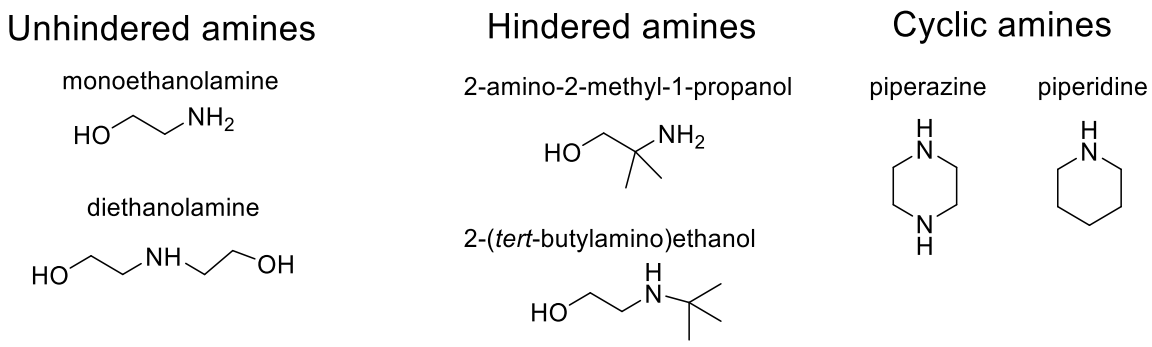

Figure 1.1. Typical amines used in aqueous media for CO_2 absorption.[13,17,30,31]

1.2 Solid Supported Amines for CO_2 Capture

Solid supported amines are one class of materials that is promising for post-combustion capture and DAC.[18,21,32,33] These materials are solid analogues of the well-established aqueous amine absorption technology, and some of the chemistry that makes aqueous amines effective for CO_2 capture is also found on solid supported analogues. For these materials, amines are typically incorporated into the pores of a metal-oxide support and act as active sites for chemisorption of CO_2. Chemisorbants, such as supported amines, have an advantage over physisorbants, such as zeolites and activated carbons, due to their

high CO_2 selectivity over other major components found in flue gas and air such as N_2 and O_2.[18] It should be noted that while a wide array of amine types has been studied in solution, studies on supported amines primarily focus on unhindered amine moieties.

1.2.1 Classes of Solid Supported Amines

Solid supported amines have been divided into four different classes (Figure 1.2).[18,32] Class 1 materials consist of aminopolymers or amine-containing small molecules that are physically impregnated into porous supports.[33–39] This class of materials is attractive for practical use because of their ease of preparation and large amounts of amines that can be incorporated into the support. However, it should be noted that if the amine-containing organics used are highly volatile, they can leach out of the support under humid conditions and/or during the regeneration step due to the physically bound nature of the amine-containing organics in this class of materials.[40,41] A particularly attractive aminopolymer used for this class of materials is low molecular weight branched poly(ethylenimine) (PEI), due to its large density of amines, good cyclic stability when used in a temperature (TSA) and/or vacuum swing adsorption (VSA) process, and commercial availability.[4,42]

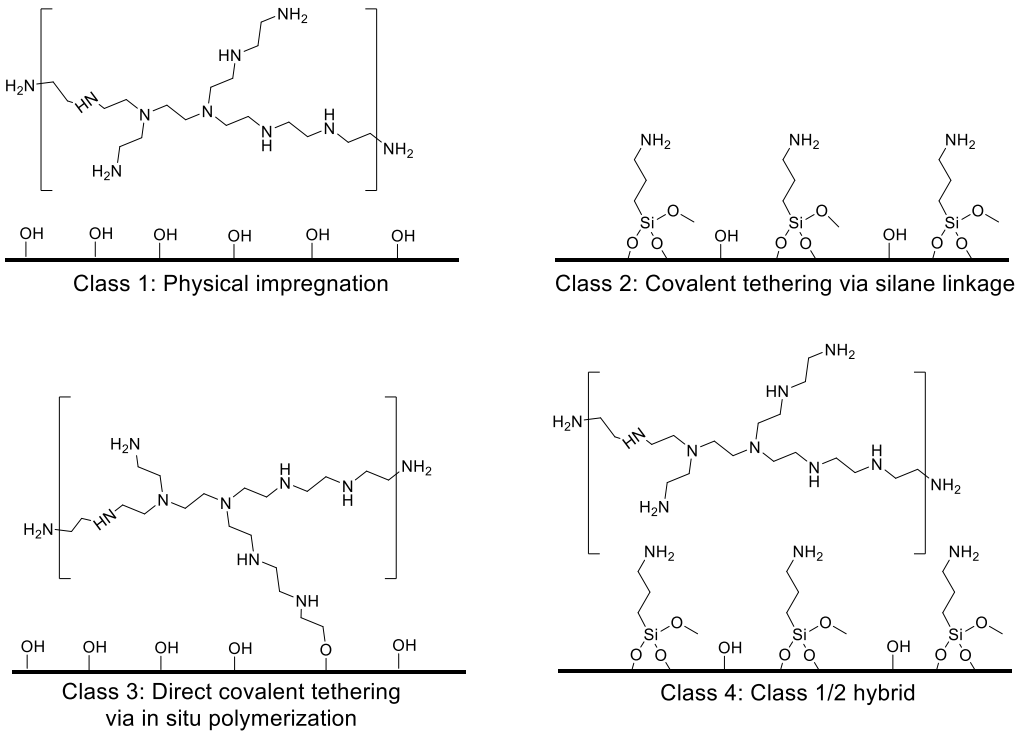

Figure 1.2. Classes of supported amine materials.

Class 3 materials consist of aminopolymers that are covalently tethered onto the support and are constructed by *in situ* polymerization inside the porous support.[43–48] While this class of materials have increased thermal stability due to the covalent bond between the support and the polymer, they are more difficult to make on a lab scale. Due to the high amine loadings that can be achieved, class 1 and 3 materials typically adsorb large quantities of CO_2; however, these materials can also suffer diffusional limitations due to pore blockage by the polymer, often resulting in slow adsorption/desorption kinetics.[33,46]

Class 2 materials consist of aminosilanes that are covalently bound to the surface of the porous support.[49–52] These materials have high thermal stability due to covalent tethering of the aminosilane onto the support, but generally low amine content is achieved. Class 2 materials have also been primarily used for fundamental studies on the role of

amine type (primary/secondary/tertiary) on CO_2 adsorption performance and oxidative stability.[49,53]

Class 4 materials are a hybrid of both class 1 and 2 materials.[54,55] Moreover, they contain both grafted molecular aminosilanes and physically impregnated aminopolymers. Class 4 materials have been reported to have better stability when compared to class 1 materials due to the hydrogen bonding interactions between the amines on the aminopolymer and the amines that are covalently bound to the surface but could still suffer diffusional limitations due to pore blockage.[54]

1.2.2 Amine-CO_2 Species Formed on Supported Amine Materials

Alkylammonium carbamates and alkylammonium bicarbonates are amine-CO_2 species that have been proposed for supported amines by extrapolation from the literature on aqueous amine solutions (Figure 1.3).[56,57] The alkylammonium carbamate species can form only on primary and secondary amines under dry and humid conditions and requires two amines to capture one molecule of CO_2 (i.e. 0.5 mol CO_2/mol N).[57]

Tertiary amines can capture CO_2 as alkylammonium bicarbonate in the presence of water.[56] The formation of such species would result in a maximum amine efficiency of 1 mol CO_2/mol N. In solution, the alkylammonium bicarbonate species is less thermally stable and has slower kinetics of formation when compared to the alkylammonium carbamate species.[13,58] It should be noted that, theoretically, primary and secondary amines can also form bicarbonate species in the presence of water. In fact, in aqueous solution, primary and secondary amines form both carbamates and bicarbonates. However, carbamates are the dominant species formed in primary and secondary amine solutions, as

carbamates are the kinetically and thermodynamically favored product.[31] Alkylammonium carbonates (0.5 mol CO_2/mol N) are another amine-CO_2 species that has been reported to form in aqueous media.[21,31] However, in solution, carbonates are typically a short-lived intermediate that evolve into the bicarbonate species.[31]

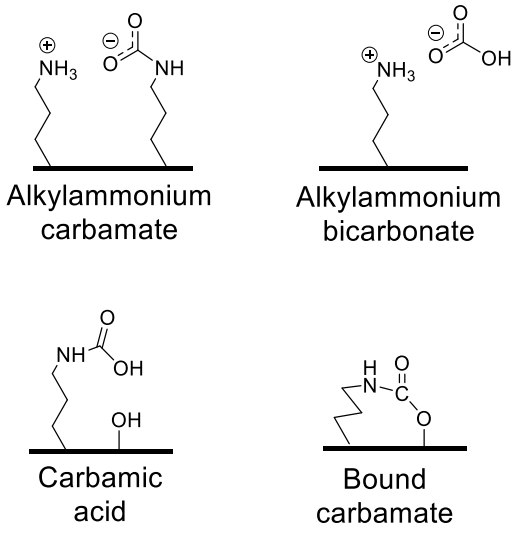

Figure 1.3. Amine-CO_2 species formed on solid supported amines.

Recently, NMR and *in situ* FTIR spectroscopy have been used to further distinguish the CO_2 adsorption products on supported amines.[59–67] Chang et al. initially proposed, using *in situ* FTIR spectroscopy that (bi)carbonates formed on a primary aminosilane functionalized sorbent under the presence of dry CO_2.[66] However, the band assignments in this initial study were not supported by subsequent work.[58,59,61,63,64,68–72] Furthermore, the initial study was conducted under dry conditions and did not consider that alkylammonium (bi)carbonate species cannot readily form without water. Subsequent FTIR and NMR spectroscopy studies suggested that the amine-CO_2 species formed on primary and

secondary amines are mostly associated with the alkylammonium carbamate species.[58,59,61,63,64,68–72]

Additional amine-CO_2 species are also observed on supported amines that are generally not found in aqueous media such as surface bound carbamate and carbamic acid (Figure 1.3).[59–61,68,71,72] Danon et al. conducted an *in situ* FTIR spectroscopy study on a primary aminosilane grafted silica sorbent.[62] They exposed the material to CO_2 and subsequently treated the material with heat and vacuum. It was observed that FTIR peaks associated with chemisorbed CO_2 (1715 and 1510 cm^{-1}) remained after vacuum and heat treatment, indicating the species associated with these peaks were strongly bound. Furthermore, the bands at 1715 and 1510 cm^{-1} were attributed to carbonyl stretching mode and a C-N stretching mode respectively of a surface bound carbamate species. Bacsik et al. also studied amine-CO_2 species on primary aminosilane grafted silica using *in situ* FTIR spectroscopy and demonstrated that there were two distinct peaks that were associated with a carbonyl stretching mode between 1680 and 1715 cm^{-1} after exposing the material to CO_2.[59] During dynamic vacuum treatment, the peak at 1680 cm^{-1} disappeared immediately, while the peak at 1715 cm^{-1} remained stable. Due to its instability under the presence of dynamic vacuum, the peak at 1680 cm^{-1} was attributed to the carbonyl stretching mode of a carbamic acid. Further evidence of the formation of carbamic acid species on supported amine sorbents in the presence of CO_2 was provided by subsequent NMR spectroscopy studies.[68,70–72]

The assignment of alkylammonium bicarbonate is not without controversy.[58,59,73–75] Some studies suggested that bicarbonates do not form on primary or secondary amine containing sorbents under humid and dry conditions.[59,64,74,76] Furthermore, in these studies,

alkylammonium carbamates and carbamic acids appeared to be major amine-CO_2 species formed. Didas et al., however, claimed that ammonium bicarbonates formed on a primary aminosilane grafted silica sorbent in the presence of humid CO_2.[58] In that study, ammonium bicarbonate formation was observed on a low amine loading sample in the presence of humid CO_2 when the contributions of fast forming carbamate and carbamic acid species were subtracted from the CO_2 adsorption FTIR spectrum. After spectral subtraction, a band at 1350 cm^{-1} was observed and was assigned to a vibrational mode of the alkylammonium bicarbonate species.

1.2.3 Effects of Humidity

There have been conflicting reports on the effects of humidity on CO_2 adsorption on supported amine materials; both enhancements and reductions of CO_2 capacity have been reported for supported amines under humid conditions.[40,58,77–82]

Goeppert et al. observed that humidity reduced the CO_2 capacity from 1.71 to 1.41 mmol CO_2/g on fumed silica impregnated with 50 wt% PEI when comparing dry to humid conditions (relative humidity of 67%) using 420 ppm CO_2 at 25 °C.[78] The authors claimed that the decrease in CO_2 capacity for the higher loading sample when comparing dry to humid conditions was due to water blocking CO_2 from accessing difficult to reach amines. In the same study, the authors observed that humidity had an enhancing effect on CO_2 adsorption on fumed silica impregnated with 33 wt% PEI. The CO_2 capacity of the material increased from 1.18 to 1.77 mmol CO_2/g when comparing dry to humid conditions. Furthermore, this indicated that the effect of water can be dependent on amine loading and amine dispersion in porous supports.

In another report, the enhancement effect of humidity on CO_2 adsorption on primary aminosilane grafted silica was observed to be a function of amine loading.[58] Furthermore, the enhancement effects of humidity on CO_2 adsorption was the least pronounced for the high amine loading material (4.33 mmol N/g). As stated in the previous section, only the low amine loading material (1.65 mmol N/g) partially adsorbed CO_2 as ammonium bicarbonates under humid conditions. A change of amine-CO_2 species from ammonium carbamates to ammonium bicarbonates can increase the CO_2 adsorption capacity, as the later species only requires one amine to adsorb one CO_2 molecule while the former species requires two amines to adsorb one CO_2 molecule.

It has also been posited that water can increase CO_2 uptake through reducing kinetic restrictions. Furthermore, adsorbed water can act as a diffusive intermediate to transport CO_2, liberate amines hydrogen bonded to surface hydroxyls, and can increase the chain mobility of amine containing molecules.[59,64,83–85] In addition, it should be noted that water can increase the thermodynamic stability of amine-CO_2 species through hydrogen bonding interactions, allowing for larger CO_2 capacities.[85,86]

While co-adsorption of water can enhance CO_2 capacity of supported amine materials, it can also increase the energy required to regenerate sorbents as some of the energy will go to heating of adsorbed water.[87] Therefore, it is also necessary to limit the amount of water adsorbed on supported amine materials for a practical separations process.

1.2.4 Degradation of Supported Amines

The sorbent lifetime is a critical parameter as it can affect the operating costs of the separations process.[32] Furthermore, the sorbent used for CO_2 capture must retain its CO_2

adsorption performance over many temperature and/or vacuum swing adsorption cycles. Supported amine materials are known to degrade by CO_2-induced urea formation, oxidation, and loss of amines through evaporation and/or leaching.[40,41,53,88–91] It should be noted that all degradation pathways are accelerated by increasing temperature.

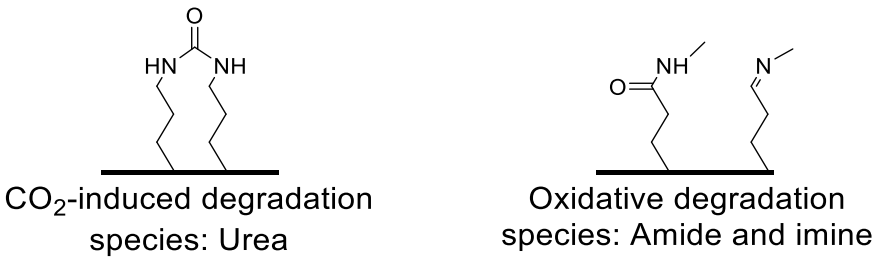

Figure 1.4. CO_2-induced and oxidative degradation species.

Supported primary amines have been found to deactivate by reacting with CO_2 to form irreversible urea linkages at temperatures (110-140 °C) that may be used for temperature swing regeneration under dry conditions (Figure 1.4).[90,92] However, this deactivation product does not form as readily in humidified gas streams.[93] It should be noted that CO_2-induced degradation by urea formation is typically not observed for secondary and tertiary amines.

Supported amines are known to deactivate in the presence of oxygen, a major component in both air (21%) and flue gas (3-10%), by formation of imines and amides (Figure 1.4).[53,88,89,91,94] It is believed that the first step of the degradation mechanism occurs through the abstraction of a hydrogen radical of the carbon adjacent to the amine group.[53] This mechanism can be accelerated in the presence of transition metal ions and/or elevated temperatures.[53] A study on how amine type affected oxidative stability was conducted using a series of aminosilane grafted silica materials.[53] It was determined from this study

that sorbents that contained solely secondary amines are prone to oxidative degradation through imine and amide formation and sorbents that contained solely primary or tertiary amines are relatively resistant to oxidation. Furthermore, imines and amides can decrease the basicity of the amine sorbent and hinder its ability to capture CO_2. In the same study it was also found that a primary amine that was separated from a secondary amine by an ethyl group was susceptible to oxidative degradation, indicating an intramolecular degradation mechanism.

Branched PEI, a commonly used aminopolymer for adsorption, has been found to oxidatively degrade.[88,95] Commercial branched PEI (M_w~800 g/mol) typically consists of 44% primary, 33% secondary, and 23% tertiary amines.[96] From the studies on isolated aminosilane grafted sorbents, it can be extrapolated that oxidative degradation can occur on secondary and primary amines of PEI. Degradation of primary amines in PEI is possible because they are attached to secondary amines by an ethyl group. Consistent with studies on grafted molecular amines, aminopolymers that only contain only primary amines, have been found to be more resistant to oxidative degradation.[95,97]

Recent studies have focused on finding aminopolymers that are more oxidatively resistant than branched PEI.[36–38,98,99] On the basis that primary and tertiary amines are oxidatively stable as isolated aminosilane grafted sorbents, Pang et al. synthesized dendrimers consisting of a combination of primary and tertiary amines.[37] However, the dendrimers were found to degrade in the presence of oxygen at high temperatures (110 °C). The authors posited that degradation occurred because the dendrimers rearranged to form secondary amine containing cyclic structures at the high temperatures used for the oxidation studies. It was also observed that aminopolymers and small molecules that

contained secondary amine spaced with propyl linkers were less likely to oxidatively degrade when compared to aminopolymers and small molecules that contained secondary amine that were spaced with ethyl linkers. Other strategies to increase the oxidative stability of aminopolymers include incorporating additives such as poly(ethylene glycol) (PEG).[100] Furthermore, the hydrogen bonding between the hydroxyl groups of PEG and amines can increase resistance to oxidative degradation.

1.3 Outlook and Scope

Supported amine sorbents are promising candidate materials for capturing CO_2 due to their low heat capacities, large CO_2 adsorption capacities, and high CO_2 selectivities at operating conditions.[18] However, the rational design of this type of sorbent remains challenging because it is not well understood how CO_2 and H_2O interacts with the sorbent on the molecular level. The amine types most commonly used on solid supports consist of unhindered primary, secondary and tertiary amines. A much larger variety has been studied in aqueous amine literature including cyclic amines and sterically hindered amines.[13,16]

To this end, this dissertation reports on the effects of water on the CO_2 adsorption performance of solid supported amines. Specifically, spectroscopic evidence of the CO_2 species formed on various amine types under dry and humid conditions is provided. This dissertation also reports on the CO_2 adsorption performance of an amine type that is widely studied in solution literature but is often ignored on solid support — sterically hindered amines.

1.4 References

(1) IPCC. *Climate Change 2007 Synthesis Report. Contribution of Working Groups I, II and III to the Fourth Assesment Report of the Intergivernmental Panel on Climate Change*; 2007.

(2) Aaron, D.; Tsouris, C. Separation of CO_2 from Flue Gas: A Review. *Sep. Sci. Technol.* **2005**, *40*, 321–348.

(3) Lackner, K. S.; Brennan, S.; Matter, J. M.; Park, A.-H. A.; Wright, A.; van der Zwaan, B. The Urgency of the Development of CO_2 Capture from Ambient Air. *Proc. Natl. Acad. Sci. U. S. A.* **2012**, *109*, 13156–13162.

(4) Choi, S.; Drese, J. H.; Jones, C. W. Adsorbent Materials for Carbon Dioxide Capture from Large Anthropogenic Point Sources. *ChemSusChem* **2009**, *2*, 796–854.

(5) Chu, S.; Majumdar, A. Opportunities and Challenges for a Sustainable Energy Future. *Nature* **2012**, *488*, 294–303.

(6) Abu-Zahra, M. R. M.; Sodiq, A.; Feron, P. H. M. Commercial Liquid Absorbent-Based PCC Processes. In *Absorption-Based Post-combustion Capture of Carbon Dioxide*; Paul Feron, Ed.; Woodhead Publishing, 2016; pp 757–778.

(7) Rochelle, G. T. Amine Scrubbing for CO_2 Capture. *Science* **2009**, *325*, 1652–1654.

(8) Bhown, A. S.; Freeman, B. C. Analysis and Status of Post-Combustion Carbon Dioxide Capture Technologies. *Environ. Sci. Technol.* **2011**, *45*, 8624–8632.

(9) Figueroa, J. D.; Fout, T.; Plasynski, S.; McIlvried, H.; Srivastava, R. D. Advances in CO2 Capture Technology—The U.S. Department of Energy's Carbon Sequestration Program. *Int. J. Greenh. Gas Control* **2008**, *2*, 9–20.

(10) Jones, C. W. CO_2 Capture from Dilute Gases as a Component of Modern Global Carbon Management. *Annu. Rev. Chem. Biomol. Eng.* **2011**, *2*, 31–52.

(11) Tokarska, K. B.; Gillett, N. P. Cumulative Carbon Emissions Budgets Consistent with 1.5 °C Global Warming. *Nat. Clim. Chang.* **2018**, *8*, 296–299.

(12) Choi, W.-J.; Seo, J.-B.; Jang, S.-Y.; Jung, J.-H.; Oh, K.-J. Removal Characteristics of CO_2 Using Aqueous MEA/AMP Solutions in the Absorption and Regeneration Process. *J. Environ. Sci.* **2009**, *21*, 907–913.

(13) Sartori, G.; Savage, D. W. Sterically Hindered Amines for Carbon Dioxide Removal from Gases. *Ind. Eng. Chem. Fundam.* **1983**, *22*, 239–249.

(14) Hook, R. J. An Investigation of Some Sterically Hindered Amines as Potential Carbon Dioxide Scrubbing Compounds. *Ind. Eng. Chem. Res.* **1997**, *36*, 1779–1790.

(15) Bernhardsen, I. M.; Knuutila, H. K. A Review of Potential Amine Solvents for CO_2 Absorption Process: Absorption Capacity, Cyclic Capacity and PKa. *Int. J. Greenh. Gas Control* **2017**, *61*, 27–48.

(16) Rochelle, G.; Chen, E.; Freeman, S.; Van Wagener, D.; Xu, Q.; Voice, A. Aqueous Piperazine as the New Standard for CO_2 Capture Technology. *Chem. Eng. J.* **2011**, *171*, 725–733.

(17) Freeman, S. A.; Dugas, R.; Van Wagener, D. H.; Nguyen, T.; Rochelle, G. T. Carbon Dioxide Capture with Concentrated, Aqueous Piperazine. *Int. J. Greenh. Gas Control* **2010**, *4*, 119–124.

(18) Bollini, P.; Didas, S. A.; Jones, C. W. Amine-Oxide Hybrid Materials for Acid Gas Separations. *J. Mater. Chem.* **2011**, *21*, 15100–15120.

(19) Yu, C.-H.; Huang, C.-H.; Tan, C.-S. A Review of CO_2 Capture by Absorption and Adsorption. *Aerosol Air Qual. Res.* **2012**, *12*, 745–769.

(20) Sayari, A.; Belmabkhout, Y.; Serna-Guerrero, R. Flue Gas Treatment via CO_2 Adsorption. *Chem. Eng. J.* **2011**, *171*, 760–774.

(21) Sanz-Pérez, E. S.; Murdock, C. R.; Didas, S. A.; Jones, C. W. Direct Capture of CO_2 from Ambient Air. *Chem. Rev.* **2016**, *116*, 11840–11876.

(22) Chue, K. T.; Kim, J. N.; Yoo, Y. J.; Cho, S. H.; Yang, R. T. Comparison of Activated Carbon and Zeolite 13X for CO_2 Recovery from Flue Gas by Pressure Swing Adsorption. *Ind. Eng. Chem. Res.* **1995**, *34*, 591–598.

(23) Cavenati, S.; Grande, C. A.; Rodrigues, A. E. Adsorption Equilibrium of Methane, Carbon Dioxide, and Nitrogen on Zeolite 13X at High Pressures. *J. Chem. Eng. Data* **2004**, *49*, 1095–1101.

(24) McDonald, T. M.; Mason, J. A.; Kong, X.; Bloch, E. D.; Gygi, D.; Dani, A.; Crocella, V.; Giordanino, F.; Odoh, S. O.; Drisdell, W. S.; et al. Cooperative Insertion of CO_2 in Diamine-Appended Metal-Organic Frameworks. *Nature* **2015**, *519*, 303–308.

(25) Darunte, L. A.; Walton, K. S.; Sholl, D. S.; Jones, C. W. CO_2 Capture via Adsorption in Amine-Functionalized Sorbents. *Curr. Opin. Chem. Eng.* **2016**, *12*, 82–90.

(26) Britt, D.; Furukawa, H.; Wang, B.; Glover, T. G.; Yaghi, O. M. Highly Efficient Separation of Carbon Dioxide by a Metal-Organic Framework Replete with Open Metal Sites. *Proc. Natl. Acad. Sci. U. S. A.* **2009**, *106*, 20637–20640.

(27) D'Alessandro, D. M.; Smit, B.; Long, J. R. Carbon Dioxide Capture: Prospects for New Materials. *Angew. Chemie Int. Ed.* **2010**, *49*, 6058–6082.

(28) Millward, A. R.; Yaghi, O. M. Metal−Organic Frameworks with Exceptionally High

Capacity for Storage of Carbon Dioxide at Room Temperature. *J. Am. Chem. Soc.* **2005**, *127*, 17998–17999.

(29) Pevida, C.; Plaza, M. G.; Arias, B.; Fermoso, J.; Rubiera, F.; Pis, J. J. Surface Modification of Activated Carbons for CO_2 Capture. *Appl. Surf. Sci.* **2008**, *254*, 7165–7172.

(30) Im, J.; Hong, S. Y.; Cheon, Y.; Lee, J.; Lee, J. S.; Kim, H. S.; Cheong, M.; Park, H. Steric Hindrance-Induced Zwitterionic Carbonates from Alkanolamines and CO_2: Highly Efficient CO_2 Absorbents. *Energy Environ. Sci.* **2011**, *4*, 4284–4289.

(31) Kortunov, P. V.; Siskin, M.; Baugh, L. S.; Calabro, D. C. *In Situ* Nuclear Magnetic Resonance Mechanistic Studies of Carbon Dioxide Reactions with Liquid Amines in Aqueous Systems: New Insights on Carbon Capture Reaction Pathways. *Energy & Fuels* **2015**, *29*, 5919–5939.

(32) Didas, S. A.; Choi, S.; Chaikittisilp, W.; Jones, C. W. Amine–Oxide Hybrid Materials for CO_2 Capture from Ambient Air. *Acc. Chem. Res.* **2015**, *48*, 2680–2687.

(33) Xu, X.; Song, C.; Andresen, J. M.; Miller, B. G.; Scaroni, A. W. Novel Polyethylenimine-Modified Mesoporous Molecular Sieve of MCM-41 Type as High-Capacity Adsorbent for CO_2 Capture. *Energy and Fuels* **2002**, *16*, 1463–1469.

(34) Chaikittisilp, W.; Khunsupat, R.; Chen, T. T.; Jones, C. W. Poly(Allylamine)–Mesoporous Silica Composite Materials for CO_2 Capture from Simulated Flue Gas or Ambient Air. *Ind. Eng. Chem. Res.* **2011**, *50*, 14203–14210.

(35) Yamada, H.; Fujiki, J.; Chowdhury, F. A.; Yogo, K. Effect of Isopropyl-Substituent Introduction into Tetraethylenepentamine-Based Solid Sorbents for CO_2 Capture. *Fuel* **2018**, *214*, 14–19.

(36) Pang, S. H.; Lively, R. P.; Jones, C. W. Oxidatively-Stable Linear Poly(Propylenimine)-Containing Adsorbents for CO_2 Capture from Ultradilute Streams. *ChemSusChem* **2018**, *11*, 2628–2637.

(37) Pang, S. H.; Lee, L.-C.; Sakwa-Novak, M. A.; Lively, R. P.; Jones, C. W. Design of Aminopolymer Structure to Enhance Performance and Stability of CO_2 Sorbents: Poly(Propylenimine) vs Poly(Ethylenimine). *J. Am. Chem. Soc.* **2017**, *139*, 3627–3630.

(38) Sarazen, M. L.; Jones, C. W. Insights into Azetidine Polymerization for the Preparation of Poly(Propylenimine)-Based CO_2 Adsorbents. *Macromolecules* **2017**, *50*, 9135–9143.

(39) Wei, J.; Liao, L.; Xiao, Y.; Zhang, P.; Shi, Y. Capture of Carbon Dioxide by Amine-Impregnated as-Synthesized MCM-41. *J. Environ. Sci.* **2010**, *22*, 1558–1563.

(40) Sanz-Pérez, E. S.; Olivares-Marín, M.; Arencibia, A.; Sanz, R.; Calleja, G.; Maroto-Valer, M. M. CO_2 Adsorption Performance of Amino-Functionalized SBA-15 under Post-Combustion Conditions. *Int. J. Greenh. Gas Control* **2013**, *17*, 366–375.

(41) Goeppert, A.; Meth, S.; Prakash, G. K. S.; Olah, G. A. Nanostructured Silica as a Support for Regenerable High-Capacity Organoamine-Based CO_2 Sorbents. *Energy Environ. Sci.* **2010**, *3*, 1949–1960.

(42) Samanta, A.; Zhao, A.; Shimizu, G. K. H.; Sarkar, P.; Gupta, R. Post-Combustion CO_2 Capture Using Solid Sorbents: A Review. *Ind. Eng. Chem. Res.* **2012**, *51*, 1438–1463.

(43) Hicks, J. C.; Drese, J. H.; Fauth, D. J.; Gray, M. L.; Qi, G.; Jones, C. W. Designing Adsorbents for CO_2 Capture from Flue Gas-Hyperbranched Aminosilicas Capable of Capturing CO_2 Reversibly. *J. Am. Chem. Soc.* **2008**, *130*, 2902–2903.

(44) Drese, J. H.; Choi, S.; Didas, S. A.; Bollini, P.; Gray, M. L.; Jones, C. W. Effect of Support Structure on CO_2 Adsorption Properties of Pore-Expanded Hyperbranched Aminosilicas. *Microporous Mesoporous Mater.* **2012**, *151*, 231–240.

(45) Choi, S.; Drese, J. H.; Eisenberger, P. M.; Jones, C. W. Application of Amine-Tethered Solid Sorbents for Direct CO_2 Capture from the Ambient Air. *Environ. Sci. Technol.* **2011**, *45*, 2420–2427.

(46) Drese, J. H.; Choi, S.; Lively, R. P.; Koros, W. J.; Fauth, D. J.; Gray, M. L.; Jones, C. W. Synthesis-Structure-Property Relationships for Hyperbranched Aminosilica CO_2 Adsorbents. *Adv. Funct. Mater.* **2009**, *19*, 3821–3832.

(47) Chaikittisilp, W.; Lunn, J. D.; Shantz, D. F.; Jones, C. W. Poly(L-lysine) Brush–Mesoporous Silica Hybrid Material as a Biomolecule-Based Adsorbent for CO_2 Capture from Simulated Flue Gas and Air. *Chem. – A Eur. J.* **2011**, *17*, 10556–10561.

(48) Qi, G.; Fu, L.; Giannelis, E. P. Sponges with Covalently Tethered Amines for High-Efficiency Carbon Capture. *Nat. Commun.* **2014**, *5*, 5796.

(49) Didas, S. A.; Kulkarni, A. R.; Sholl, D. S.; Jones, C. W. Role of Amine Structure on Carbon Dioxide Adsorption from Ultradilute Gas Streams Such as Ambient Air. *ChemSusChem* **2012**, *5*, 2058–2064.

(50) Serna-Guerrero, R.; Belmabkhout, Y.; Sayari, A. Further Investigations of CO_2 Capture Using Triamine-Grafted Pore-Expanded Mesoporous Silica. *Chem. Eng. J.* **2010**, *158*, 513–519.

(51) Harlick, P. J. E.; Sayari, A. Applications of Pore-Expanded Mesoporous Silica. 5. Triamine Grafted Material with Exceptional CO_2 Dynamic and Equilibrium Adsorption Performance. *Ind. Eng. Chem. Res.* **2007**, *46*, 446–458.

(52) Gebald, C.; Wurzbacher, J. A.; Tingaut, P.; Steinfeld, A. Stability of Amine-Functionalized Cellulose during Temperature-Vacuum-Swing Cycling for CO_2 Capture from Air. *Environ. Sci. Technol.* **2013**, *47*, 10063–10070.

(53) Bollini, P.; Choi, S.; Drese, J. H.; Jones, C. W. Oxidative Degradation of Aminosilica Adsorbents Relevant to Postcombustion CO_2 Capture. *Energy & Fuels* **2011**, *25*, 2416–2425.

(54) Wilfong, W. C.; Kail, B. W.; Jones, C. W.; Pacheco, C.; Gray, M. L. Spectroscopic Investigation of the Mechanisms Responsible for the Superior Stability of Hybrid Class 1/Class 2 CO_2 Sorbents: A New Class 4 Category. *ACS Appl. Mater. Interfaces* **2016**, *8*, 12780–12791.

(55) Choi, S.; Gray, M. L.; Jones, C. W. Amine-Tethered Solid Adsorbents Coupling High Adsorption Capacity and Regenerability for CO_2 Capture From Ambient Air. *ChemSusChem* **2011**, *4*, 628–635.

(56) Donaldson, T. L.; Nguyen, Y. N. Carbon Dioxide Reaction Kinetics and Transport in Aqueous Amine Membranes. *Ind. Eng. Chem. Fundam.* **1980**, *19*, 260–266.

(57) Caplow, M. Kinetics of Carbamate Formation and Breakdown. *J. Am. Chem. Soc.* **1968**, *90*, 6795–6803.

(58) Didas, S. A.; Sakwa-Novak, M. A.; Foo, G. S.; Sievers, C.; Jones, C. W. Effect of Amine Surface Coverage on the Co-Adsorption of CO_2 and Water: Spectral Deconvolution of Adsorbed Species. *J. Phys. Chem. Lett.* **2014**, *5*, 4194–4200.

(59) Bacsik, Z.; Ahlsten, N.; Ziadi, A.; Zhao, G. Y.; Garcia-Bennett, A. E.; Martín-Matute, B.; Hedin, N. Mechanisms and Kinetics for Sorption of CO_2 on Bicontinuous Mesoporous Silica Modified with n-Propylamine. *Langmuir* **2011**, *27*, 11118–11128.

(60) Foo, G. S.; Lee, J. J.; Chen, C.-H.; Hayes, S. E.; Sievers, C.; Jones, C. W. Elucidation of Surface Species through in Situ FTIR Spectroscopy of Carbon Dioxide Adsorption on Amine-Grafted SBA-15. *ChemSusChem* **2017**, *10*, 266–276.

(61) Hahn, M. W.; Jelic, J.; Berger, E.; Reuter, K.; Jentys, A.; Lercher, J. A. Role of Amine Functionality for CO_2 Chemisorption on Silica. *J. Phys. Chem. B* **2016**, *120*, 1988–1995.

(62) Danon, A.; Stair, P. C.; Weitz, E. FTIR Study of CO_2 Adsorption on Amine-Grafted SBA-15: Elucidation of Adsorbed Species. *J. Phys. Chem. C* **2011**, *115*, 11540–11549.

(63) Knofel, C.; Martin, C.; Hornebecq, V.; Llewellyn, P. L. Study of Carbon Dioxide Adsorption on Mesoporous Aminopropylsilane-Functionalized Silica and Titania Combining Microcalorimetry and in Situ Infrared Spectroscopy. *J. Phys. Chem. C* **2009**, *113*, 21726–21734.

(64) Aziz, B.; Hedin, N.; Bacsik, Z. Quantification of Chemisorption and Physisorption of Carbon Dioxide on Porous Silica Modified by Propylamines: Effect of Amine Density. *Microporous Mesoporous Mater.* **2012**, *159*, 42–49.

(65) Yu, J.; Chuang, S. S. C. The Role of Water in CO_2 Capture by Amine. *Ind. Eng. Chem. Res.* **2017**, *56*, 6337–6347.

(66) Chang, A. C. C.; Chuang, S. S. C.; Gray, M.; Soong, Y. In-Situ Infrared Study of CO_2 Adsorption on SBA-15 Grafted with Gamma-(Aminopropyl)Triethoxysilane. *Energy & Fuels* **2003**, *17*, 468–473.

(67) Wilfong, W. C.; Srikanth, C. S.; Chuang, S. S. C. In Situ ATR and DRIFTS Studies of the Nature of Adsorbed CO_2 on Tetraethylenepentamine Films. *ACS Appl. Mater. Interfaces* **2014**, *6*, 13617–13626.

(68) Pinto, M. L.; Mafra, L.; Guil, J. M.; Pires, J.; Rocha, J. Adsorption and Activation of CO_2 by Amine-Modified Nanoporous Materials Studied by Solid-State NMR and $^{13}CO_2$ Adsorption. *Chem. Mater.* **2011**, *23*, 1387–1395.

(69) Bacsik, Z.; Atluri, R.; Garcia-Bennett, A. E.; Hedin, N. Temperature-Induced Uptake of CO_2 and Formation of Carbamates in Mesocaged Silica Modified with n-Propylamines. *Langmuir* **2010**, *26*, 10013–10024.

(70) Shimon, D.; Chen, C. H.; Lee, J. J.; Didas, S. A.; Sievers, C.; Jones, C. W.; Hayes, S. E. ^{15}N Solid State NMR Spectroscopic Study of Surface Amine Groups for Carbon Capture: 3-Aminopropylsilyl Grafted to SBA-15 Mesoporous Silica. *Environ. Sci. Technol.* **2018**, *52*, 1488–1495.

(71) Chen, C.-H.; Shimon, D.; Lee, J. J.; Didas, S. A.; Mehta, A. K.; Sievers, C.; Jones, C. W.; Hayes, S. E. Spectroscopic Characterization of Adsorbed $^{13}CO_2$ on 3-Aminopropylsilyl-Modified SBA15 Mesoporous Silica. *Environ. Sci. Technol.* **2017**, *51*, 6553–6559.

(72) Mafra, L.; Čendak, T.; Schneider, S.; Wiper, P. V.; Pires, J.; Gomes, J. R. B.; Pinto, M. L. The Structure of Chemisorbed CO_2 Species in Amine-Functionalized Mesoporous Silicas Studied by Solid-State NMR and Computer Modeling. *J. Am. Chem. Soc.* **2017**, *139*, 389–408.

(73) Hahn, M. W.; Steib, M.; Jentys, A.; Lercher, J. A. Mechanism and Kinetics of CO_2 Adsorption on Surface Bonded Amines. *J. Phys. Chem. C* **2015**, *119*, 4126–4135.

(74) Li, K.; Kress, J. D.; Mebane, D. S. The Mechanism of CO_2 Adsorption under Dry and Humid Conditions in Mesoporous Silica-Supported Amine Sorbents. *J. Phys. Chem. C* **2016**, *120*, 23683–23691.

(75) Yu, J.; Zhai, Y.; Chuang, S. S. C. Water Enhancement in CO_2 Capture by Amines: An Insight into CO_2 –H_2O Interactions on Amine Films and Sorbents. *Ind. Eng. Chem. Res.* **2018**, *57*, 4052–4062.

(76) Wang, X.; Schwartz, V.; Clark, J. C.; Ma, X.; Overbury, S. H.; Xu, X.; Song, C. Infrared Study of CO_2 Sorption over "Molecular Basket" Sorbent Consisting of Polyethylenimine-Modified Mesoporous Molecular Sieve. *J. Phys. Chem. C* **2009**, *113*, 7260–7268.

(77) Zhang, H.; Goeppert, A.; Olah, G. A.; Prakash, G. K. S. Remarkable Effect of Moisture on the CO_2 Adsorption of Nano-Silica Supported Linear and Branched Polyethylenimine. *J. CO2 Util.* **2017**, *19*, 91–99.

(78) Goeppert, A.; Czaun, M.; May, R. B.; Prakash, G. K. S.; Olah, G. A.; Narayanan, S. R. Carbon Dioxide Capture from the Air Using a Polyamine Based Regenerable Solid Adsorbent. *J. Am. Chem. Soc.* **2011**, *133*, 20164–20167.

(79) Belmabkhout, Y.; Serna-Guerrero, R.; Sayari, A. Amine-Bearing Mesoporous Silica for CO_2 Removal from Dry and Humid Air. *Chem. Eng. Sci.* **2010**, *65*, 3695–3698.

(80) Belmabkhout, Y.; Serna-Guerrero, R.; Sayari, A. Adsorption of CO_2-Containing Gas Mixtures over Amine-Bearing Pore-Expanded MCM-41 Silica: Application for Gas Purification. *Ind. Eng. Chem. Res.* **2010**, *49*, 359–365.

(81) Brilman, D. W. F.; Veneman, R. Capturing Atmospheric CO_2 Using Supported Amine Sorbents. *Energy Procedia* **2013**, *37*, 6070–6078.

(82) Chen, C.; Yang, S.-T.; Ahn, W.-S.; Ryoo, R. Amine-Impregnated Silica Monolith with a Hierarchical Pore Structure: Enhancement of CO_2 Capture Capacity. *Chem. Commun.* **2009**, *0*, 3627.

(83) Fan, Y.; Labreche, Y.; Lively, R. P.; Jones, C. W.; Koros, W. J. Dynamic CO_2 Adsorption Performance of Internally Cooled Silica-Supported Poly(Ethylenimine) Hollow Fiber Sorbents. *AIChE J.* **2014**, *60*, 3878–3887.

(84) Mebane, D. S.; Kress, J. D.; Storlie, C. B.; Fauth, D. J.; Gray, M. L.; Li, K. Transport, Zwitterions, and the Role of Water for CO_2 Adsorption in Mesoporous Silica-Supported Amine Sorbents. *J. Phys. Chem. C* **2013**, *117*, 26617–26627.

(85) Sumon, K. Z.; Bains, C. H.; Markewich, D. J.; Henni, A.; East, A. L. L. Semicontinuum Solvation Modeling Improves Predictions of Carbamate Stability in the CO_2 + Aqueous Amine Reaction. *J. Phys. Chem. B* **2015**, *119*, 12556–12264.

(86) Thirion, D.; Rozyyev, V.; Park, J.; Byun, J.; Jung, Y.; Atilhan, M.; Yavuz, C. T. Observation of the Wrapping Mechanism in Amine Carbon Dioxide Molecular Interactions on Heterogeneous Sorbents. *Phys. Chem. Chem. Phys* **2016**, *18*, 14177.

(87) Min, K.; Choi, W.; Kim, C.; Choi, M. Rational Design of the Polymeric Amines in Solid Adsorbents for Postcombustion Carbon Dioxide Capture. *ACS Appl. Mater. Interfaces* **2018**, *10*, 23825–23833.

(88) Heydari-Gorji, A.; Sayari, A. Thermal, Oxidative, and CO_2-Induced Degradation of

Supported Polyethylenimine Adsorbents. *Ind. Eng. Chem. Res.* **2012**, *51*, 6887–6894.

(89) Ahmadalinezhad, A.; Tailor, R.; Sayari, A. Molecular-Level Insights into the Oxidative Degradation of Grafted Amines. *Chem. - A Eur. J.* **2013**, *19*, 10543–10550.

(90) Didas, S. A.; Zhu, R.; Brunell, N. A.; Sholl, D. S.; Jones, C. W. Thermal, Oxidative and CO_2 Induced Degradation of Primary Amines Used for CO_2 Capture: Effect of Alkyl Linker on Stability. *J. Phys. Chem. C* **2014**, *118*, 12302–12311.

(91) Calleja, G.; Sanz, R.; Arencibia, A.; Sanz-Pérez, E. S. Influence of Drying Conditions on Amine-Functionalized SBA-15 as Adsorbent of CO_2. *Top. Catal.* **2011**, *54*, 135–145.

(92) Sayari, A.; Heydari-Gorji, A.; Yang, Y. CO_2-Induced Degradation of Amine-Containing Adsorbents: Reaction Products and Pathways. *J. Am. Chem. Soc.* **2012**, *134*, 13834–13842.

(93) Heydari-Gorji, A.; Belmabkhout, Y.; Sayari, A. Degradation of Amine-Supported CO_2 Adsorbents in the Presence of Oxygen-Containing Gases. *Microporous Mesoporous Mater.* **2011**, *145*, 146–149.

(94) Srikanth, C. S.; Chuang, S. S. C. Spectroscopic Investigation into Oxidative Degradation of Silica-Supported Amine Sorbents for CO_2 Capture. *ChemSusChem* **2012**, *5*, 1435–1442.

(95) Wang, D.; Wang, X.; Song, C. Comparative Study of Molecular Basket Sorbents Consisting of Polyallylamine and Polyethylenimine Functionalized SBA-15 for CO_2 Capture from Flue Gas. *ChemPhysChem* **2017**, *18*, 3163–3173.

(96) Holewinski, A.; Sakwa-Novak, M. A.; Jones, C. W. Linking CO_2 Sorption Performance to Polymer Morphology in Aminopolymer/Silica Composites through Neutron Scattering. *J. Am. Chem. Soc.* **2015**, *137*, 11749–11759.

(97) Bali, S.; Chen, T. T.; Chaikittisilp, W.; Jones, C. W. Oxidative Stability of Amino Polymer-Alumina Hybrid Adsorbents for Carbon Dioxide Capture. *Energy & Fuels* **2013**, *27*, 1547–1554.

(98) Choi, W.; Min, K.; Kim, C.; Ko, Y. S.; Jeon, J. W.; Seo, H.; Park, Y. K.; Choi, M. Epoxide-Functionalization of Polyethyleneimine for Synthesis of Stable Carbon Dioxide Adsorbent in Temperature Swing Adsorption. *Nat. Commun.* **2016**, *7*, 12640−12648.

(99) Sarazen, M. L.; Sakwa-Novak, M. A.; Ping, E. W.; Jones, C. W. Effect of Different Acid Initiators on Branched Poly(Propylenimine) Synthesis and CO_2 Sorption Performance. *ACS Sustain. Chem. Eng.* **2019**, *7*, 7338–7345.

(100) Tanthana, J.; Chuang, S. S. C. In Situ Infrared Study of the Role of PEG in Stabilizing Silica-Supported Amines for CO_2 Capture. *ChemSusChem* **2010**, *3*, 957–964.

CHAPTER 2. EFFECT OF HUMIDITY ON THE CO_2 ADSORPTION OF TERTIARY AMINE GRAFTED SBA-15

Parts of this chapter are adapted from 'Lee, J. J.; Chen, C.-H.; Hayes, S. E.; Sievers, C.; Jones, C. W. Effect of Humidity on the CO_2 Adsorption of Tertiary Amine grafted SBA-15 *J. Phys. Chem. C* **2018**, *121*, 23480-23487 with permission of The American Chemical Society.

2.1 Background

Bicarbonate formation is known to occur in aqueous amine solutions in the presence of CO_2, but there has been conflicting evidence regarding the formation of such species on solid supported analogues during CO_2 capture. Ammonium bicarbonate formation could be beneficial for solid supported amines because of its lower heat of adsorption compared to the ammonium carbamate species.[1,2] Moreover, a low heat of adsorption could help reduce energy costs associated with the desorption process. In addition, the ammonium carbamate species that dominate adsorption on sorbents containing primary and/or secondary amines have been shown to slow down diffusion of CO_2 by crosslinking aminopolymer chains.[3] The formation of ammonium bicarbonate species would not lead to crosslinking because only one nitrogen site is needed to capture a molecule of CO_2.

Few reports have provided experimental evidence for bicarbonate formation over solid amine sorbents. Didas et al. observed a band assigned to a vibrational mode of bicarbonate using *in situ* FTIR spectroscopy on supported primary amines under humid CO_2 capture conditions, but only in (apparently) small amounts.[4] Furthermore, bicarbonate

formation was observed only when the bands associated with fast forming species were subtracted from the FTIR spectrum. Foo et al. recently claimed that bicarbonates can form on tertiary amine [N,N-dimethyl-3-aminopropyltrimethoxysilane (DMAPS)] grafted SBA-15 under nominally dry conditions.[5] Residual physisorbed water after pretreatment at 110 °C for 3 h under helium flow was thought to allow for the formation of bicarbonate species in the presence of otherwise dry CO_2. However, the reported CO_2 capacity of <0.01 mmol CO_2/g shows that the bicarbonate species only formed in very small quantities in nominally dry conditions.

The bicarbonate species has been postulated by ^{13}C solid-state NMR studies in several solid amine sorbents, but the assignments are complicated because the bicarbonate species isotropic chemical shift is in the same region where ^{13}C signals of carbamate and carbamic acid are found (165-160 ppm). Hahn et al. observed a ^{13}C CPMAS solid-state NMR resonance at 162.4 ppm and assigned the peak to bicarbonate for a tetraethylenepentamine/silica composite that was doused with water and exposed to $^{13}CO_2$.[6] Moore et al. showed that multiple chemical entities associated with amine-CO_2 species formed when hyperbranched aminosilica was exposed to $^{13}CO_2$; furthermore, evidence for bicarbonate was supported by the lack of splitting of the low-field ^{13}C NMR from ^{14}N dipolar coupling and by bimodal T_2 relaxation times.[7] Recently, Chen et al. studied the amine-CO_2 species formed on primary amine grafted silica materials. Furthermore, they revealed through $^{13}C\{^{15}N\}$ and $^{15}N\{^{13}C\}$ rotational echo double-resonance (REDOR) NMR that a fraction of the ^{13}C intensity at the resonance frequency corresponding to both bicarbonate and carbamate chemical shifts (~165 ppm) was absent under REDOR dephasing, while the $^{15}N\{^{13}C\}$ REDOR behaved as expected for a ^{15}N-^{13}C

spin pair.[8] This result implied that some of the ^{13}C intensity was missing because it was not in dipolar contact with nitrogen — a result consistent with bicarbonate formation.

In this chapter, to provide clearer evidence for bicarbonate formation on amine sorbents, CO_2 capture on tertiary amine [N,N-dimethyl-3-aminopropyltrimethoxysilane (DMAPS)] supported SBA-15 sorbents were studied under dry and humid conditions (Figure 2.1). Tertiary amine grafted sorbents are rarely studied in this application, but they were chosen here because it is known that tertiary amines do not form alkylammonium carbamates, so such adsorbed species can be removed from consideration when making assignments of adsorbed CO_2. To observe effects of amine loading under both dry and humid CO_2 conditions, samples with a high loading (HLDMAPS-SBA) and a medium loading (DMAPS-SBA) of supported tertiary amine were synthesized. Differences in amine loading can affect the hydrophilicity of the sorbent and could also lead to different CO_2 species adsorbed.[9] Dry and humid CO_2 uptakes and amine efficiencies of the supported tertiary amines were measured using fixed bed breakthrough experiments. NMR and *in situ* FTIR spectroscopy studies were used to identify chemisorbed species under dry and humid conditions.

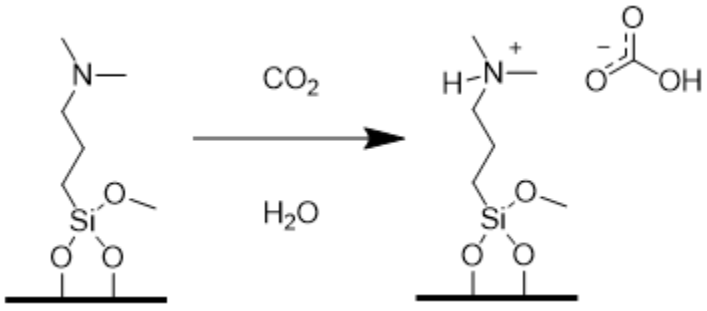

Figure 2.1. DMAPS and its hypothesized adsorbed bicarbonate species using humid CO_2.

2.2 Experiments

2.2.1 Materials

Dimethylaminopropyltrimethoxysilane (DMAPS) and hydrochloric acid (36 wt%) were purchased from Alfa Aesar. Toluene (99.5%), pluronic-123 (P123), and tetraethylorthosilicate (TEOS, 98%) were obtained from Sigma-Aldrich. Hexanes (98.5%) was obtained from BDH. Ethanol (100%) was obtained from Koptec.

Pluronic P-123 (24.0 g) was dissolved in distilled water (636 mL) and concentrated HCl (120 mL) in a 2 L Erlenmeyer flask. The mixture was stirred for 3 h at room temperature. Tetraethyl orthosilicate (46.24 g) was added dropwise to the mixture. The mixture was then stirred continuously for 20 h at 40 °C. The stir bar was removed, and the mixture temperature was maintained at 100 °C for 24 h. The mixture was then quenched and filtered with copious amounts of distilled water. The resulting white powder was then dried in an oven overnight at 75 °C. Afterwards, the sample was put into a calcination oven. To calcine the white powder, it was heated to 200 °C at 1.2 °C min^{-1}, held at that temperature for 2 h, heated to 550 °C at 1.2 °C min^{-1}, held at that temperature for 6 h, and finally cooled to room temperature.

To graft DMAPS on to SBA-15, SBA-15 was dried on a Schlenk line at 110 °C under a pressure of <20 mTorr overnight. Afterwards, SBA-15 was added to a flask with toluene. DMAPS was then added to the mixture and was stirred at 85 °C for 24 h. The following product was washed using copious amounts of toluene, hexane, and ethanol. Next, the sample was dried on a Schlenk line at 110 °C and under a pressure of <20mTorr overnight.

2.2.2 Materials Characterization

Nitrogen physisorption was performed using a Micromeritics Tristar II 3020 instrument at -196 ℃. Samples were activated under vacuum at 110 ℃ for 12 h. Surface areas were calculated by the Brunauer–Emmett–Teller (BET) method (P/P_o range used to calculate BET surface areas was $0 - 0.3$), and the pore volumes were calculated based on the total amount of N_2 adsorbed at $P/P_o=0.95$.[10] Amine loadings were based on measurements on a Netzch STA409PG TGA. The organic content was estimated from mass loss between 120 and 900 ℃ under nitrogen diluted air flow.

2.2.3 CO_2 and H_2O Adsorption Measurements

Dry CO_2 uptake measurements were performed by thermogravimetric analysis (TGA) with a TA Instruments Q500 analyzer. Each sample was pretreated at 110 °C for 3 h under He flow and then cooled to 30 ℃. The gas flow was then switched to 1% CO_2/He for 12 h. The CO_2 capacities of the samples were calculated by the weight change between the activated sample and the sample after exposure to 1% CO_2/He for 12 h.

Humid and dry CO_2 capacities were obtained by fixed bed breakthrough experiments. A 6.35 mm x 3.86 mm (outer diameter x inner diameter) stainless steel tube was used as the fixed bed and glass wool was used to support the sample. A schematic of the apparatus is seen in Appendix A (Figure A.1). The outlet gas was analyzed using a Li-COR Li-840A CO_2/H_2O IR gas analyzer. All runs were conducted at 1 atm and used a CO_2 concentration of 1% CO_2/He. A typical run used 300-500 mg of pelletized sample at a size of 53-150 μm. Flow rates of all gases were held constant at 50 mL/min. For both dry and humid experiments, samples were pretreated by flowing He at 110 ℃ until the outlet flow

of CO_2 and H_2O was less than $3*10^{-4}$ mL/min and $5*10^{-3}$ mL/min respectively. Afterwards the temperature of the bed was reduced to 30 °C for uptake measurements. For dry experiments, 1% CO_2/He was then introduced to the bed. For humid experiments, a humid He stream (P_{H2O} = 21 mbar) was first introduced into the bed until the outlet stream concentration matched the inlet stream concentration of H_2O. Humidity was generated by flowing gases through a sparger containing deionized H_2O at 18 °C. Once the bed was saturated with H_2O, a humid CO_2 stream was introduced to the bed. The adsorption experiments ended once the outlet stream concentration of CO_2 matched the inlet stream concentration of CO_2. For both dry and humid experiments, the CO_2 was desorbed from the bed by flowing dry helium through the bed at a temperature of 110 °C. Desorption experiments ended once the outlet flow of CO_2 and H_2O was less than $3*10^{-4}$ mL/min and $5*10^{-3}$ mL/min respectively.

The CO_2 adsorption capacities of the sorbents were calculated by evaluating the area confined between the CO_2 breakthrough curve for a bed containing the sorbent and the CO_2 breakthrough curve for a bed containing glass wool. The CO_2 desorption capacities were calculated by evaluating the area under the CO_2 desorption curve. Dead-time was also accounted for in desorption measurements.

A Hiden IGASorp was used to measure water vapor isotherms. The sorbents were pretreated at 110 °C for 3 h under nitrogen flow and cooled to 30 °C. Varying partial pressures of water vapor were then introduced in nitrogen flow. H_2O capacities of the samples were calculated by the weight change between the activated sample and the sample after exposure to varying partial pressures of water vapor.

2.2.4 In Situ FTIR spectroscopy

A Harrick High Temperature Transmission Cell with CaF_2 windows was used for *in situ* IR spectroscopy experiments. Each sample was pressed into a self-supported wafer and loaded into the IR cell. The spectrometer used was a Thermo Nicolet iS10 with a mercury cadmium telluride (MCT) detector. Flow rates of all gases were held constant at 100 mL/min. The sample was activated at 110 °C for 3 h under helium flow. Afterwards, the sample was cooled to 30 °C, and a background spectrum was collected. For dry experiments, a 1% CO_2/He mixture was then introduced into the cell for 30 min. For humid experiments, after activation, humid helium was introduced into the cell for 1 h, and a background spectrum was collected. Next, humid CO_2 was introduced into the cell for 30 min. To eliminate water vapor peaks for humid CO_2 adsorption experiments, a background containing water vapor and helium was subtracted from the results. After each experiment, the wafer was cut with a circular stamp (6.35 mm in diameter) and was weighed to determine its density. All spectra were normalized by the density of the wafer. Each spectrum was collected with 64 scans at a resolution of 4 cm^{-1}.

2.2.5 Solid State NMR Spectroscopy

The samples were activated at 105 °C under vacuum at 40 mTorr for 12 h, then cooled down to room temperature. For dry experiments, the sample was transferred to a glove bag under continuous nitrogen flow and packed in a zirconia rotor for solid-state NMR. The rotor was placed in a glass tube that was subsequently connected to a gas manifold. The manifold was then evacuated to 40 mTorr and subsequently loaded with 1 atm of $^{13}CO_2$ (Sigma-Aldrich, 99%) for 20 h. For wet experiments, 80 mg deionized water

was added to hydrate 80 mg of sample—enough to cause the solid to clump but less than the amount needed to create a slurry. The damp solid was then packed in a zirconia rotor. The loading of $^{13}CO_2$ followed, using the same procedure that was used for the dry experiment.

$^{13}C\{^{1}H\}$ static Hahn spin-echo experiments with ^{1}H decoupling were performed using a 6.93 T magnet with a 5 mm HXY Chemagnetics MAS NMR probe at a ^{13}C resonance frequency of 74.18 MHz, and ^{1}H frequency of 294.97 MHz. The following parameters were used for the spin-echo pulse sequence: $\pi/2$ pulse length for ^{13}C of 5.5 µs, τ echo delay time (between first and second pulses) of 200 µs, ^{1}H decoupling strength of 50 kHz, TPPM phase cycling during signal acquisition, number of scans 2828, and a recycle delay of 10 s.

2.3 Results and Discussion

2.3.1 Materials Characterization

Nitrogen adsorption-desorption isotherms for the sorbents are displayed in Figure 2.2. Mesoporosity in all materials was confirmed by the presence of a hysteresis loop in each of the adsorption-desorption isotherms. BET surface areas, pore volumes, and amine loadings determined by TGA are shown in Table 2.1. The surface areas and pore volumes of the sorbents decreased with increasing amine loading, as expected.

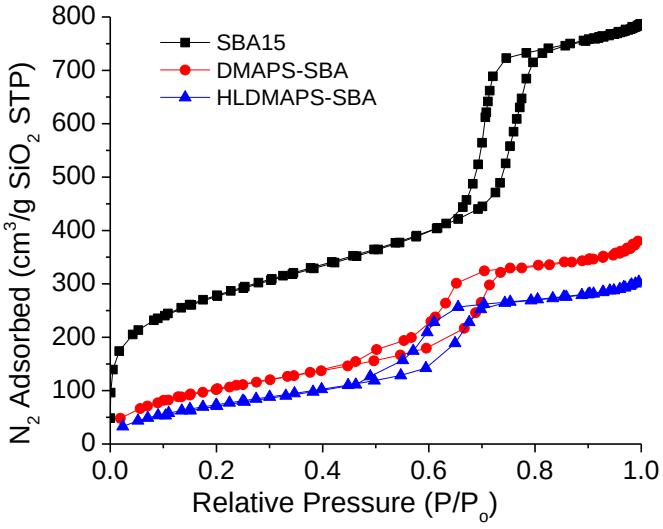

Figure 2.2. Nitrogen physisorption isotherms for SBA-15, DMAPS-SBA, and HLDMAPS-SBA.

Table 2.1. Textural and physical properties of sorbents.

Materials	BET Surface Area (m^2/g_{SiO2})	Volume of Pore (cm^3/g_{SiO2})	Estimated Amine Loading ($mmol_N/g$)
SBA-15	961	1.19	-
DMAPS-SBA	386	0.55	1.9
HLDMAPS-SBA	289	0.45	2.5

FTIR spectra of the sorbents following activation at 110 °C under He flow for 3 h are shown in Figure 2.3. All spectra were recorded at a cell temperature of 30 °C. A peak at 3741 cm^{-1} was observed in the IR spectrum of SBA-15 and is attributed to the OH

stretching vibration of free silanol groups.[11,12] Peaks at 1977 cm^{-1} and 1875 cm^{-1} are overtones of Si-O vibrational modes and were seen in all spectra.[11] A water deformation peak at 1648 cm^{-1} was present in all spectra even after activation, indicating that a residual amount of water remained on all sorbents.[13] In addition, a broad peak between 3700-2500 cm^{-1} indicated hydrogen bonding of silanol groups and water molecules on all sorbents.[13] The peak of free silanol stretching modes was absent in the spectra of DMAPS-SBA and HLDMAPS-SBA, indicating that the silanols had reacted with the aminosilanes or were engaged in hydrogen bonds. Peaks associated with CH_3 and CH_2 stretching modes were seen in the spectra of tertiary amine sorbents in the 3000-2800 cm^{-1} region.[5,11,14] A moderately sharp peak containing contributions from asymmetric CH_3 deformations and CH_2 deformations was observed at 1467 cm^{-1}. Symmetric CH_3 deformations gave rise to peaks at 1443 cm^{-1} and 1411 cm^{-1}, while peaks at 1378 cm^{-1}, 1345 cm^{-1}, and 1321 cm^{-1} are attributed to CH_2 wagging vibrations.[5,14,15]

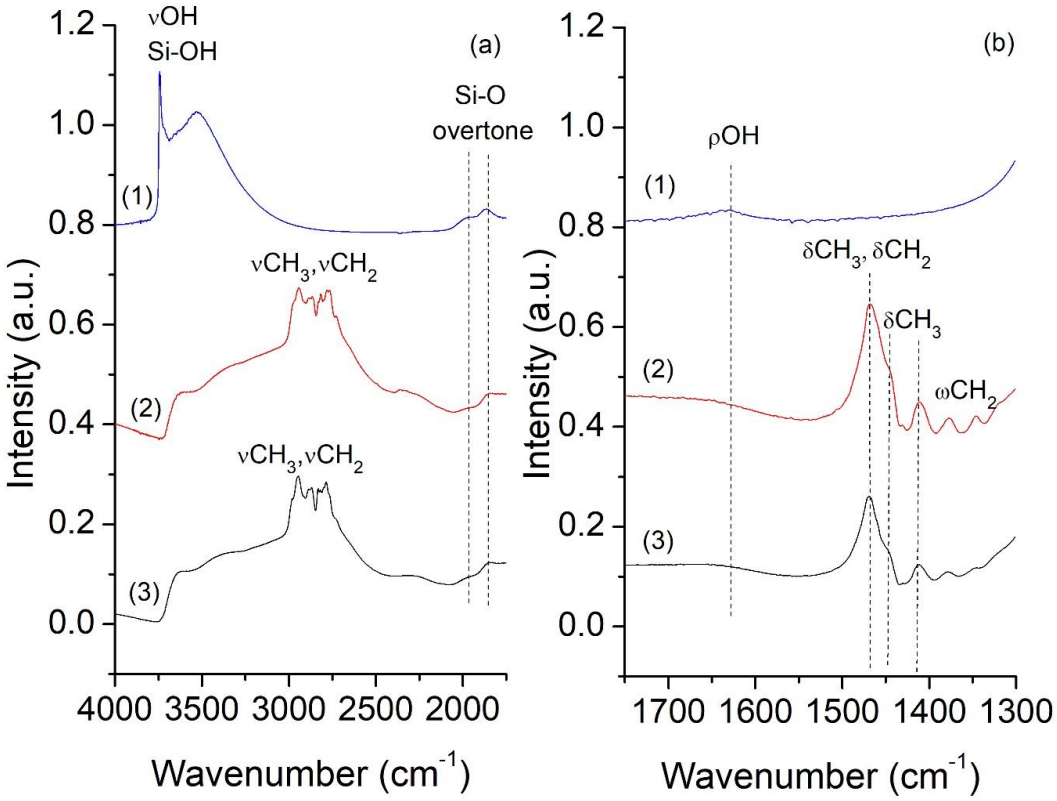

Figure 2.3. FTIR spectra of activated sorbents: (1) SBA-15 (2) HLDMAPS-SBA (3) DMAPS-SBA from (a) 4000-1800 wavenumbers and (b) 1800-1300 wavenumbers.

2.3.2 CO_2 and H_2O Adsorption

The CO_2 capacities of the sorbents were measured using a 1% CO_2/He gas mixture under dry and humid conditions at 30 °C. Each humid run was conducted at 49% relative humidity (RH) or P_{H2O} = 21 mbar. Dry CO_2 capacities were measured using both thermal gravimetric analysis and fixed bed breakthrough measurements. Both methods resulted in the same CO_2 capacity for each adsorbent. For all fixed bed measurements, both the adsorption and desorption CO_2 capacities were measured. There was no discrepancy of CO_2 adsorption and desorption under dry conditions. However, the CO_2 adsorption capacities were consistently higher than the CO_2 desorption capacities for each adsorbent

under humid conditions for all sorbents studied. To determine if the discrepancy between adsorption and desorption was an artifact, each humid fixed bed run was conducted two times in series using the same sample (Table A.1). It is expected that the CO_2 adsorption capacity would decrease after each adsorption/desorption cycle if CO_2 was not fully desorbing off the sorbents. However, from these cycling experiments, it was observed that the adsorption and desorption capacity remained the same for each cycle on all sorbents. The discrepancy between adsorption and desorption capacity was thus not likely due to incomplete CO_2 desorption and is likely an instrumental error.

For both humid and dry conditions, the tertiary amine grafted sorbents exhibited poor CO_2 capacities compared to primary and secondary amine grafted sorbents (Table 2.2).[5] However, all sorbents showed an increase in CO_2 capacity in the presence of humidity when compared to their dry CO_2 capacities. DMAPS-SBA was observed to have the highest CO_2 capacity under humid conditions. The increase in CO_2 capacity in the presence of humidity for the tertiary amine sorbents is likely due to formation of ammonium bicarbonates, which will be explored further below.

Table 2.2. Dry and humid CO_2 capacities.

Adsorbent	Amine Loading [$mmol_N/g_]$	Dry CO_2 Uptake [$mmol_{CO2}/g$]	Dry Amine Efficiency [%]	Humid CO_2 Uptake (Adsorption) [$mmol_N/g$]	Humid CO_2 Uptake (Desorption) [$mmol_N/g$]	Humid Amine Efficiency (Desorption) [%]
DMAPS-SBA	1.9	0.01	0.5	0.10	0.04	2
HLDMAPS-SBA	2.5	0.01	0.4	0.06	0.02	1

For ammonium bicarbonates to form on amine sorbents, both H_2O and CO_2 must be present. However, the amount of water adsorbed on each of the sorbents is expected to vary based on their hydrophilicity at fixed relative humidities and temperatures. The varying amounts of water adsorbed on the surface could affect the concentration of ammonium bicarbonates that are formed. To this end, a water adsorption isotherm was measured at 30 °C for all sorbents (Figure 2.4). The bare silica support had the highest uptake of water. Water adsorption decreased with the addition of tertiary amines onto the sorbent.[9] The low CO_2 capacities for DMAPS-SBA and HLDMAPS-SBA under humid conditions could be due, in part, to their low water capacities. If the amount of adsorbed water is too low, it is possible that ammonium bicarbonate formation may not occur to a measurable extent. Even though HLDMAPS-SBA has more tertiary amine sites for bicarbonates to form, HLDMAPS-SBA has a lower CO_2 capacity under humid conditions than DMAPS-SBA. This may be due to HLDMAPS-SBA having a lower affinity for water than DMAPS-SBA (Table 2.3).

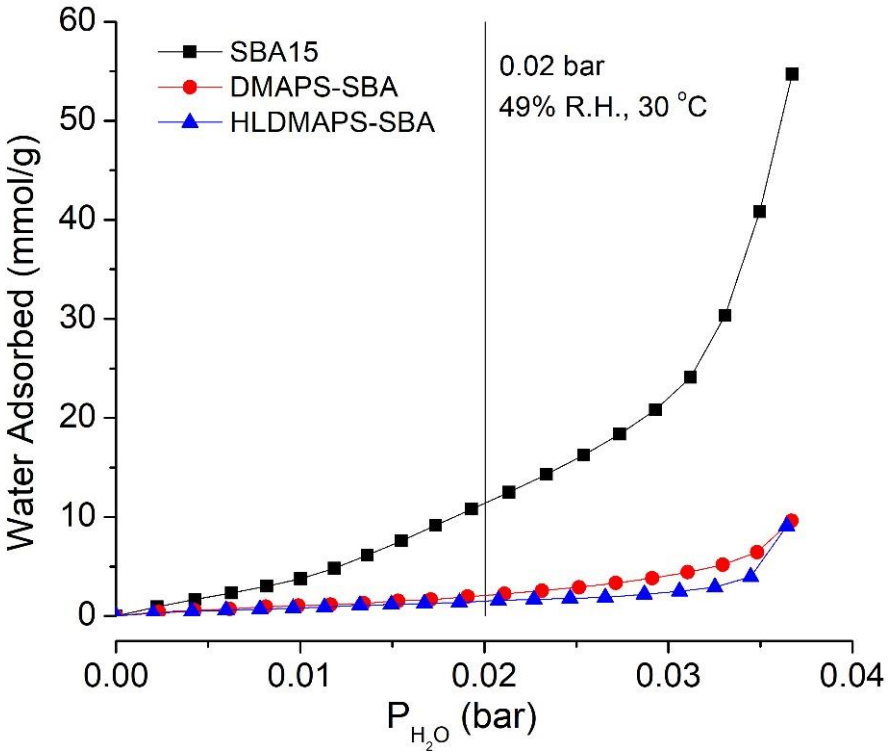

Figure 2.4 Water adsorption isotherm of the sorbents.

Table 2.3. Water adsorbed at P_{H2O} = 21 mbar and 30 °C.

	SBA-15	DMAPS-SBA	HLDMAPS-SBA
Water Adsorbed (mmol/g)	11.4	3.9	1.5

2.3.3 FTIR spectra of Adsorbed H_2O

The effects of water on the sorbents were probed using *in situ* FTIR spectroscopy. After activation for 3 h at 110 °C, a humid He stream (P_{H2O} = 21 mbar) at 30 °C was

introduced into the IR cell. Peaks in the 1800-1300 cm^{-1} region arose in the presence of humid He for all sorbents (Figure 2.5). The water adsorption spectra for all sorbents showed a peak at 1648 cm^{-1} attributed to the OH deformation vibrations of physisorbed H_2O.[13] A broad peak between 3500-3000 cm^{-1} associated with the OH stretching vibrations of H_2O and hydrogen bonded silanols also appeared (Figure A.4, Figure A.5, and Figure A.6). Additionally, the spectra of DMAPS-SBA and HLDMAPS-SBA showed a sharp peak at 1488 cm^{-1} and multiple peaks centered around 1388 cm^{-1}. The peak at 1488 cm^{-1} may be due to a NH deformation of a protonated tertiary amine, or it could originate from a blueshift of the CH_3 deformation in the presence of water. Peaks associated with NH stretching vibrations of a protonated tertiary amine were observed between 2500-2000 cm^{-1} (Figure A.4 and Figure A.5).[14] Multiple peaks centered around 1388 cm^{-1} are postulated to be due to perturbations of multiple CH_3 and CH_2 deformation and wagging modes in the presence of water. A decrease of the intensities of the methyl and methylene stretching bands of the supported tertiary amines between 3000-2800 cm^{-1} was also observed in the presence of water (Figure A.4, Figure A.5). Water is known to induce shifts in peak intensity and position of methyl and methylene vibrational modes in polymers and alkyl ammonium cations.[16–20] Foo et al. conducted an *in situ* IR study on a tertiary amine sorbent under nominally dry CO_2 flow and found similar peaks to those shown in Figure 2.5.[5] Based on the experiments shown here, it is likely that the peaks in the region of 1800-1300 cm^{-1} that are seen in that study are a combination of (i) changes of CH_2 and CH_3 deformation modes by water, (ii) a NH deformation mode of a protonated amine, and/or (iii) modes of bicarbonates.

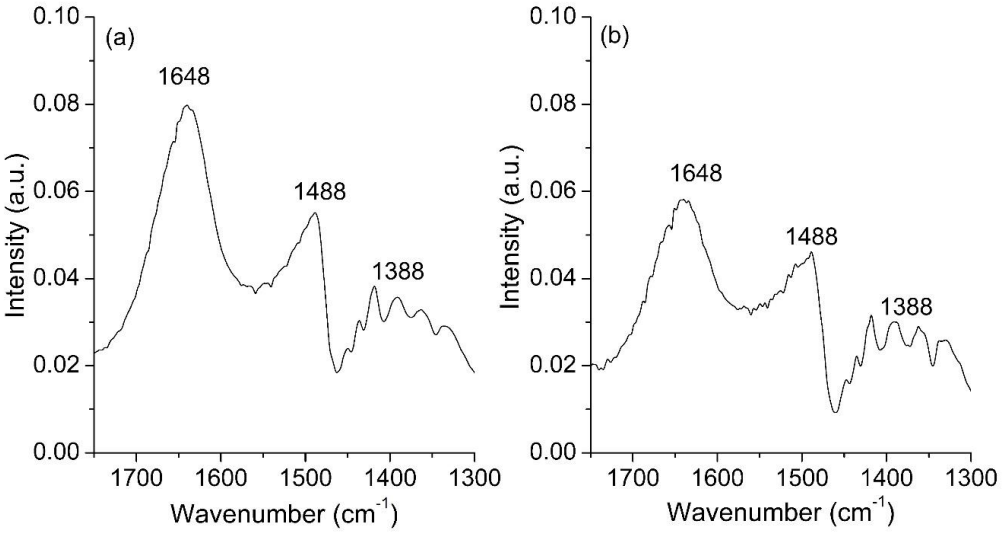

Figure 2.5. FTIR spectra of (a) DMAPS-SBA and (b) HLDMAPS-SBA after 2 h of humid He exposure with the activated sample as the background.

2.3.4 FTIR spectra of Adsorbed CO_2

To probe the structure of chemisorbed CO_2 species on the tertiary amine sorbents, *in situ* FTIR spectroscopy was conducted under humid and dry CO_2 flow. Peaks were observed in the 1800-1300 cm^{-1} region under dry conditions for the tertiary amine sorbents (Figure A.10 and Figure A.11). Using a mass spectrometer, it was revealed that the amount of water in the CO_2-in-helium gas cylinder was approximately 30 ppm. The peaks observed in the 1800-1300 cm^{-1} region for the tertiary amine sorbents under dry conditions could be a result of adsorbed water and/or bicarbonate formation. Owing to the residual water found in the CO_2 cylinder and the tertiary amine sorbents, after activation, ammonium bicarbonate formation on the tertiary amine sorbents cannot be ruled out for the nominally dry CO_2 runs.[5]

After humid CO_2 was introduced into the IR cell, additional peaks arose for the two tertiary amine sorbents in the 1800-1300 cm^{-1} region (Figure 2.6). A broad peak between 2500-2000 cm^{-1} was also observed and is associated with the NH stretch of a tertiary ammonium ion (Figure A.7 and Figure A.8).[14,21] The peak at 1616 cm^{-1} is attributed to the asymmetric COO^- stretch of a bicarbonate ion, and the peak at 1358 cm^{-1} is attributed to the symmetric COO^- stretch of a bicarbonate ion.[22–24] It should be noted that the peaks were more intense in the 1800-1300 cm^{-1} region for the DMAPS-SBA spectrum when compared to the HLDMAPS-SBA spectrum. Furthermore, this observation indicates that more bicarbonates formed on the sample with the lower amine loading, likely due to HLDMAPS-SBA having less affinity for water. These spectra confirm the existence of ammonium bicarbonate species on solid supported tertiary amines. However, the low IR peak intensities of bicarbonates combined with the low CO_2 capacity for both HLDMAPS-SBA and DMAPS-SBA suggest that bicarbonate formation is not highly favored for tertiary amine containing sorbents even in the presence of humid CO_2.

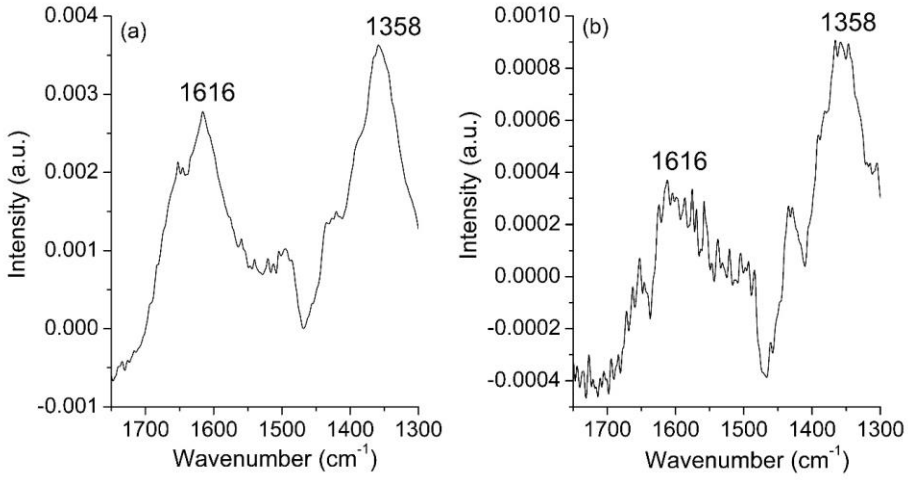

Figure 2.6. FTIR spectra of (a) DMAPS-SBA and (b) HLDMAPS-SBA after humid 1% CO_2 exposure with the sample presaturated with water as the background.

2.3.5 Solid-state NMR Spectroscopy

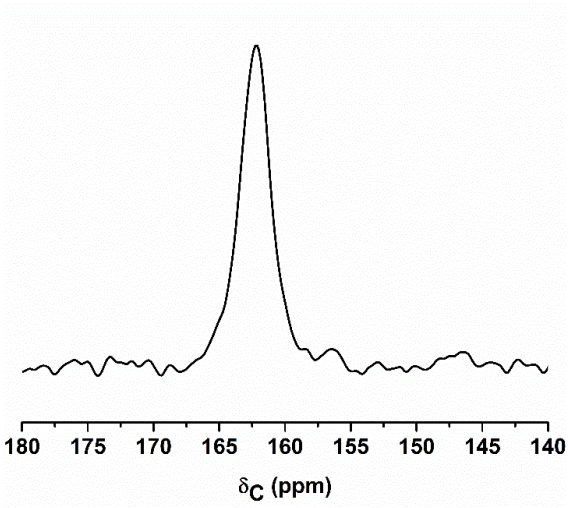

Figure 2.7. $^{13}C\{^{1}H\}$ static spin-echo NMR spectrum of $^{13}CO_2$ exposed DMAPS-SBA, doused with water prior to CO_2 exposure.

Solid-state NMR can be used as a complimentary tool to determine the products of CO_2 chemisorption by DMAPS-SBA and SBA-15. As expected, there was no evidence of chemisorbed species in either dry or humid conditions on bare SBA-15. No evidence of chemisorbed or physisorbed CO_2 was also observed on DMAPS-SBA under dry conditions. Figure 2.7 shows the $^{13}C\{^{1}H\}$ static NMR spectrum that was acquired using the Hahn spin-echo pulse sequence on a sample of DMAPS-SBA that was doused with water and then loaded with $^{13}CO_2$. A ^{13}C resonance at 162.2 ppm was found only for $^{13}CO_2$ exposed DMAPS-SBA that was doused with water. It should be noted that many attempts were made to find amine-CO_2 species on DMAPS-SBA using H_2O-saturated $^{13}CO_2$ gas, and "lightly-hydrated" DMAPS-SBA samples. Ultimately, CO_2 adsorption was only detectable by CPMAS NMR on DMAPS-SBA samples that were near-saturated with water. This resonance is assigned to bicarbonate; mechanistically, the only chemisorbed product expected for tertiary amine sorbents is bicarbonate.[6] This resonance is shifted

slightly to lower frequency when compared to the resonance that has been previously observed for bicarbonate formation on $^{13}CO_2$-reacted primary amine grafted silica; however, this is unsurprising because the resonance for bicarbonate is highly dependent upon pH, ranging from 160 to 170 ppm.[25] The peak width (full-width half-maximum) of the resonance is 3 ppm (225 Hz), which is narrower than typically found in static solid-state NMR experiments, even with ^{1}H decoupling.[5,7,8] The unusually narrow lineshape suggests that the species experiences some form of motional averaging. These results confirm that formation of bicarbonate needs the presence of water, and when water is not in abundance, DMAPS-SBA shows little or no evidence for chemisorption of CO_2.

2.3.6 Conclusions

This fundamental study explored the behavior of solid supported tertiary amine sorbents under dry and humid CO_2 capture conditions. Bicarbonate formation on tertiary amine sorbents in the presence of humid CO_2 was confirmed using *in situ* FTIR and ^{13}C NMR spectroscopy. The tertiary amine sorbents showed a dramatic increase in CO_2 capacity when water was present in the gas mixture, as water is necessary for bicarbonate formation. However, the CO_2 capacity of these sorbents were poor, even in the presence of humidity. This result implies that bicarbonate formation over tertiary amine sorbents are less practically useful for CO_2 capture than carbamate formation over primary and secondary amine sorbents. Using *in situ* IR spectroscopy and under humid CO_2 flow, it was seen that the peaks associated with bicarbonates were more intense for the medium loading tertiary amine sample when compared to that of the high loading tertiary amine sample, indicating that more bicarbonates formed on the medium amine loading sample. This is proposed to be due to the more optimal balance of water and CO_2 loading on the surface

of the medium loading sorbents, with the high loading amine sorbent having more unfavorable hydrophobicity. These new insights show that bicarbonate formation may not be favored for tertiary amines at flue gas capture or direct air capture conditions.

It should also be noted that water affects the spectroscopic region where chemisorbed CO_2 appears, 1800-1300 cm^{-1}, for supported amine sorbents. These peaks are sometimes falsely associated with vibrations of amine-CO_2 species. Peaks associated with water and perturbations of aminosilane modes due to water were even observed under purportedly dry conditions due to residual water found both in the gas cylinder and on the sorbent after activation. Careful consideration and appropriate control/background spectra must be obtained when conducting IR studies in the presence of water, and it should be recognized that even under ostensibly "dry conditions", water often remains on the surface of amine sorbents.

2.4 References

(1) Kortunov, P. V.; Siskin, M.; Baugh, L. S.; Calabro, D. C. *In Situ* Nuclear Magnetic Resonance Mechanistic Studies of Carbon Dioxide Reactions with Liquid Amines in Aqueous Systems: New Insights on Carbon Capture Reaction Pathways. *Energy & Fuels* **2015**, *29*, 5919–5939.

(2) Zhang, R.; Liang, Z.; Liu, H.; Rongwong, W.; Luo, X.; Idem, R.; Yang, Q. Study of Formation of Bicarbonate Ions in CO_2-Loaded Aqueous Single 1DMA2P and MDEA Tertiary Amines and Blended MEA–1DMA2P and MEA–MDEA Amines for Low Heat of Regeneration. *Ind. Eng. Chem. Res.* **2016**, *55*, 3710–3717.

(3) Wilfong, W. C.; Srikanth, C. S.; Chuang, S. S. C. In Situ ATR and DRIFTS Studies of the Nature of Adsorbed CO_2 on Tetraethylenepentamine Films. *ACS Appl. Mater. Interfaces* **2014**, *6*, 13617–13626.

(4) Didas, S. A.; Sakwa-Novak, M. A.; Foo, G. S.; Sievers, C.; Jones, C. W. Effect of Amine Surface Coverage on the Co-Adsorption of CO_2 and Water: Spectral Deconvolution of Adsorbed Species. *J. Phys. Chem. Lett.* **2014**, *5*, 4194–4200.

(5) Foo, G. S.; Lee, J. J.; Chen, C.-H.; Hayes, S. E.; Sievers, C.; Jones, C. W. Elucidation of Surface Species through in Situ FTIR Spectroscopy of Carbon Dioxide Adsorption on Amine-Grafted SBA-15. *ChemSusChem* **2017**, *10*, 266–276.

(6) Hahn, M. W.; Steib, M.; Jentys, A.; Lercher, J. A. Mechanism and Kinetics of CO_2 Adsorption on Surface Bonded Amines. *J. Phys. Chem. C* **2015**, *119*, 4126–4135.

(7) Moore, J. K.; Sakwa-Novak, M. A.; Chaikittisilp, W.; Mehta, A. K.; Conradi, M. S.; Jones, C. W.; Hayes, S. E. Characterization of a Mixture of CO_2 Adsorption Products in Hyperbranched Aminosilica Adsorbents by ^{13}C Solid-State NMR. *Environ. Sci. Technol.* **2015**, *49*, 13684–13691.

(8) Chen, C.-H.; Shimon, D.; Lee, J. J.; Didas, S. A.; Mehta, A. K.; Sievers, C.; Jones, C. W.; Hayes, S. E. Spectroscopic Characterization of Adsorbed $^{13}CO_2$ on 3-Aminopropylsilyl-Modified SBA15 Mesoporous Silica. *Environ. Sci. Technol.* **2017**, *51*, 6553–6559.

(9) Didas, S. A.; Kulkarni, A. R.; Sholl, D. S.; Jones, C. W. Role of Amine Structure on Carbon Dioxide Adsorption from Ultradilute Gas Streams Such as Ambient Air. *ChemSusChem* **2012**, *5*, 2058–2064.

(10) Brunauer, S.; Emmett, P. H.; Teller, E. Adsorption of Gases in Multimolecular Layers. *J. Am. Chem. Soc.* **1938**, *60*, 309–319.

(11) Hiyoshi, N.; Yogo, K.; Yashima, T. Adsorption Characteristics of Carbon Dioxide on Organically Functionalized SBA-15. *Microporous Mesoporous Mater.* **2005**, *84*, 357–365.

(12) Benesi, H. A.; Jones, A. C. An Infrared Study of the Water-Silica Gel System. *J. Phys. Chem.* **1959**, *63*, 179–182.

(13) Asay, D. B.; Kim, S. H. Evolution of the Adsorbed Water Layer Structure on Silicon Oxide at Room Temperature. *J. Phys. Chem. B* **2005**, *109*, 16760–16763.

(14) Socrates, G. *Infrared and Raman Characteristic Group Frequencies*, Third.; John Wiley & Sons LTD, 2001.

(15) Colthup, N. B.; Daly, L. H.; Wiberley, S. E. *Introduction to Infrared and Raman Spectroscopy*, Third Edit.; Academic Press, 1990.

(16) Yanliang Gu; Tapas Kar; Scheiner, S. Fundamental Properties of the CH···O Interaction: Is It a True Hydrogen Bond? *J. Am. Chem. Soc.* **1999**, *121*, 9411–9422.

(17) Maeda, Y. IR Spectroscopic Study on the Hydration and the Phase Transition of Poly(Vinyl Methyl Ether) in Water. *Langmuir* **2001**, *17*, 1737–1742.

(18) Fan, Y. F.; Lively, R. P.; Labreche, Y.; Rezaei, F.; Koros, W. J.; Jones, C. W. Evaluation of CO_2 Adsorption Dynamics of Polymer/Silica Supported

Poly(Ethylenimine) Hollow Fiber Sorbents in Rapid Temperature Swing Adsorption. *Int. J. Greenh. Gas Control* **2014**, *21*, 61–71.

(19) Su, Y.; Wang, J.; Liu, H. Melt, Hydration, and Micellization of the PEO–PPO–PEO Block Copolymer Studied by FTIR Spectroscopy. *J. Colloid Interface Sci.* **2002**, *251*, 417–423.

(20) Stevens, J. J.; Anderson, S. J. An FTIR Study of Water Sorption on TMA- and TMPA-Montmorillonites. *Clays Clay Miner.* **1996**, *44*, 142–150.

(21) Yu, J.; Chuang, S. S. C. The Role of Water in CO_2 Capture by Amine. *Ind. Eng. Chem. Res.* **2017**, *56*, 6337–6347.

(22) Richner, G.; Puxty, G. Assessing the Chemical Speciation during CO_2 Absorption by Aqueous Amines Using in Situ FTIR. *Ind. Eng. Chem. Res.* **2012**, *51*, 14317–14324.

(23) Garand, E.; Wende, T.; Goebbert, D. J.; Bergmann, R.; Meijer, G.; Neumark, D. M.; Asmis, K. R. Infrared Spectroscopy of Hydrated Bicarbonate Anion Clusters: $HCO_3^-(H_2O)_{1-10}$. *J. Am. Chem. Soc.* **2010**, *132*, 849–856.

(24) Robinson, K.; McCluskey, A.; Attalla, M. I. An FTIR Spectroscopic Study on the Effect of Molecular Structural Variations on the CO_2 Absorption Characteristics of Heterocyclic Amines. *ChemphysChem* **2011**, *12*, 1088–1099.

(25) Moret, S.; Dyson, P. J.; Laurenczy, G. Direct, in Situ Determination of PH and Solute Concentrations in Formic Acid Dehydrogenation and CO_2 Hydrogenation in Pressurised Aqueous Solutions Using ^2H and ^2C NMR Spectroscopy. *Dalt. Trans.* **2013**, *42*, 4353.

CHAPTER 3. SILICA SUPPORTED STERICALLY HINDERED AMINES FOR CO_2 CAPTURE

Parts of this chapter are adapted from 'Lee, J. J.; Yoo, C.-J.; Chen, C.-H.; Hayes, S. E.; Sievers, C.; Jones, C. W. Silica Supported Sterically Hindered Amines for CO_2 Capture. *Langmuir* **2018**, *34*, 12279–12292' with permission of The American Chemical Society.

3.1 Background

Sterically hindered primary and secondary amines in aqueous solutions, hereafter referred to simply as "hindered amines", have been used for CO_2 absorption due to their high selectivity towards bicarbonate formation.[1–4] A hindered amine is defined as a primary or secondary amine with a secondary or tertiary α-carbon. The higher selectivity of bicarbonate formation of hindered amines is attributed in part due to poor carbamate stability, which originates from unfavorable steric interactions between the COO^- group and the methyl and methylene substituents on the α-carbon.[1,5,6] Due to the increase in bicarbonate formation with such structures, hindered amines have increased amine efficiency when compared to unhindered primary and secondary amines.[1] Moderately hindered amines (hindered secondary amines that have no more than one secondary α-carbon or hindered primary amines) are of specific interest due to bicarbonate formation at practical time scales. Moderately hindered amine solutions have slower CO_2 absorption rates than unhindered primary and secondary amine solutions but have faster CO_2 absorption rates compared to tertiary amines.[1,7] Severely hindered amine solutions

(hindered secondary amines that have a tertiary α-carbon) do not form carbamates and have poor absorption kinetics, as observed for tertiary amines.[1,7]

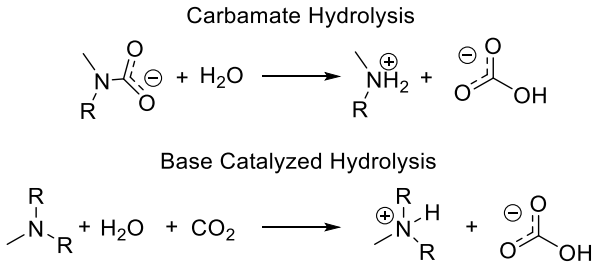

Figure 3.1. Proposed mechanisms of bicarbonate formation: carbamate hydrolysis[8] and base catalyzed hydrolysis.[9] R denotes a hydrogen atom or an alkyl group.

The causes of the differences between the kinetics of bicarbonate formation on various amines remain unclear. One hypothesis is that moderately hindered amines allow for faster formation of bicarbonates than tertiary and severely hindered amines due to a different mechanism of formation.[1,7] Furthermore, the fast formation of the bicarbonate species on moderately hindered amines is attributed to carbamate hydrolysis, whereas slow formation of bicarbonates on tertiary and severely hindered amines are attributed to base catalyzed hydrolysis (Figure 3.1). In the carbamate hydrolysis pathway, carbamates are initially formed, but due to their low stability on hindered amines, they are further hydrolyzed into bicarbonates. However, recent computational studies suggest that carbamate hydrolysis on unhindered and hindered amines are equally unlikely at relevant timescales due to the high activation barrier of the pathway and that it is more likely that all amines form bicarbonates through base catalyzed hydrolysis of CO_2.[10–14] Stowe and Hwang, using *ab initio* molecular dynamic simulations combined with metadynamics, suggested that differences in kinetics of bicarbonate formation between different amine

solutions, given the same base catalyzed hydrolysis mechanism, can be influenced by entropic factors.[15] Furthermore, the authors suggested that the faster kinetics of a hindered primary amine (2-amino-2-methyl-1-propanol) when compared to a tertiary amine (diethylethanolamine) could be attributed to the primary hindered amine's comparatively smaller entropic penalty associated with the rearrangement of water molecules near the amine to stabilize transition states of reaction intermediates.

While hindered amines have been widely studied in aqueous solution, as noted above, very little research has been conducted on solid supported analogues. Lee et al. studied the CO_2 adsorption performance on low molecular weight hindered alkanolamines impregnated on activated carbon.[16] However, likely due to amine leaching concerns, they did not study the effects of humidity on hindered amine sorbents. Zhao and Ho demonstrated that hindered amine membranes displayed enhanced CO_2/N selectivity and CO_2 permeability when compared to their unhindered counterparts at 110 °C and a feed pressure of 2 atm.[17,18] The Yogo research group recently studied supported tetraethylenepentamine (TEPA) with hindered functional groups on the terminal amines for CO_2 capture and observed improved regeneration compared to unfunctionalized TEPA.[19–21]

It has been previously suggested that unhindered amine adsorbents are poor at forming bicarbonates.[22,23] Due to the reduced ability of the carbon atom in CO_2 to form covalent bonds with the amine, supported hindered amines may help promote formation of ionically bonded bicarbonates, thus increasing theoretical amine efficiency, reducing diffusional limitations, and reducing energy requirements for regeneration. This study aims to better understand the effects of steric hindrance on the adsorption performance of

supported amines under dry and humid conditions. To this end, a moderately hindered primary amine, (3-amino-3-methylbutyl)triethoxysilane (AMBS); a moderately hindered secondary amine, (N-cyclohexylaminopropyl)trimethoxysilane (CHAPS); and a severely hindered secondary amine, (*tert*-butylaminopropyl)trimethoxysilane (TBAPS) were grafted onto a prototypical mesoporous silica SBA-15 support at similar loadings (Figure 3.2), and the CO_2 capacities under dry and humid conditions were evaluated for these materials. Mesoporous SBA-15 was chosen as a support due to its high surface area and uniform pores, as well as extensive literature of comparable sorbents with different amine structures. *In situ* IR spectroscopy was also utilized to identify chemisorbed CO_2 species formed under both dry and humid conditions. Supported amines with varying levels of steric hindrance were studied here to observe how different bulky α-carbon substituents affected the formation of adsorbed CO_2 species. It should be noted that bicarbonate formation in amine solutions is a strong function of CO_2 concentration. It is less likely for bicarbonates to form in amine solutions at low CO_2 concentrations (<1% CO_2).[2] Therefore, concentrations of CO_2 found in flue gas (10% CO_2) were used in this study.

Also, an important requirement associated with a viable CO_2 capture technology is finding a sorbent with a sufficiently long cyclic lifetime. Specifically, dilute CO_2 sources such as air and flue gas contain O_2 at concentrations of 21% and 3-10%, respectively, making it critical for the sorbent employed to be oxidatively stable under such conditions.[24–29] In addition, the sorbent must be able to withstand elevated temperatures used in the regeneration step of the temperature swing adsorption processes. To this end, the oxidative and thermal stabilities of each sorbent were also studied to help assess the potential lifetime of the sorbents.

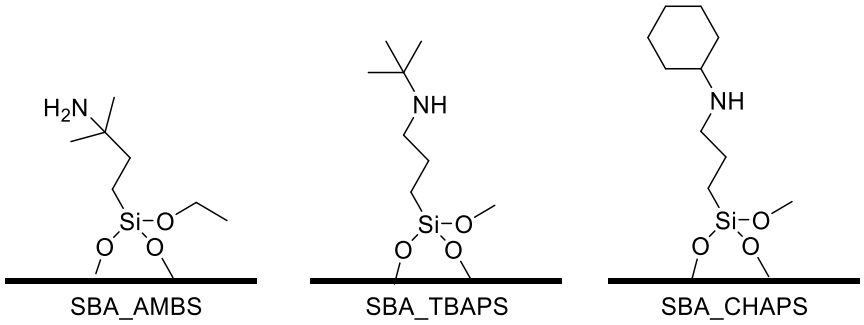

Figure 3.2. Hindered aminosilanes, (3-amino-3-methylbutyl)triethoxysilane (AMBS); (*tert*-butylaminopropyl)trimethoxysilane (TBAPS); and (N-cyclohexylaminopropyl)trimethoxysilane (CHAPS), grafted onto SBA-15.

3.2 Experiments

3.2.1 Materials

Hydrochloric acid (36 wt%) was purchased from Alfa Aesar. Toluene (99.5%), Pluronic P-123, tetraethylorthosilicate (TEOS, 98%), $^{13}CO_2$ (99%), and all materials used for the synthesis of (3-amino-3-methylbutyl)triethoxysilane and (E)-2-methyl-4-(triethoxysilyl)but-3-en-2-amine were obtained from Sigma-Aldrich. Hexanes (98.5%) was obtained from BDH. Ethanol (100%) was obtained from Koptec. The following gases were purchased from Airgas: ultra-high purity N_2 , ultra-zero air, ultra-high purity He, and 10% CO_2/He were purchased from Airgas. (N-cyclohexylaminopropyl)trimethoxysilane and (*tert*-butyl)aminopropyltrimethoxysilane were purchased from Gelest.

3.2.2 Materials Synthesis

SBA-15 synthesis is based on a previous procedure.[30] Pluronic P-123 (24.0 g) was dissolved in concentrated hydrochloric acid (120 mL) and distilled water (636 mL) in a 2 L Erlenmeyer flask. The solution was stirred for 3 h at room temperature. Tetraethyl

orthosilicate (46.24 g) was added dropwise to the solution. The mixture was then stirred continuously for 20 h at 40 °C. The stir bar was removed, and the mixture temperature was maintained at 100 °C for 24 h. The mixture was then quenched and filtered with copious amounts of distilled water. The resulting white powder was then dried overnight in an oven at 75 °C. The white powder was calcined using the following procedure: ramp to 200 °C at 1.2 °C min^{-1}, hold at 200 °C for 2 h, ramp to 550 °C at 1.2 °C min^{-1}, hold at 550 °C for 6 h, and cool to room temperature.

The synthesis of (E)-2-methyl-4-(triethoxysilyl)but-3-en-2-amine and (3-amino-3-methylbutyl)triethoxysilane are based on a previous procedure.[31,32] A 100 mL flame-dried three-neck round-bottom flask equipped with a condenser was charged with 2 wt% Platinum(0)-1,3-divinyl-1,1,3,3-tetramethyldisiloxane complex (Pt-DVDS) in xylenes (3.43 mL, 0.3 mmol Pt, 1 mol% catalyst) and 0.6 mL (0.5 M) of triisobutyl base solution (0.103 g of 2,8,9-triisobutyl-2,5,8,9-tetraaza-1-phosphabicyclo[3.3.3]undecane in 0.6 mL of diethyl ether). The mixture was stirred at 60 °C for 10 min and then diluted with inhibitor-free anhydrous tetrahydrofuran (20 mL) at room temperature. The mixture temperature was cooled down to about -10 °C in an ice and brine bath. Triethoxysilane (5.54 mL, 30 mmol) was then added dropwise into the mixture, followed by stirring for 5 min. Next, 2-methyl-3-butyn-2-amine (2.5 mL, 23.75 mmol) was added dropwise into the mixture at -10 °C. The mixture was then stirred at room temperature overnight. Crude (E)-2-methyl-4-(triethoxysilyl)but-3-en-2-amine was concentrated by a rotary evaporator and was purified by distillation under reduced pressure (200 mtorr) at about 60 °C. ^{1}H NMR (400 MHz, $CDCl_3$): δ (ppm) 6.52 (d, J = 5.6 Hz, 1H) 6.47 (d, 1H), 3.82 (q, 6H), 1.23 (t,

9H), 1.19 (s, 6H). ^{13}C NMR (100 MHz, $CDCl_3$): δ (ppm) 162.21, 112.44, 58.41, 52.29, 29.73, 18.15.

Next, a 50 mL flame-dried round-bottom flask was charged with (E)-2-methyl-4-(triethoxysilyl)but-3-en-2-amine (2.5 g, 10 mmol), anhydrous ethanol (10 mL) and 5 wt% Pd/C (30 mg). The flask was purged under He for 15 min, followed by bubbling with hydrogen for additional 20 min. The flask was then pressurized with hydrogen using a two layered balloon and stirred at room temperature for 18 h. The mixture was filtered and washed with anhydrous ethanol several times. Crude (3-amino-3-methylbutyl)triethoxysilane was concentrated by a rotary evaporator, and subsequently purified by distillation under reduced pressure (200 mTorr) at about 60 ^{o}C. ^{1}H NMR (400 MHz, $CDCl_3$): δ (ppm) 3.84 (q, 6H) 1.45 (m, 2H), 1.25 (t, 9H), 1.08 (s, 6H), 0.64 (m, 2H). ^{13}C NMR (100 MHz, $CDCl_3$): δ (ppm) 58.40, 49.89, 37.66, 29.57, 18.31, 4.75.

Aminosilane grafted silica was prepared by first drying SBA-15 in a round bottom flask overnight on a Schlenk line at 100 ^{o}C and under vacuum (<20 mTorr). After drying, toluene was added to the round bottom flask, and the flask was capped with a rubber septum. The flask was purged with Ar for 30 min while the solution was stirred at 85 °C. Afterwards, silane was added to the solution and was stirred at 85 °C for 24 h. The following product was washed using copious amounts of toluene, hexane, and ethanol. Next, the sample was dried overnight on a Schlenk line at 110 ^{o}C and under vacuum (<20 mTorr).

3.2.3 Materials Characterization

Nitrogen physisorption was performed on a Micromeritics Tristar II instrument at -196 ℃. All samples were degassed at 110 ℃ for 12 h before the measurement. The resulting isotherms were used to obtain surface area and pore volume. The Brunauer–Emmett–Teller (BET) method was used to calculate surface area (P/P_o range used to calculate BET surface areas was $0 - 0.3$), pore size distributions were calculated from N_2 physisorption isotherms using the BdB-FHH method, and the pore volumes were determined by the total amount of nitrogen adsorbed at $P/P_o=0.95$.[33] Elemental analysis (Atlantic Microlabs, Norcross, GA) was used to determine amine loadings of the sorbents.

3.2.4 CO_2 and H_2O Adsorption Measurements

A Hiden IGASorp was used to measure water vapor isotherms. The sorbents were pretreated at 110 ℃ for 3 h under nitrogen flow and cooled to 30 °C. Varying partial pressures of water vapor were then introduced in nitrogen flow, followed by equilibration. H_2O capacities of the samples were calculated by the weight change between the activated sample and the sample after exposure to varying partial pressures of water vapor.

A TA Instruments Q500 thermogravimetric analyzer (TGA) was used to measure dry CO_2 capacity. About 10-15 mg of sample was used for each run. Each sample was activated in He flow at 110 ℃ for 3 h. The sample was then cooled to 30 ℃, and the gas was switched to 10% CO_2 in He for 3 h. Measurement of CO_2 capacity was based on the weight change between the activated sample and the sample after exposure to 10% CO_2 in He for 3 h.

Humid and dry CO_2 capacities were obtained by using a 6 mm x 4 mm (outer diameter x inner diameter) fritted glass fixed bed. A schematic of the apparatus can be seen in Appendix A.[23] The accuracy of the apparatus was verified by comparing dry CO_2 capacities calculated between the TGA and fixed bed of the hindered amine sorbents at 30 °C in 10% CO_2/He flow. The outlet gas was analyzed using an Omnistar GSD 320 mass spectrometer. All adsorption studies used a 10% CO_2/He mixture at 1 bar, and all flow rates used were held constant at 50 mL/min. A typical run used 100-200 mg of pelletized sample at a size of 53-150 μm. For both dry and humid experiments, samples were pretreated by flowing He at 110 ℃ for 3 h. Afterwards, the temperature of the bed was reduced to 30 °C. For dry experiments, 10% CO_2/He was then introduced to the bed. For humid experiments, a humid He stream (P_{H2O} = 21 mbar at 30 °C) was first introduced into the bed until the outlet stream concentration matched the inlet stream concentration of H_2O. Humidity was generated by flowing gases through a sparger containing DI H_2O at a controlled temperature of 18 °C. Once the bed was saturated with H_2O, a humid CO_2 stream was introduced to the bed. Desorption started once the outlet stream concentration of CO_2 reached 98% of the inlet stream concentration of CO_2. For both dry and humid experiments, the CO_2 was desorbed from the bed by flowing dry helium through the bed at a temperature of 110 ℃. Desorption ended after approximately 2 h. The psuedo-equilibrium CO_2 capacities measured were obtained from the breakthrough curves generated from adsorption. The dead-time of the fixed bed system was accounted for in all capacity measurements and was calculated based on the breakthrough curve of 10% CO_2/He through a bed filled with glass wool.

CO_2 adsorption isotherms and heats of adsorption for aminosilane grafted SBA-15 materials were measured by a combined calorimeter-volumetric adsorption apparatus, which consists of a gas dosing manifold and a Tian-Calvet Calorimeter (Sensys Evo DSC, Setaram).[34] Approximately 50 mg of pelletized sample (150-250 μm) was inserted in one side of a sample glass cell that has two prongs. Another side of the cell was left empty as a reference. This cell is connected to the dosing manifold and encased in an aluminum block that contains highly sensitive thermophiles. The samples were pretreated at 120 ℃ for 3 h under vacuum (<15 Pa) and then cooled down to 30 ℃. Two pressure transducers were connected to the reservoir and sample cell areas, which were maintained at 30 ℃ with heating tape. The amount of adsorbed CO_2 after dosing was calculated by mole balance using initial and final pressure values from the sample cell and reservoir sides. Heats of CO_2 adsorption were simultaneously recorded, while the dosed CO_2 was adsorbed by the adsorbents. When the rate of pressure change became lower than 0.01 Pa/min, the system was considered to have reached a pseudo-equilibrium state.

3.2.5 In Situ FTIR Spectroscopy

The spectrometer used for all IR experiments was a Thermo Nicolet iS10 with a mercury cadmium telluride **(**MCT) detector. A Harrick High Temperature Transmission Cell equipped with CaF_2 windows was used for *in situ* IR spectroscopy experiments. Self-supporting wafers were used for all *in situ* IR spectroscopy experiments. The wafers were made using a Carver Press and a pellet die set. Powders were pressed into wafers at ~2000 psig for 30 to 60 s. Gas flow rates were held constant at 50 mL/min at a pressure of 1 bar. Typically, each sample was activated at 110 ℃ for 3 h under helium flow and was cooled to 30 ℃ subsequently. For dry CO_2 adsorption experiments, a 10% CO_2/He mixture was

then introduced into the cell for 65 min, and spectra were recorded throughout this period using the activated sample as the background spectrum. For humid experiments, after activation, humid helium was introduced into the cell for 2 h, and a background spectrum was collected subsequently. Next, humid CO_2 was introduced into the cell for 65 min and spectra were recorded throughout this period using the presaturated sample as the background spectrum. CO_2 adsorption spectra from 0-5 min were collected with 1 scan at a resolution of 4 cm^{-1} every 5 sec, and spectra from 5-65 min were collected with 64 scans at a resolution of 4 cm^{-1} every 2 min. To eliminate water vapor peaks for humid CO_2 adsorption experiments, a background spectrum containing water vapor and helium was subtracted from the results. After each experiment, the wafer was cut with a circular stamp (6.35 mm in diameter) and was weighed to determine its mass. CO_2 adsorption spectra were normalized by the mass of the wafer (mg).

3.2.6 Solid State NMR Spectroscopy

Each sample was activated under vacuum (40 mTorr) at 105 ^oC for 4 h. The sample was then cooled to room temperature and was transferred to a continuous-flow nitrogen bag to be packed into a zirconia NMR rotor. The rotor (packed with the sample) was then placed into a glass vessel, connected to a gas manifold system, and loaded with $^{13}CO_2$ for 20 h. $^{13}C\{^1H\}$ cross-polarization magic-angle spinning (CPMAS) experiments were performed with a 4 mm HXY MAS Chemagnetics probe at Larmor frequencies, ^1H at 294.97 MHz, and ^{13}C at 74.17 MHz. The initial $\pi/2$ excitation pulse width was in the range of 4 - 4.25 μs, the contact time was 2 ms, and a recycle delay of 4s was used. The MAS spinning frequency was controlled at 5 kHz.

3.2.7 Degradation Studies

The same TGA used to measure dry CO_2 capacities was used for degradation experiments. Approximately 20-30 mg of sample was used on each run. The sample was first activated at 110 °C in He flow for 3 h. Afterwards, the temperature was increased to 135 °C, and the gas was switched to either ultra-zero grade air (21% O_2 in N_2) for oxidative degradation experiments or ultra-high purity grade N_2 for thermal degradation experiments. The samples were exposed to degradative conditions for 24 h. Afterwards, approximately 10-15 mg of the sample was taken out for elemental analysis and *ex-situ* transmission IR spectroscopy experiments. CO_2 adsorption experiments were then conducted on the same TGA for samples exposed to degradative conditions using the procedure listed above. The same IR spectrometer used for *in situ* IR spectroscopy experiments was used for the degradation studies. Wafers consisting of a mixture of 100 mg of KBr to 1 mg of sample were used. The wafers were activated in a vacuum oven at 100 °C for 3 h before spectra were recorded. Each spectrum was collected with 64 scans at a resolution of 4 cm^{-1} and was normalized by the Si-O vibrational mode at 1977 cm^{-1}.

3.3 Results and Discussion

3.3.1 Material Characterization

All materials were characterized by nitrogen physisorption and elemental analysis (Table 3.1). All functionalized materials have similar amine content ranging from 1.86 to 1.94 mmol N/g. Pore volumes and BET surface areas were reduced, as expected, upon functionalization. The presence of a hysteresis loop in the N_2 adsorption/desorption isotherms of all materials confirmed mesoporosity (Figure B.1).

Table 3.1. Physical and textural properties of materials.

Material	BET Surface Area (m^2/g_{SiO2})	Pore Volume (cm^3/g_{SiO2})	Amine Loading ($mmol_N/g$)
SBA15	961	1.19	–
SBA_AMBS	415	0.61	1.94
SBA_TBAPS	385	0.57	1.89
SBA_CHAPS	372	0.54	1.86

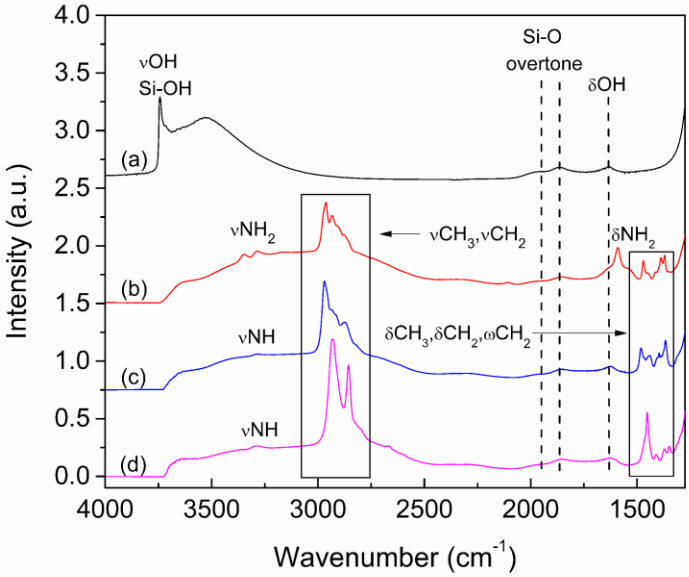

Figure 3.3. FTIR spectra of activated sorbents: (a) SBA-15, (b) SBA_AMBS, (c) SBA_TBAPS, (d) SBA_CHAPS. All IR spectra were taken under He flow at 30 °C.

The functionalization of the silica support was further confirmed using IR spectroscopy. FTIR spectra of the sorbents following activation at 110°C under He flow for 3 h are displayed in Figure 3.3. For the bare support SBA-15, the peak at 3741 cm^{-1} is attributed to the stretching vibration of free silanols.[23,35] The free silanol stretching mode was not observed in the activated spectra of the amine sorbents, indicating that aminosilanes reacted with the free silanol groups. It is also possible that some unreacted free silanol groups were engaged in hydrogen bonding interactions with the amines after grafting. The stretching vibration of such silanol groups would be observed as a redshifted and significantly broadened peak. The peaks at 1977 and 1866 cm^{-1} are assigned to Si-O vibrational modes for all sorbents.[23,35,36] A large broad peak between 3750 and 2500 cm^{-1}, indicated that all sorbents contained hydrogen bonding OH groups, which may include water. The peak at 1634 cm^{-1} is assigned to the bending mode of physisorbed water on all sorbents. Physisorbed water remained on the surface even after activation due to the hygroscopic nature of the silica support. For SBA_AMBS, peaks located at 3356 and 3283 cm^{-1} are assigned to NH_2 asymmetric and symmetric stretching modes and the peak found at 1597 cm^{-1} is associated with the NH_2 deformation mode.[37,38] The peak at 3285 cm^{-1} in the spectra for SBA_CHAPS and SBA_TBAPS is assigned to a NH stretching mode. For the functionalized sorbents, peaks between 3000 and 2750 cm^{-1} are attributed to stretching modes of CH_2/CH_3 groups.[37,38] Peaks between 1400 and 1300 cm^{-1} are attributed to wagging modes of CH_2 for all functionalized sorbents.[37,38] For SBA_AMBS and SBA_TBAPS, the CH_2 wagging modes overlapped with symmetric deformations of the branched CH_3 groups.[37] Peaks at 1500 and 1400 cm^{-1} are assigned to symmetric CH_2 and asymmetric CH_3 deformations for all functionalized sorbents.[37] For SBA_CHAPS, the

sharp peak at 1453 cm^{-1} is attributed to the methylene deformation of the cyclohexyl functional group.[37] The region below 1300 cm^{-1} was not evaluated due to strong Si-O vibrational modes.

3.3.2 CO_2 and H_2O Adsorption

Fixed bed measurements and thermogravimetric analysis were conducted on the hindered amine sorbents in 10% CO_2/He flow to determine their CO_2 capacities under dry and humid conditions (Figure 3.4). Under dry conditions, the SBA_AMBS sorbent had the highest CO_2 capacity, followed by SBA_CHAPS and SBA_TBAPS. All hindered amine sorbents exhibited increases in CO_2 capacity when comparing humid to dry conditions. Under humid conditions, SBA_TBAPS had the highest CO_2 capacity, followed by SBA_AMBS and SBA_CHAPS. To help compare the increases in CO_2 capacity when comparing humid to dry conditions, the efficiency enhancement was calculated (Table 3.2). The efficiency enhancement is defined as the amine efficiency of a sorbent at humid conditions divided by the amine efficiency under nominally dry conditions. The SBA_TBAPS sorbent had the largest efficiency enhancement out of all the hindered amine sorbents, indicating the largest increase in CO_2 capacity when comparing humid to dry conditions. The SBA_AMBS and SBA_CHAPS sorbents both adsorbed more than three times the amount of CO_2 under humid conditions compared to dry conditions. While increases in CO_2 capacity were seen in all sorbents with the addition of water, the maximum theoretical amine efficiency associated with ammonium bicarbonates of 1 CO_2/N was not observed under the conditions employed for any of the sorbents.

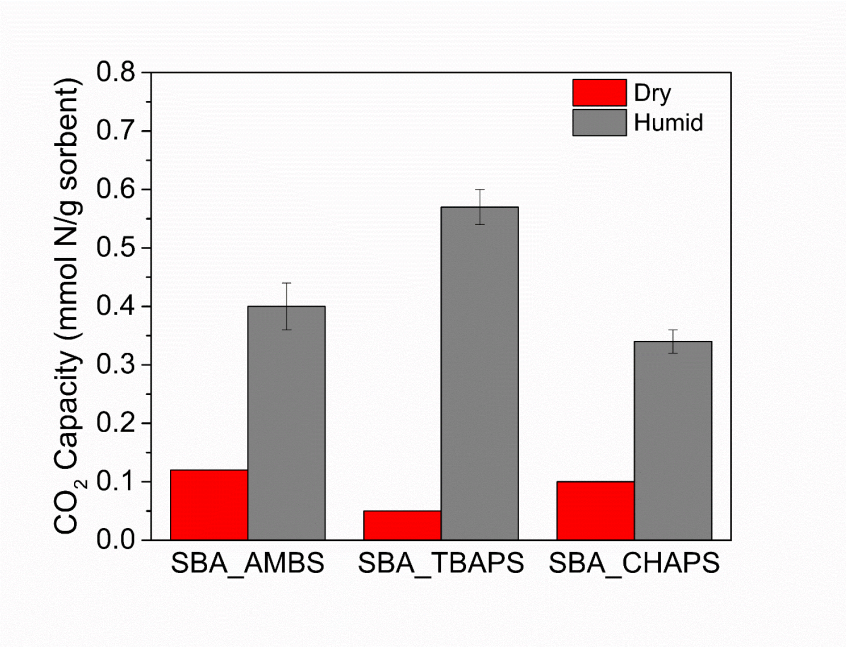

Figure 3.4. CO_2 adsorption capacities under dry and humid conditions (P_{H2O} = 21 mbar) under 10% CO_2 in He flow at 30 °C. Dry capacities were determined by thermogravimetric analysis, and humid capacities were determined using a fixed bed. The reported error in the humid runs is the standard deviation calculated from three consecutive runs.

Table 3.2. CO_2 capacities, H_2O capacities, amine efficiencies (A.E.) and efficiency enhancement (E.E.) under 10% CO_2 in He flow at 30 °C. Dry CO_2 capacities were determined by thermogravimetric analysis, and humid CO_2 capacities (P_{H2O} = 21 mbar) were determined using a fixed bed.

Material	Dry CO_2 Capacity (mmol/g)	Humid CO_2 Capacity (mmol/g)	Dry A.E. (CO_2/N)	Humid A.E. (CO_2/N)	E.E. (Humid A.E./Dry A.E.)	H_2O Capacity (mmol/g)
SBA_AMBS	0.12	0.40	0.06	0.21	3.5	2.6
SBA_TBAPS	0.05	0.57	0.03	0.31	10.3	2.4
SBA_CHAPS	0.10	0.34	0.05	0.18	3.6	1.7

Single component water adsorption isotherms were measured for all the sorbents at the temperature used for the humid, fixed bed experiments (Table 3.2, Figure B.4). As expected, the hindered amine sorbents were less hydrophilic than the bare silica support. At the relative humidity used for the fixed bed experiments (49% RH or P_{H2O} = 21 mbar), it was observed that SBA_CHAPS adsorbed the lowest amount of water. The effects of water on the CO_2 adsorption capacity are further explored in the discussion section below.

Previous studies on unhindered amine sorbents indicate that increases of CO_2 capacity in the presence of water are not necessarily due to formation of ammonium bicarbonates.[9,11] Moreover, it has been proposed that more ammonium carbamates can form when comparing humid and dry conditions due to water acting as a diffusive intermediate, increased chain mobility, and/or liberation of amines interacting with surface silanols when water is present on the sorbent.[22,39–43] Spectroscopic studies are needed to further verify if there is any change in the nature of the species adsorbed under humid conditions.

3.3.3 FTIR Spectra of Adsorbed CO_2 on the Hindered Amine Sorbents

In situ IR spectroscopy was used to probe the nature of the adsorbed species formed in the presence of both humid and dry CO_2. Multiple overlapping peaks formed between 1750 and 1275 cm^{-1} in the presence of dry and humid CO_2 for each sorbent, indicating that chemisorbed species formed on the sorbents in both runs (Figure 3.5). The humid CO_2 adsorption spectrum for all sorbents appeared to have larger peak intensity when compared to their respective dry CO_2 adsorption spectrum, indicating that more of the same species and/or new species formed in the presence of humidity. Peak shifts observed when

comparing the $^{12}CO_2$ to $^{13}CO_2$ adsorption spectra were used to assist in peak assignments for all sorbents under both dry and humid conditions.

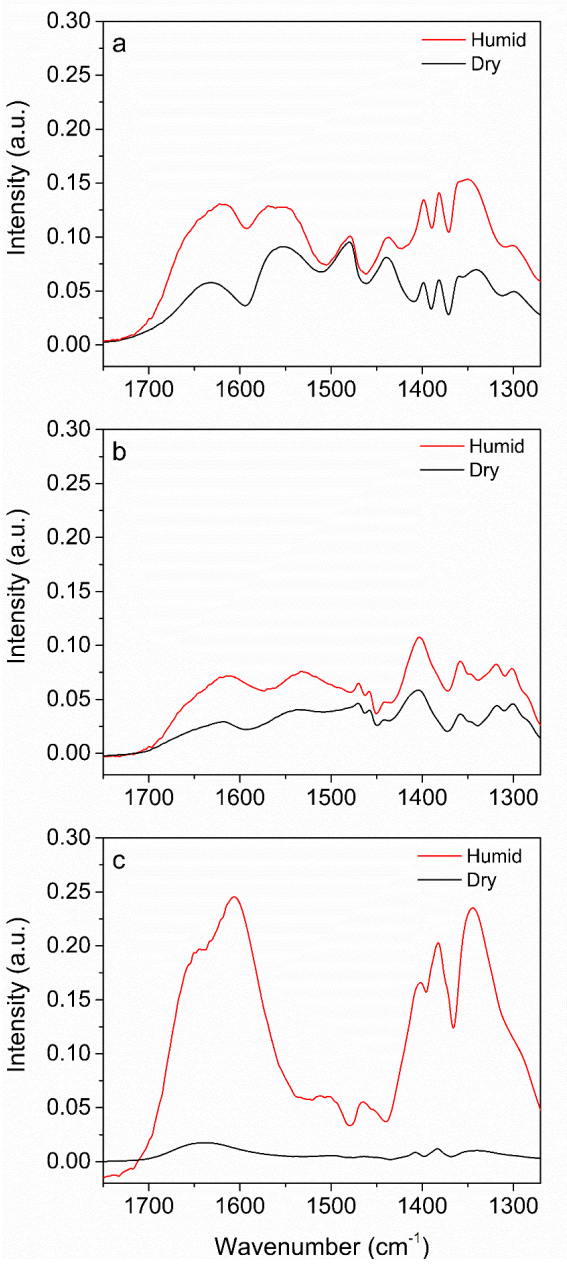

Figure 3.5. FTIR spectra for 10% CO_2 adsorption on (a) SBA_AMBS, (b) SBA_CHAPS, and (c) SBA_TBAPS under dry and humid conditions (P_{H2O} = 21 mbar) at 30 °C after 65 min.

For the SBA_AMBS sorbent under dry conditions, peaks observed for $^{12}CO_2$-derived species and the shifts for the $^{13}CO_2$-derived analogs resembled what was seen in a previous spectroscopic study on an unhindered primary amine grafted sorbent (Figure 3.6a).[35] Furthermore, several peaks in the $^{13}CO_2$ adsorption spectrum shifted to a lower wavenumber when compared to the $^{12}CO_2$ adsorption spectrum, indicating that they could be traced to the carbon atom from CO_2. Peaks at 1552 and 1439 cm^{-1} redshifted to 1539 and 1430 cm^{-1}, respectively, and are assigned to the asymmetric and symmetric stretch of the carboxylate anion of ammonium carbamate.[22,35,44] The peak at 1342 cm^{-1} redshifted to 1329 cm^{-1} and is attributed to the skeletal vibration of carbamate.[22] The shoulder at 1680 cm^{-1} redshifted and merged with the peak at 1632 cm^{-1} and is attributed to the carbonyl stretch of carbamic acid. The peak at 1632 cm^{-1} does not appear to shift and is attributed to a deformation mode of NH_3^+.[22,37,45] The shoulder at 1495 cm^{-1} appeared to redshift to form a peak at 1477 cm^{-1}. Previous reports have attributed peaks around 1477 cm^{-1} to both the NH stretch of the carbamate anion and a deformation mode of NH_3^+.[22,35] Consistent with a previous computational study, the shoulder at 1495 cm^{-1} may be associated with a C-N stretch of a carbamic acid or carbamate.[46,47] No shifts were seen for the peaks at 1398 and 1380 cm^{-1}. These peaks are likely due to perturbations of CH_2 or CH_3 modes in the carbon backbone of the grafted aminosilane.

Peak shifts were also observed when comparing the $^{12}CO_2$ to $^{13}CO_2$ adsorption spectra for SBA_AMBS under humid conditions (Figure 3.6b). The broad peak at 1614 cm^{-1} seen after $^{12}CO_2$ adsorption merged with the peak at 1565 cm^{-1}. This peak shift did not occur in the dry adsorption spectrum and can be attributed to a new adsorbed species. In addition, this peak shift revealed an underlying peak at 1632 cm^{-1} attributed to the

deformation mode of an alkylammonium ion. Similar peak shifts to what was observed in the dry adsorption spectra were seen at 1342, 1439, 1495, 1680 to 1329, 1430, 1477, and 1626 cm^{-1}, indicating that carbamates and carbamic acids were still present under humid conditions. The peaks around 1342 cm^{-1} in the presence of $^{12}CO_2$ increased in intensity when comparing the dry and humid spectra, indicating that there may be a new peak associated with a new chemisorbed species around that region. However, the peak shift of that band remained the same as what was seen in the dry adsorption spectra. To further clarify what new peaks arose in the presence of humidity, the spectrum of adsorbed CO_2 under dry conditions was subtracted from the spectrum of adsorbed CO_2 under humid conditions (Figure 3.6c). Two peaks at 1611 and 1354 cm^{-1} were then clearly revealed in the $^{12}CO_2$ adsorption spectrum, which shifted to 1574 and 1329 cm^{-1}, respectively, in the $^{13}CO_2$ adsorption spectrum. These peaks at 1611 and 1354 cm^{-1} are respectively assigned to the asymmetric and symmetric stretches of the carboxylate group in ammonium bicarbonate.[23,48,49]

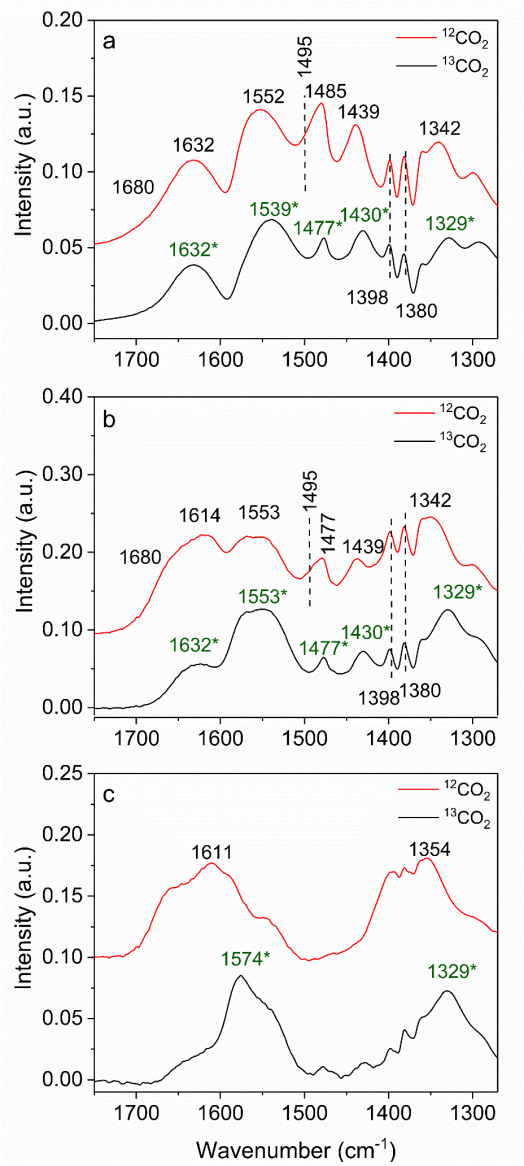

Figure 3.6. FTIR spectra for 10% $^{12}CO_2$ and $^{13}CO_2$ adsorption on SBA_AMBS at 30 °C after 65 min under (a) dry conditions, (b) humid conditions (P_{H2O} = 21 mbar), and (c) residual of humid-minus-dry conditions.

For the SBA_CHAPS material, peaks at 1535 and 1401 cm^{-1} shifted to 1514 and 1393 cm^{-1} when comparing the dry adsorption spectrum of $^{12}CO_2$ to $^{13}CO_2$. These peaks are attributed to the asymmetric and symmetric stretching modes of the carboxylate group in ammonium carbamate (Figure 3.7a).[35] The shoulder at 1667 cm^{-1} redshifted and combined with the peak at 1617 cm^{-1} to form a new peak at 1624 cm^{-1}. The shoulder at

1667 cm^{-1} is attributed to the carbonyl stretch of carbamic acid and the peak at 1617 cm^{-1} is attributed to a deformation mode of the alkylammonium cation.[35] Peaks at 1468 and 1457 cm^{-1} did not appear to shift, indicating that they are either associated with perturbations of NH or CH modes. The peak at 1357 cm^{-1} did not shift, indicating that it is attributed to a CH mode. The peak at 1298 cm^{-1} appeared to become more intense than the peak at 1317 cm^{-1}, indicating that there was some contribution of CO_2 in that region. This peak is attributed to a skeletal vibrational mode of carbamate.[22]

In the isotopic labeling experiments for the SBA_CHAPS material, similar peak shifts that were found under dry conditions were also observed under humid conditions (Figure 3.7b). Furthermore, peaks at 1317, 1402, 1531, and 1661 cm^{-1} shifted to 1295, 1393, 1491, and 1620 cm^{-1}, respectively, indicating that carbamates and carbamic acids formed under humid conditions. The peak centered at 1612 cm^{-1} increased in intensity when comparing the adsorption spectra under humid and dry conditions. A peak of similar intensity at 1617 cm^{-1} was attributed to a deformation of alkylammonium cation in the dry $^{12}CO_2$ adsorption spectrum, as it did not redshift. However, under humid conditions the peak at 1612 cm^{-1} shifted to 1574 cm^{-1}, indicating that the peak centered at 1612 cm^{-1} in the humid $^{12}CO_2$ adsorption spectrum consisted of both a deformation of alkylammonium cation and a newly adsorbed species.

Again, the dry CO_2 adsorption spectrum was subtracted from the humid CO_2 adsorption spectrum to clarify what new species may be present under humid conditions (Figure 3.7c). Peaks at 1602 cm^{-1} and 1357 cm^{-1} redshifted to 1574 and 1323 cm^{-1} in the presence of $^{13}CO_2$ and are associated with the vibrational modes of ammonium bicarbonate species.[49] The SBA_CHAPS sorbent also appeared to form more carbamates and carbamic

acids in the presence of humidity, as the plot of the residual (humid-minus-dry spectrum) revealed peaks associated with such species.

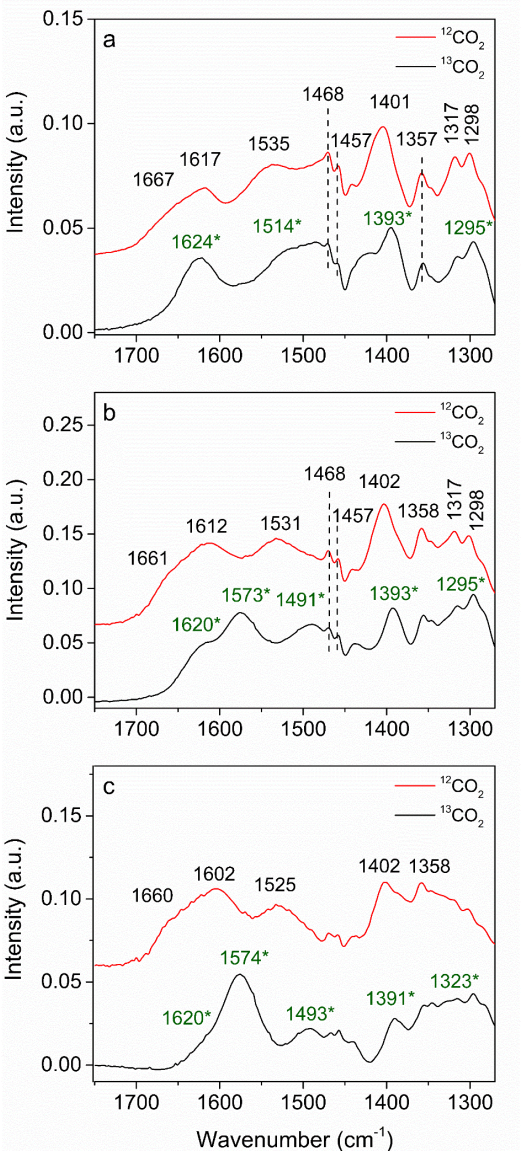

Figure 3.7. FTIR spectra for 10% $^{12}CO_2$ and $^{13}CO_2$ adsorption on SBA_CHAPS at 30 °C after 65 min under (a) dry conditions, (b) humid conditions (P_{H2O} = 21 mbar), and (c) residual of humid-minus-dry conditions.

The broad peak at 1640 cm^{-1} in the dry $^{12}CO_2$ spectrum of SBA_TBAPS was revealed to consist of multiple vibrational modes, as two peaks at 1629 and 1578 cm^{-1} appeared in the presence of $^{13}CO_2$ (Figure 3.8a). Moreover, the peak at 1629 cm^{-1} is in part associated

with a deformation of an alkylammonium cation, and the peak at 1575 cm^{-1} is attributed to the asymmetric stretch of the bicarbonate anion in the $^{13}CO_2$ spectrum. The peak at 1343 cm^{-1} shifted to 1324 cm^{-1} and is assigned to the symmetric stretching mode of the bicarbonate anion. As observed in the IR spectra, severely hindered amines such as SBA_TBAPS cannot chemisorb CO_2 in the form of ammonium carbamate. Due to the tertiary α-carbon of SBA_TBAPS, the formation of a covalent bond between the carbon atom in CO_2 and the amine is thermodynamically unfavorable.[50–52] It is noteworthy that small quantities of bicarbonate formation may be possible even under dry conditions due to the residual amounts of water on the sorbent even after activation.[23,35] The peaks at 1607 and 1349 cm^{-1} in the humid CO_2 adsorption spectrum of SBA_TBAPS are also associated with the bicarbonate species (Figure 3.8b). Again, these peaks shifted in the presence of $^{13}CO_2$, indicating that they are associated with carbon from CO_2. In both the dry and humid spectra, the peaks at 1497, 1461, 1406, and 1384 cm^{-1} did not noticeably shift in the presence of $^{13}CO_2$ (Figure 3.8b). The peaks at 1497 and 1461 cm^{-1} could thus be assigned to the deformation modes of the alkylammonium ion or perturbations in the NH deformation mode.[23,35] The peaks at 1406 and 1384 cm^{-1} are attributed to perturbations in CH_2 or CH_3 modes associated with the carbon backbone of the grafted aminosilane. There appeared to be a difference of relative peak intensity between 1629 cm^{-1} and the peak below 1576 cm^{-1} when comparing the dry and humid $^{13}CO_2$ adsorption spectra. In both dry and humid conditions, it is possible that an additional bicarbonate mode existed around 1640 cm^{-1} in the presence of $^{12}CO_2$ and merged with the peak associated with the ammonium deformation mode at 1629 cm^{-1} in the $^{13}CO_2$ spectra. Consistent with a previous NMR study on supported primary and tertiary amines, it is postulated that ammonium

bicarbonates with varying amounts of water molecules interacting with the anion existed on the sorbent.[53] Bicarbonate asymmetric stretching modes are known to redshift when the amount of water molecules surrounding the anion increases.[49] The higher peak intensities when comparing the peak at 1576 to 1629 cm^{-1} in the humid $^{13}CO_2$ adsorption spectrum would be consistent with more water interactions with the bicarbonate anions. If two distinct bicarbonates species existed on SBA_TBAPS in the presence of CO_2, a total of four asymmetric and symmetric carboxylate stretching modes would be expected—an asymmetric and symmetric carboxylate stretch for each chemically distinct bicarbonate species. The broad peak between 1360 and 1275 cm^{-1} for both dry and humid $^{12}CO_2$ adsorption spectra may be a combination of two symmetric carboxylate stretching modes.

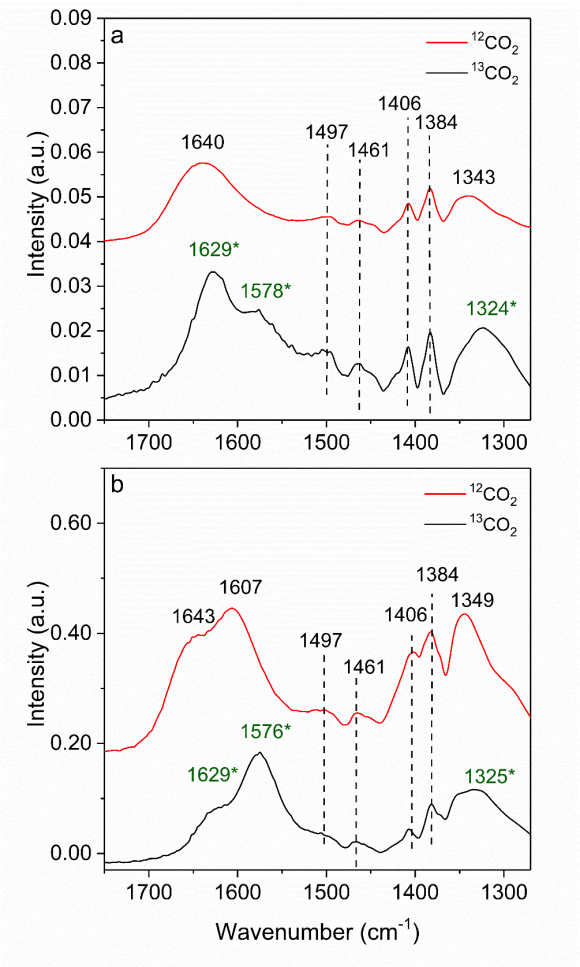

Figure 3.8. FTIR spectra for 10% $^{12}CO_2$ and $^{13}CO_2$ adsorption on SBA_TBAPS at 30 °C after 65 min under (a) dry conditions, (b) humid conditions (P_{H2O} = 21 mbar).

3.3.4 NMR Spectra of Adsorbed CO_2 on the Hindered Amine Sorbents under Nominally Dry Conditions

Ex-situ solid state ^{13}C NMR spectroscopy was used to confirm the existence of chemisorbed species after extended exposure to CO_2 under dry conditions (Figure 3.9). The chemisorption products are assigned through their ^{13}C isotropic chemical shifts: the carbamate species (at ~164 ppm) is found on SBA_CHAPS and SBA_AMBS, but carbamic acid (~162 ppm) was not observed on either sample. The absence of carbamic

acid may reflect very low signal-to-noise ratios as well as carbamic acid's unstable nature in comparison to that of carbamate's.[54] No resonances associated with chemisorbed species were discovered on SBA_TBAPS by NMR spectroscopy; this may be due to limited amounts (below the detection threshold for NMR) and the possible instability of the bicarbonate species formed on that sorbent under nominally dry conditions. Both ^{13}C Bloch decay and spin echo sequences were tested for these samples under dry conditions, in keeping with a recent study of CO_2 exposure that detected bicarbonate unexpectedly on amine sorbents.[53] In that study, ^{1}H-^{13}C CPMAS failed to detect bicarbonates because of motion disrupting the ^{1}H-^{13}C dipole-dipole interaction required for cross-polarization.[53] No bicarbonate signals were found for dry CO_2 exposed samples here.

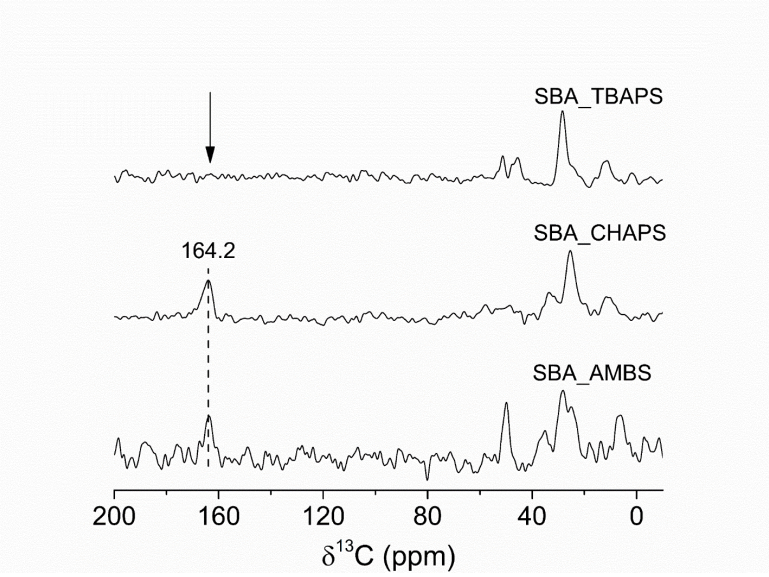

Figure 3.9. $^{13}C\{^{1}H\}$ CPMAS of $^{13}CO_2$ loaded SBA_TBAPS, SBA_CHAPS, and SBA_AMBS. The arrow points to the expected region where chemisorbed products introduced with ^{13}C enrichment would be found. Resonances below 60 ppm are associated with the aminosilane pendant species (at natural abundance).

3.3.5 Isosteric Heats of CO_2 Adsorption

Isosteric heats of adsorption of dry CO_2 were measured at 30 °C on all the sorbents to investigate the thermodynamics of adsorption of CO_2 (Figure 3.10). It should be noted that the amine loadings of the functionalized sorbents studied here are above the threshold of ~1.2-1.4 mmol N/g needed for strong amine-CO_2-amine interactions previously reported with the less bulky aminopropylsilane-functionalized primary amine sorbents.[55] Furthermore, in that study it was demonstrated that there was no change in heat of adsorption at close to zero coverage when the amine loading was at or above the threshold amine loading on primary amine functionalized SBA-15.

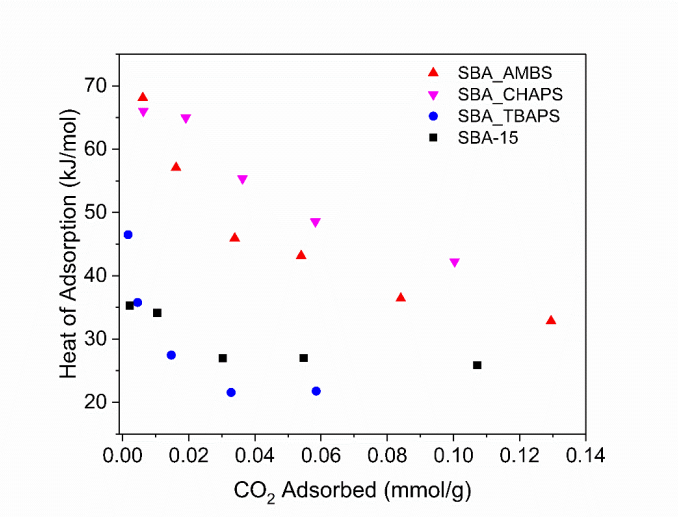

Figure 3.10. Isosteric heats of CO_2 adsorption under dry conditions for all sorbents at 30 °C.

The bare support, SBA-15, had the lowest heat of adsorption at close to zero coverage when compared to the functionalized sorbents with a value of 35 kJ/mol. Physisorption on oxide surfaces typically has low heats of adsorption of 20-40 kJ/mol.[34,55] Furthermore, the heat of adsorption of the silica support is attributed exclusively to physisorption of CO_2 on

surface silanols or siloxane bridges. All hindered amine sorbents studied here had lower initial heats of adsorption than what has been found for unhindered primary and secondary amine grafted sorbents at similar amine loadings (i.e., 86-92 kJ/mol).[55] The low initial heats of adsorption measured for hindered amine sorbents indicate that they contain only weakly chemisorbed CO_2. At high surface coverages of CO_2, there was a dramatic reduction of the heat of adsorption indicating that physisorption became dominant. The adsorption isotherms displayed linearity at higher CO_2 coverages, also indicating physisorption under such conditions (Figure B.10b, Figure B.11b, and Figure B.12b). The inability for available amines to strongly chemisorb CO_2 in nominally dry conditions is due to large amounts of steric hindrance and/or poor spacing.

The initial heats of adsorption of SBA_AMBS and SBA_CHAPS were the highest of all the materials studied here at 65-70 kJ/mol. As shown above via IR spectroscopy, these two hindered amine sorbents were found to chemisorb dry CO_2 as carbamates and carbamic acids – the same species that form on unhindered primary and secondary amine sorbents.[35] The formation of ammonium bicarbonates in large quantities in the presence of humid CO_2 on SBA_AMBS and SBA_CHAPS when compared to their unhindered counterparts could be explained in part by the differences of thermal stability of carbamates/carbamic acids between hindered and unhindered amines. The introduction of steric hindrance on the α-carbon weakens the stability of carbamates and carbamic acids making bicarbonate formation more common on hindered amines when compared to unhindered amines.

Of the hindered amine sorbents, SBA_TBAPS had the lowest initial heat of adsorption at 46 kJ/mol, indicating more weakly CO_2 interactions than the other two

hindered amine sorbents. This value is slightly higher than the reported value for physisorption, indicating weakly chemisorption on SBA_TBAPS. As noted above, carbamates and carbamic acids are unlikely to form on SBA_TBAPS due to the severe steric hindrance of the *t*-butyl functional group.[50–52] The initial heat evolved when CO_2 adsorbs onto SBA_TBAPS is consistent with bicarbonate formation, as indicated above by IR spectroscopy. Tertiary amine solutions, which only chemisorb CO_2 as bicarbonates, are found to have initial heats of absorption in the range of 40-60 kJ/mol.[56] Due to the hygroscopic nature of the sorbents, residual water that is present on the sorbent after activation may allow small quantities of bicarbonates to form even under nominally dry conditions.

3.3.6 CO_2 Desorption Kinetics

All hindered amine sorbents appeared to readily desorb CO_2 at 30 °C under He flow (50 mL/min) (Figure 3.11). Less than 20 percent of the integrated peak area in the 1750-1275 cm^{-1} region remained after 1 h of desorption for the hindered sorbents under both dry and humid conditions at this temperature. In a previous *in situ* IR spectroscopy study, unhindered primary and secondary amines desorbed less chemisorbed CO_2 under dry conditions. Furthermore, after 90 minutes of desorption under He flow (80 mL/min), 60 percent and 30 percent of the integrated peak area in the region evaluated for chemisorbed CO_2 remained for an unhindered primary and secondary amine, respectively.[35] Consistent with the heat of adsorption data, the desorption kinetics imply that the chemisorbed species formed are weakly bound on these hindered amine sorbents, indicating that regeneration of these materials may be less energy intensive than their unhindered counterparts.

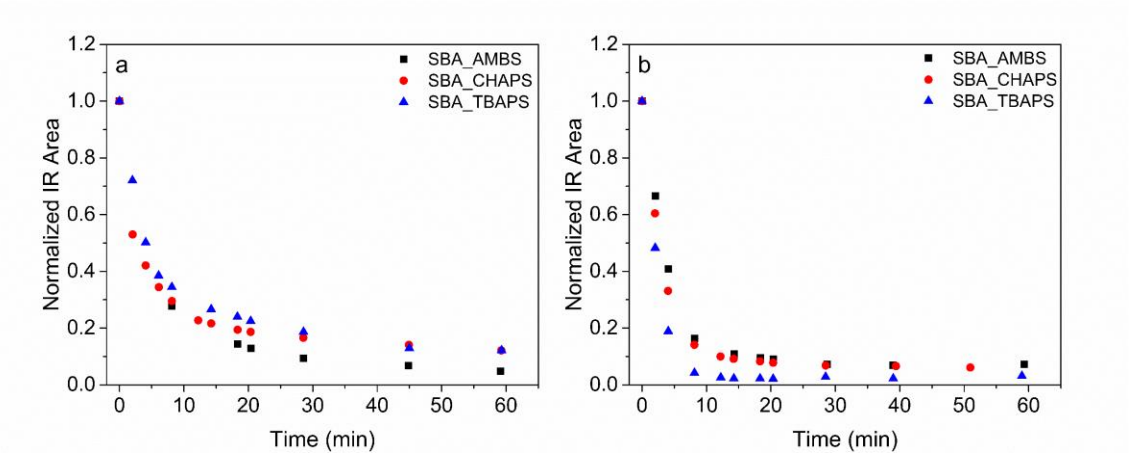

Figure 3.11. Normalized integrated FTIR peak area between 1750 and 1275 cm^{-1} during desorption of 10% CO_2 under (a) dry and (b) humid conditions at 30 °C. Desorption was conducted with dry He in the dry run and humid He (P_{H2O} = 21 mbar) in the humid run. The curves are normalized such that the start of the desorption run equals 1.

3.3.7 Kinetics of Ammonium Bicarbonate Formation

Severely hindered and tertiary amines in solution have slow kinetics when compared to moderately hindered amines. Therefore, it would be expected that the severely hindered SBA_TBAPS material would have slower kinetics than the other two hindered amine sorbents. Interestingly, all supported hindered amines appeared to have similar rates of bicarbonate formation under 10% CO_2/He flow under humid conditions (Figure 3.12). It is unclear why the rates of bicarbonate formation on solid supported amines do not appear to change with increasing amounts of steric hindrance. The ease of intermediate species forming hydrogen bonds with nearby water molecules and/or differences in the adsorption mechanism are thought to factor into the kinetics of bicarbonate formation in solution.[1,15] However, the experiments conducted here do not give insight into these factors. Since SBA_TBAPS is a severely hindered amine, it should only form bicarbonates by base catalyzed hydrolysis. The SBA_AMBS and SBA_CHAPS sorbents, in principle, could

form bicarbonates by both base catalyzed hydrolysis and carbamate hydrolysis. There is no direct evidence of the carbamate hydrolysis mechanism for moderately hindered amine sorbents under the conditions employed here, as there appeared to be no reduction in ammonium carbamate content when comparing humid to dry runs for SBA_AMBS and SBA_CHAPS.

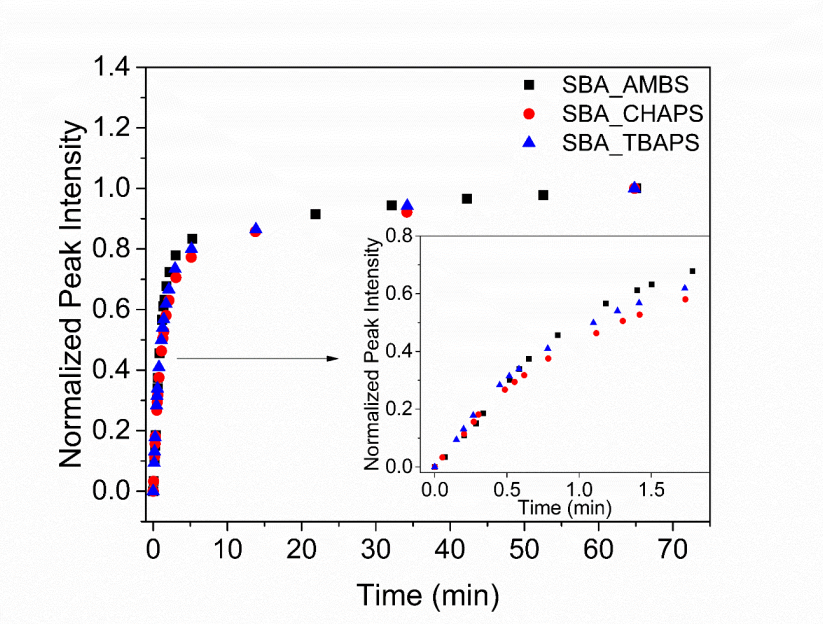

Figure 3.12. Normalized peak intensity of the asymmetric stretching mode of the bicarbonate species (1602 cm^{-1} for SBA_CHAPS, 1611 cm^{-1} for SBA_AMBS, and 1607 cm^{-1} for SBA_TBAPS) during adsorption of 10% CO_2 under humid conditions (P_{H2O} = 21 mbar) at 30 °C. The curves are normalized such that the end of the adsorption run (65 min) equals 1.

3.3.8 Discussion on the Nature of the Chemisorbed Species

All hindered amine sorbents had poor adsorption performance under nominally dry conditions as they all had CO_2 capacities within the range of the bare silica support (Figure B.13b). The SBA_AMBS and SBA_CHAPS sorbents were found to have larger CO_2 capacities than SBA_TBAPS. Moreover, the chemisorbed CO_2 species were identified to

be carbamates and carbamic acids on SBA_AMBS and SBA_CHAPS and as bicarbonates on SBA_TBAPS at those conditions. Very small quantities of bicarbonates, which require one molecule of water per CO_2 to form, were discovered on SBA_TBAPS under nominally dry conditions due to residual water on the sorbent surface that remained after activation.

The adsorbed CO_2 species on supported hindered amines under dry conditions were determined to have lower initial heats of adsorption than their unhindered counterparts, implying formation of weakly chemisorbed species on hindered amines. Bulky α-carbon substituents on hindered amines weaken covalent bonds between the nitrogen in the amine group and the carbon in CO_2. If the amine is too sterically hindered, species that require covalent bonding between CO_2 and the amine such as carbamates and carbamic acids cannot form.[7] The inability to form such species explains the observed low CO_2 capacities under nominally dry conditions for SBA_TBAPS. Furthermore, the bulky *t*-butyl substituent adjacent to the nitrogen atom in SBA_TBAPS makes it unfavorable for CO_2 to form carbamates and carbamic acids. Yoo et al. also demonstrated that supported amines that were in hydrophobic environments had reduced isosteric heats of CO_2 adsorption and CO_2 capacities when compared to amines that were in hydrophilic environments; this result implies that hydrogen bonding can increase thermal stability of chemisorbed species.[34] The hindered amine sorbents studied here are less hydrophilic than their unhindered counterparts implying that after activation there will fewer water molecules around to hydrogen bond with CO_2-derived species on hindered amine sorbents.[57]

The CO_2 capacity of all sorbents increased in the presence of humidity, which was revealed using IR spectroscopy to be due to bicarbonate formation for SBA_AMBS and SBA_TBAPS and a combination of carbamates, carbamic acids, and bicarbonates for

SBA_CHAPS. As seen in solution, ammonium bicarbonates are more common on supported hindered amines than on supported unhindered primary amines previously studied under similar conditions.[7,41]. In hindered amines, bicarbonates, which are predicted to be ionically bonded to the amines, are more common due in part to the reduction of the stability of species requiring covalent bonds such as carbamates and carbamic acids.[1,5,6] In addition, the preferential formation of bicarbonates on hindered amines has also been thought to be due to kinetic factors.[10,58] Steric hindrance on the α-carbon can block pathways of CO_2 to get to the nitrogen atom in the amine, making it more likely for the nitrogen atom to be protonated by smaller water molecules instead. It has also been reported in solution studies that ammonium bicarbonate formation is more likely for amines that are stronger bases.[59,60] Furthermore, the hindered amines studied here are expected to be stronger Brønsted bases than supported unhindered primary amines employed in previous studies due to electron donating methyl and methylene groups on the α-carbon.[9,11]

Severely hindered SBA_TBAPS had the highest CO_2 capacities and amine efficiencies followed by moderately hindered SBA_AMBS and SBA_CHAPS under humid conditions. The SBA_TBAPS material had larger amounts of bicarbonate formation leading to higher amine efficiencies than the moderately hindered amines. The amine efficiencies found for the hindered amine sorbents under humid conditions are within range of what has been reported for SBA-15 supported primary amines grafted at similar amine loadings and under CO_2 capture conditions employed here. Furthermore, supported primary amines have been reported to have an amine efficiency of 0.21-0.24 CO_2/N in 10% CO_2 under both dry[55] and humid[61] conditions, while the amine efficiencies of the hindered

amines sorbents studied here under humid conditions were found to be between 0.18 and 0.31 CO_2/N. Although similar CO_2 capacities are observed between hindered and unhindered amines, regeneration of hindered amine sorbents may be less energy intensive on unhindered amines due to weakly bound chemisorbed species.

Ammonium bicarbonate formation, however, appears less favorable on solid supported amines than in amine solutions under the conditions employed. In aqueous solution, amine efficiencies for hindered amines have been reported in the range of 0.65 to 1 CO_2/N under conditions similar to those employed here.[7] Variations of bicarbonate formation between the different types of hindered amine sorbents as well as variations between the solid sorbents and solutions may be due to the reasons listed below.

(1) In a computational study, Sumon et al. suggested that water can increase thermodynamic stability of ionic species formed in amine solutions through solvation and hydrogen bonding.[62] There is less water available for hydrogen bonding on solid supports, possibly making it less favorable for bicarbonates to form when compared to aqueous amine solutions. The hindered amine sorbents vary in water content at the same temperature and relative humidity, as shown by the water adsorption isotherms (Table 3.2 and Figure B.4), with SBA_CHAPS having the least amount of water adsorbed. How the water molecules are arranged on the surface for each hindered amine sorbent may also play a factor in determining favorability of bicarbonate formation.[58]

(2) It is assumed that there is a monolayer surface coverage of aminosilanes on the silica support at the amine loadings used here. However, it is also possible that some of the

aminosilanes have condensed with each other during the silane grafting step, resulting in multilayer surface coverage in some regions. Some amine sites may be less accessible to CO_2 and H_2O due to amine clustering. If multilayer surface coverage of aminosilanes exist in the hindered sorbents, SBA_TBAPS may have more amines available to interact with CO_2 when compared to SBA_CHAPS and SBA_AMBS because of reduced mass transfer limitations associated with the lack of formation of the cross-linking ammonium carbamate species on SBA_TBAPS.

3.3.9 Sorbent Degradation Experiments

The sorbents were exposed to both an inert stream of N_2 and simulated air (21% O_2 in N_2) at a temperature of 135 °C for a prolonged time (24 h) to evaluate their thermal and oxidative stability, respectively. All hindered amine sorbents retained at least 90% of their original nitrogen content after oxidative and thermal treatments (Figure B.15). However, the SBA_CHAPS and SBA_TBAPS sorbents had significant reductions in capacity after exposure to accelerated oxidative conditions (Table 3.3).

Table 3.3. CO_2 adsorption capacities (mmol/g) under dry conditions before and after degradation.

Material	CO_2 Capacity of Fresh Material	CO_2 Capacity after Oxidation	CO_2 Capacity after Thermal Degradation
SBA_AMBS	0.12	0.11	0.12
SBA_CHAPS	0.10	0.03	0.08
SBA_TBAPS	0.05	0.02	0.04

Unhindered secondary amine sorbents have been previously shown to be susceptible to oxidative degradation.[25,26] Oximes, imines, and amides have been previously reported as species associated with oxidative degradation on amine sorbents.[25,26,63] Peaks associated with degradation products were identified in the IR spectra of SBA_CHAPS and SBA_TBAPS after oxidative and thermal treatments (Figure B.16 and Figure B.17). Furthermore, SBA_CHAPS and SBA_TBAPS had multiple overlapping peaks appearing between 1700-1500 cm^{-1}, which could be associated with multiple degradation products such as imines, oximes, and amides. As expected, the primary hindered amine SBA_AMBS did not readily oxidize under the conditions employed here. Moreover, no noticeable peaks associated with degradation products were found using IR spectroscopy (Figure B.18). These results are consistent with a previous studies that have demonstrated that sorbents that consist of solely primary amines or tertiary amines are less prone to oxidization than ones that contain solely secondary amines.[26,64,65] Bollini et al. demonstrated that supported primary amines are prone to degradation when spaced from a secondary amine by an ethyl group, implying an intramolecular degradation mechanism.[26] The initial degradation events are thought to occur via proton abstraction from the carbon alpha to the amine nitrogen. Because SBA_AMBS does not contain any C-H bonds on the α-carbon, enhanced oxidative stability is expected for hindered primary amines in "blended" amine systems.

3.4 Conclusions

The effects of humidity on CO_2 adsorption on solid supported hindered amines were explored in this fundamental study. While the adsorption performance of the hindered amine sorbents in nominally dry conditions was poor, amine efficiencies and CO_2

capacities under humid conditions were comparable to values previously reported for unhindered primary amine sorbents at similar amine loadings. It was found that SBA_TBAPS achieved the highest CO_2 adsorption capacities under humid conditions followed by SBA_AMBS and SBA_CHAPS. It was confirmed by *in situ* FTIR spectroscopy that all hindered amine sorbents studied were prone to form bicarbonates under humid conditions. Furthermore, the amount of bicarbonates formed on these sorbents are the largest amount reported on solid supported amines to date, to the best of our knowledge. More bicarbonates formed on hindered amines than were observed on their unhindered counterparts, due in part to limited or no carbamate formation on such sites. Weakly chemisorbed species led to facile desorption at 30 °C for the hindered amine sorbents. This result implies hindered amine sorbents have potential for reduced energy costs for regeneration.

The large amine efficiencies observed in hindered amine solutions were not achieved on the solid analogues. The lower extent of bicarbonate formation on solid supports when compared to solution may be a function of water loading, as in solution the amines are in a large excess of water when compared to their solid counterparts. A better understanding of how solvation and hydrogen bonding affect chemisorbed CO_2 on solid supported amines is needed to further explain discrepancies in CO_2 capacity between solid supported amines and amines in aqueous solution.

Oxidative and thermal degradation of the sorbents was also studied to help evaluate sorbent lifetimes. All sorbents retained most of their amine content and CO_2 adsorption capacity when exposed to high temperatures under inert He flow at long timescales. The SBA_AMBS sorbent retained most of its dry CO_2 capacity after exposure to accelerating

oxidizing conditions and was the most oxidatively stable sorbent studied here. Both the secondary hindered amine sorbents had significant decreases in CO_2 capacity after exposure to accelerated oxidizing conditions, and peaks associated with degradation products were observed using IR spectroscopy. Due to their oxidative stability, hindered primary amines are better candidates than hindered secondary amines for future studies on CO_2 adsorption.

3.5 References

(1) Sartori, G.; Savage, D. W. Sterically Hindered Amines for Carbon Dioxide Removal from Gases. *Ind. Eng. Chem. Fundam.* **1983**, *22*, 239–249.

(2) Hook, R. J. An Investigation of Some Sterically Hindered Amines as Potential Carbon Dioxide Scrubbing Compounds. *Ind. Eng. Chem. Res.* **1997**, *36*, 1779–1790.

(3) Chakraborty, A. K.; Astarita, G.; Bischoff, K. B. CO_2 Absorption in Aqueous Solutions of Hindered Amines. *Chem. Eng. Sci.* **1986**, *41*, 997–1003.

(4) Vaidya, P. D.; Kenig, E. Y. CO_2-Alkanolamine Reaction Kinetics: A Review of Recent Studies. *Chem. Eng. Technol.* **2007**, *30*, 1467–1474.

(5) Fernandes, D.; Conway, W.; Burns, R.; Lawrance, G.; Maeder, M.; Puxty, G. Investigations of Primary and Secondary Amine Carbamate Stability by ^{1}H NMR Spectroscopy for Post Combustion Capture of Carbon Dioxide. *J. Chem. Thermodyn.* **2012**, *54*, 183–191.

(6) Da Silva, E. F.; Svendsen, H. F. Study of the Carbamate Stability of Amines Using Ab Initio Methods and Free-Energy Perturbations. *Ind. Eng. Chem. Res.* **2006**, *45*, 2497–2504.

(7) Kortunov, P. V.; Siskin, M.; Paccagnini, M.; Thomann, H. CO_2 Reaction Mechanisms with Hindered Alkanolamines: Control and Promotion of Reaction Pathways. *Energy & Fuels* **2016**, *30*, 1223–1236.

(8) Smith, D. R.; Quinn, J. A. The Prediction of Facilitation Factors for Reaction Augmented Membrane Transport. *AIChE J.* **1979**, *25*, 197–200.

(9) Donaldson, T. L.; Nguyen, Y. N. Carbon Dioxide Reaction Kinetics and Transport in Aqueous Amine Membranes. *Ind. Eng. Chem. Fundam.* **1980**, *19*, 260–266.

(10) Stowe, H. M.; Hwang, G. S. Fundamental Understanding of CO_2 Capture and

Regeneration in Aqueous Amines from First-Principles Studies: Recent Progress and Remaining Challenges. *Ind. Eng. Chem. Res.* **2017**, *56*, 6887–6899.

(11) da Silva, E. F.; Svendsen, H. F. Computational Chemistry Study of Reactions, Equilibrium and Kinetics of Chemical CO_2 Absorption. *Int. J. Greenh. Gas Control* **2007**, *1*, 151–157.

(12) Davran-Candan, T. DFT Modeling of CO_2 Interaction with Various Aqueous Amine Structures. *J. Phys. Chem. A* **2014**, *118*, 4582–4590.

(13) Xie, H.-B.; He, N.; Song, Z.; Chen, J.; Li, X. Theoretical Investigation on the Different Reaction Mechanisms of Aqueous 2-Amino-2-Methyl-1-Propanol and Monoethanolamine with CO_2. *Ind. Eng. Chem. Res.* **2014**, *53*, 3363–3372.

(14) Yamada, H.; Matsuzaki, Y.; Higashii, T.; Kazama, S. Density Functional Theory Study on Carbon Dioxide Absorption into Aqueous Solutions of 2-Amino-2-Methyl-1-Propanol Using a Continuum Solvation Model. *J. Phys. Chem. A* **2011**, *115*, 3079–3086.

(15) Stowe, H. M.; Hwang, G. S. Molecular Insights into the Enhanced Rate of CO_2 Absorption to Produce Bicarbonate in Aqueous 2-Amino-2-Methyl-1-Propanol. *Phys. Chem. Chem. Phys.* **2017**, *19*, 32116–32124.

(16) Lee, C. S.; Ong, Y. L.; Aroua, M. K.; Daud, W. M. A. W. Impregnation of Palm Shell-Based Activated Carbon with Sterically Hindered Amines for CO_2 Adsorption. *Chem. Eng. J.* **2013**, *219*, 558–564.

(17) Zhao, Y.; Winston Ho, W. S. Steric Hindrance Effect on Amine Demonstrated in Solid Polymer Membranes for CO_2 Transport. *J. Memb. Sci.* **2012**, *415–416*, 132–138.

(18) Zhao, Y.; Ho, W. S. W. CO_2-Selective Membranes Containing Sterically Hindered Amines for CO_2/H_2 Separation. *Ind. Eng. Chem. Res.* **2013**, *52*, 8774–8782.

(19) Yamada, H.; Fujiki, J.; Chowdhury, F. A.; Yogo, K. Effect of Isopropyl-Substituent Introduction into Tetraethylenepentamine-Based Solid Sorbents for CO_2 Capture. *Fuel* **2018**, *214*, 14–19.

(20) Numaguchi, R.; Fujiki, J.; Yamada, H.; Firoz; Chowdhury, A.; Kida, K.; Goto, K.; Okumura, T.; Yoshizawa, K.; Yogo, K. Development of Post-Combustion CO_2 Capture System Using Amine-Impregnated Solid Sorbent. *Energy Procedia* **2017**, *114*, 2304–2312.

(21) Fujiki, J.; Chowdhury, F. A.; Yamada, H.; Yogo, K. Highly Efficient Post-Combustion CO_2 Capture by Low-Temperature Steam-Aided Vacuum Swing Adsorption Using a Novel Polyamine-Based Solid Sorbent. *Chem. Eng. J.* **2017**, *307*, 273–282.

(22) Didas, S. A.; Sakwa-Novak, M. A.; Foo, G. S.; Sievers, C.; Jones, C. W. Effect of Amine Surface Coverage on the Co-Adsorption of CO_2 and Water: Spectral Deconvolution of Adsorbed Species. *J. Phys. Chem. Lett.* **2014**, *5*, 4194–4200.

(23) Lee, J. J.; Chen, C.-H.; Shimon, D.; Hayes, S. E.; Sievers, C.; Jones, C. W. Effect of Humidity on the CO_2 Adsorption of Tertiary Amine Grafted SBA-15. *J. Phys. Chem. C* **2017**, *121*, 23480–23487.

(24) Chi, S.; Rochelle, G. T. Oxidative Degradation of Monoethanolamine. *Ind. Eng. Chem. Res.* **2002**, *41*, 4178–4186.

(25) Heydari-Gorji, A.; Sayari, A. Thermal, Oxidative, and CO_2-Induced Degradation of Supported Polyethylenimine Adsorbents. *Ind. Eng. Chem. Res.* **2012**, *51*, 6887–6894.

(26) Bollini, P.; Choi, S.; Drese, J. H.; Jones, C. W. Oxidative Degradation of Aminosilica Adsorbents Relevant to Postcombustion CO_2 Capture. *Energy & Fuels* **2011**, *25*, 2416–2425.

(27) Calleja, G.; Sanz, R.; Arencibia, A.; Sanz-Pérez, E. S. Influence of Drying Conditions on Amine-Functionalized SBA-15 as Adsorbent of CO_2. *Top. Catal.* **2011**, *54*, 135–145.

(28) Bali, S.; Chen, T. T.; Chaikittisilp, W.; Jones, C. W. Oxidative Stability of Amino Polymer-Alumina Hybrid Adsorbents for Carbon Dioxide Capture. *Energy & Fuels* **2013**, *27*, 1547–1554.

(29) Heydari-Gorji, A.; Belmabkhout, Y.; Sayari, A. Degradation of Amine-Supported CO_2 Adsorbents in the Presence of Oxygen-Containing Gases. *Microporous Mesoporous Mater.* **2011**, *145*, 146–149.

(30) Moschetta, E. G.; Sakwa-Novak, M. A.; Greenfield, J. L.; Jones, C. W. Post-Grafting Amination of Alkyl Halide-Functionalized Silica for Applications in Catalysis, Adsorption, and N-15 NMR Spectroscopy. *Langmuir* **2015**, *31*, 2218–2227.

(31) Switzer, J. R.; Ethier, A. L.; Hart, E. C.; Flack, K. M.; Rumple, A. C.; Donaldson, J. C.; Bembry, A. T.; Scott, O. M.; Biddinger, E. J.; Talreja, M.; et al. Design, Synthesis, and Evaluation of Nonaqueous Silylamines for Efficient CO_2 Capture. *ChemSusChem* **2014**, *7*, 299–307.

(32) Rohan, A. L.; Switzer, J. R.; Flack, K. M.; Hart, R. J.; Sivaswamy, S.; Biddinger, E. J.; Talreja, M.; Verma, M.; Faltermeier, S.; Nielsen, P. T.; et al. The Synthesis and the Chemical and Physical Properties of Non-Aqueous Silylamine Solvents for Carbon Dioxide Capture. *ChemSusChem* **2012**, *5*, 2181–2187.

(33) Brunauer, S.; Emmett, P. H.; Teller, E. Adsorption of Gases in Multimolecular Layers. *J. Am. Chem. Soc.* **1938**, *60*, 309–319.

(34) Yoo, C.-J.; Lee, L.-C.; Jones, C. W. Probing Intramolecular versus Intermolecular CO_2 Adsorption on Amine-Grafted SBA-15. *Langmuir* **2015**, *31*, 13350–13360.

(35) Foo, G. S.; Lee, J. J.; Chen, C.-H.; Hayes, S. E.; Sievers, C.; Jones, C. W. Elucidation of Surface Species through in Situ FTIR Spectroscopy of Carbon Dioxide Adsorption on Amine-Grafted SBA-15. *ChemSusChem* **2017**, *10*, 266–276.

(36) Bacsik, Z.; Atluri, R.; Garcia-Bennett, A. E.; Hedin, N. Temperature-Induced Uptake of CO_2 and Formation of Carbamates in Mesocaged Silica Modified with N-Propylamines. *Langmuir* **2010**, *26*, 10013–10024.

(37) Socrates, G. *Infrared and Raman Characteristic Group Frequencies*, Third.; John Wiley & Sons LTD, 2001.

(38) Colthup, N. B.; Daly, L. H.; Wiberley, S. E. *Introduction to Infrared and Raman Spectroscopy*, Third Edit.; Academic Press, 1990.

(39) Mebane, D. S.; Kress, J. D.; Storlie, C. B.; Fauth, D. J.; Gray, M. L.; Li, K. Transport, Zwitterions, and the Role of Water for CO_2 Adsorption in Mesoporous Silica-Supported Amine Sorbents. *J. Phys. Chem. C* **2013**, *117*, 26617–26627.

(40) Fan, Y.; Labreche, Y.; Lively, R. P.; Jones, C. W.; Koros, W. J. Dynamic CO_2 Adsorption Performance of Internally Cooled Silica-Supported Poly(ethylenimine) Hollow Fiber Sorbents. *AIChE J.* **2014**, *60*, 3878–3887.

(41) Bacsik, Z.; Ahlsten, N.; Ziadi, A.; Zhao, G. Y.; Garcia-Bennett, A. E.; Martín-Matute, B.; Hedin, N. Mechanisms and Kinetics for Sorption of CO_2 on Bicontinuous Mesoporous Silica Modified with N-Propylamine. *Langmuir* **2011**, *27*, 11118–11128.

(42) Aziz, B.; Hedin, N.; Bacsik, Z. Quantification of Chemisorption and Physisorption of Carbon Dioxide on Porous Silica Modified by Propylamines: Effect of Amine Density. *Microporous Mesoporous Mater.* **2012**, *159*, 42–49.

(43) Koutsianos, A.; Barron, A. R.; Andreoli, E. CO_2 Capture Partner Molecules in Highly Loaded PEI Sorbents. *J. Phys. Chem. C* **2017**, *121*, 21772–21781.

(44) Danon, A.; Stair, P. C.; Weitz, E. FTIR Study of CO_2 Adsorption on Amine-Grafted SBA-15: Elucidation of Adsorbed Species. *J. Phys. Chem. C* **2011**, *115*, 11540–11549.

(45) Danon, A.; Stair, P. C.; Weitz, E. FTIR Study of CO_2 Adsorption on Amine-Grafted SBA-15: Elucidation of Adsorbed Species. *J. Phys. Chem. C* **2011**, *115*, 11540–11549.

(46) Bossa, J.-B.; Borget, F.; Duvernay, F.; Theulé, P.; Chiavassa, T. Formation of Neutral Methylcarbamic Acid ($CH_3NHCOOH$) and Methylammonium Methylcarbamate [$CH_3NH_3^+$][$CH_3NHCO_2^-$] at Low Temperature. *J. Phys. Chem. A*

2008, *112*, 5113–5120.

(47) Mafra, L.; Čendak, T.; Schneider, S.; Wiper, P. V.; Pires, J.; Gomes, J. R. B.; Pinto, M. L. The Structure of Chemisorbed CO_2 Species in Amine-Functionalized Mesoporous Silicas Studied by Solid-State NMR and Computer Modeling. *J. Am. Chem. Soc.* **2017**, *139*, 389–408.

(48) Richner, G.; Puxty, G. Assessing the Chemical Speciation during CO_2 Absorption by Aqueous Amines Using in Situ FTIR. *Ind. Eng. Chem. Res.* **2012**, *51*, 14317–14324.

(49) Garand, E.; Wende, T.; Goebbert, D. J.; Bergmann, R.; Meijer, G.; Neumark, D. M.; Asmis, K. R. Infrared Spectroscopy of Hydrated Bicarbonate Anion Clusters: $HCO_3^-(H_2O)_{1-10}$. *J. Am. Chem. Soc.* **2010**, *132*, 849–856.

(50) Choi, Y.-S.; Im, J.; Jeong, J. K.; Hong, S. Y.; Jang, H. G.; Cheong, M.; Lee, J. S.; Kim, H. S. CO_2 Absorption and Desorption in an Aqueous Solution of Heavily Hindered Alkanolamine: Structural Elucidation of CO_2-Containing Species. *Environ. Sci. Technol.* **2014**, *48*, 4163–4170.

(51) Im, J.; Hong, S. Y.; Cheon, Y.; Lee, J.; Lee, J. S.; Kim, H. S.; Cheong, M.; Park, H. Steric Hindrance-Induced Zwitterionic Carbonates from Alkanolamines and CO_2: Highly Efficient CO_2 Absorbents. *Energy Environ. Sci.* **2011**, *4*, 4284–4289.

(52) Xie, H.-B.; Wei, X.; Wang, P.; He, N.; Chen, J. CO_2 Absorption in an Alcoholic Solution of Heavily Hindered Alkanolamine: Reaction Mechanism of 2-(Tert-Butylamino)ethanol with CO_2 Revisited. *J. Phys. Chem. A* **2015**, *119*, 6346–6353.

(53) Chen, C. H.; Shimon, D.; Lee, J. J.; Mentink-Vigier, F.; Hung, I.; Sievers, C.; Jones, C. W.; Hayes, S. E. The "Missing" Bicarbonate in CO_2 Chemisorption Reactions on Solid Amine Sorbents. *J. Am. Chem. Soc.* **2018**, *140*, 8648–8651.

(54) Shimon, D.; Chen, C. H.; Lee, J. J.; Didas, S. A.; Sievers, C.; Jones, C. W.; Hayes, S. E. ^{15}N Solid State NMR Spectroscopic Study of Surface Amine Groups for Carbon Capture: 3-Aminopropylsilyl Grafted to SBA-15 Mesoporous Silica. *Environ. Sci. Technol.* **2018**, *52*, 1488–1495.

(55) Alkhabbaz, M. A.; Bollini, P.; Foo, G. S.; Sievers, C.; Jones, C. W. Important Roles of Enthalpic and Entropic Contributions to CO_2 Capture from Simulated Flue Gas and Ambient Air Using Mesoporous Silica Grafted Amines. *J. Am. Chem. Soc.* **2014**, *136*, 13170–13173.

(56) Svensson, H.; Hulteberg, C.; Karlsson, H. T. Heat of Absorption of CO_2 in Aqueous Solutions of N-Methyldiethanolamine and Piperazine. *Int. J. Greenh. Gas Control* **2013**, *17*, 89–98.

(57) Didas, S. A.; Kulkarni, A. R.; Sholl, D. S.; Jones, C. W. Role of Amine Structure on Carbon Dioxide Adsorption from Ultradilute Gas Streams such as Ambient Air.

ChemSusChem **2012**, *5*, 2058–2064.

(58) Stowe, H. M.; Vilčiauskas, L.; Paek, E.; Hwang, G. S. On the Origin of Preferred Bicarbonate Production from Carbon Dioxide (CO_2) Capture in Aqueous 2-Amino-2-Methyl-1-Propanol (AMP). *Phys. Chem. Chem. Phys.* **2015**, *17*, 29184–29192.

(59) Bernhardsen, I. M.; Knuutila, H. K. A Review of Potential Amine Solvents for CO_2 Absorption Process: Absorption Capacity, Cyclic Capacity and pKa. *Int. J. Greenh. Gas Control* **2017**, *61*, 27–48.

(60) Chowdhury, F. A.; Yamada, H.; Higashii, T.; Goto, K.; Onoda, M. CO_2 Capture by Tertiary Amine Absorbents: A Performance Comparison Study. *Ind. Eng. Chem. Res.* **2013**, *52*, 8323–8331.

(61) Hicks, J. C.; Drese, J. H.; Fauth, D. J.; Gray, M. L.; Qi, G.; Jones, C. W. Designing Adsorbents for CO_2 Capture from Flue Gas-Hyperbranched Aminosilicas Capable of Capturing CO_2 Reversibly. *J. Am. Chem. Soc.* **2008**, *130*, 2902–2903.

(62) Sumon, K. Z.; Bains, C. H.; Markewich, D. J.; Henni, A.; East, A. L. L. Semicontinuum Solvation Modeling Improves Predictions of Carbamate Stability in the CO_2 + Aqueous Amine Reaction. *J. Phys. Chem. B* **2015**, *119*, 12556–12264.

(63) Didas, S. A.; Zhu, R.; Brunell, N. A.; Sholl, D. S.; Jones, C. W. Thermal, Oxidative and CO_2 Induced Degradation of Primary Amines Used for CO_2 Capture: Effect of Alkyl Linker on Stability. *J. Phys. Chem. C* **2014**, *118*, 12302–12311.

(64) Heydari-Gorji, A.; Belmabkhout, Y.; Sayari, A. Degradation of Amine-Supported CO_2 Adsorbents in the Presence of Oxygen-Containing Gases. *Microporous Mesoporous Mater.* **2011**, *145*, 146–149.

(65) Calleja, G.; Sanz, R.; Arencibia, A.; Sanz-Pérez, E. S. Influence of Drying Conditions on Amine-Functionalized SBA-15 as Adsorbent of CO_2. *Top. Catal.* **2011**, *54*, 135–145.

CHAPTER 4. STERICALLY HINDERED AMINOPOLYMERS FOR CO_2 CAPTURE

4.1 Background

One type of solid supported amine that is heavily researched are aminopolymer/metal-oxide composites, in which the aminopolymer is physically incorporated into the pores of the metal-oxide support.[1–7] These aminopolymer/metal-oxide composites are attractive for practical use due to the ease of incorporating aminopolymers into porous solids and the large CO_2 capacities associated with the large amine densities of the aminopolymer. A variety of aminopolymers have been studied for CO_2 adsorption, including poly(ethylenimine) (PEI),[1,2,8] poly(allylamine) (PAA),[9] and poly(propylenimine) (PPI).[4,10–12]

Out of all the polymers studied, branched poly(ethylenimine) is particularly attractive for practical use due to its commercial availability and good CO_2 capacities and kinetics.[8] However, PEI is prone to oxidative degradation due to the high temperatures used for regeneration.[4,13] In addition, recent studies have suggested that the energy required for regenerating such sorbents are a key cost driver of the separations process.[14,15] Min et al. demonstrated that sorbents that contain PEI functionalized with various epoxide groups required lower amounts of energy for regeneration than sorbents that contain unfunctionalized PEI, due to weak amine-CO_2 species formed and the sorbents more hydrophobic nature.[15] Another possible route to reduce energy and temperatures required for regeneration is to use primary amines that have a tertiary α-carbon or secondary amines

that have a secondary or tertiary α-carbons, otherwise known as sterically hindered amines.[16] Hindered amines have been effective for energy efficient CO_2 capture and desorption in aqueous solution due to their weak amine-CO_2 binding and high amine efficiencies (up to 1 mol CO_2 adsorbed/mol N)..[16,17] In addition, hindered primary amines are expected to be oxidatively stable because there are no hydrogen atoms to abstract on their α-carbon.[18] This is important because the initial degradation event of oxidation is thought to occur by hydrogen abstraction from the α-carbon.[19–21]

While hindered amine solutions have been researched for the past 30 years[16,17,22] and have been commercially employed by Mitsubishi Heavy Industries,[23] studies on solid supported hindered amines are limited.[18,24–26] In Chapter 3, it was observed that silane grafted sterically hindered molecular amines had similar CO_2 capacities and weaker amine-CO_2 species when compared to a supported unhindered primary amine under humid conditions.[18] However, low amine loadings were achieved in that study (1.8 mmol N/g_{SiO2}), resulted in modest CO_2 capacities. This study aims to synthesize an aminopolymer with large densities of hindered amine moieties, incorporate the polymer into mesoporous SBA-15, and compare the CO_2 adsorption performance of the resulting composite material to silica composites that are incorporated with unhindered aminopolymer PEI, which is the benchmark aminopolymer for CO_2 capture.[27]

4.2 Experiments

4.2.1 Materials

Hydrochloric acid (36 wt%) was purchased from Alfa Aesar and 2-methylpropane-1,2-diamine dihydrochloride was purchased from Enamine. Deuterated methanol (CD_3OD), deuterated chloroform ($CDCl_3$), deuterium oxide (D_2O), chromium (III) acetylacetonate, Poly(ethylenimine) (M_w 800), Pluronic P-123, tetraethyl orthosilicate (TEOS, 98%), chlorosulfonic acid (99%), sodium hydroxide, potassium hydroxide, 2-amino-2-methyl-1-propanol (AMP, 95%), and AMBERSEP 900 ion exchange resin were purchased from Sigma Aldrich. Methanol and diethyl ether were purchased from BDH chemicals. Ultra-high purity N_2, ultra-high purity He, bone dry CO_2, and 10% CO_2/10% He/80% N_2 were purchased from Airgas.

4.2.2 Materials Synthesis

SBA-15 synthesis was based on a previous procedure.[28] Pluronic P-123 (24.0 g) was dissolved in concentrated hydrochloric acid (120 mL) and deionized (DI) water (636 mL) in a 2 L Erlenmeyer flask. The solution was stirred for 3 h at room temperature. Tetraethyl orthosilicate (46.24 g) was added dropwise to the solution, and the mixture was subsequently stirred for 20 h at 40 °C. Afterwards, the stir bar was removed, and the mixture temperature was maintained at 100 °C for 24 h. The mixture was then quenched and filtered with copious amounts of distilled water, and the resulting white powder was then dried overnight in an oven at 75 °C. Afterwards, the white powder was calcined using the following procedure: ramp to 200 °C at 1.2 °C min^{-1}, hold at 200 °C for 2 h, ramp to 550 °C at 1.2 °C min^{-1}, hold at 550 °C for 6 h, and cool to room temperature.

The synthesis of poly(2,2-dimethylenimine) was based on a previous procedure.[1,29–32] First, AMP (5.64 g) was dissolved in diethyl ether (600 mL) in a 1 L round bottom flask. The mixture was cooled to 0 °C by an ice bath. Next, chlorosulfonic acid (5.4 mL) was added dropwise, and a white precipitate immediately formed. The mixture was then stirred for 3 h and the resultant product, 2-amino-2-methyl-1-propanol hydrogen sulfate, was washed with copious amounts of diethyl ether and dried overnight on a Schlenk line under vacuum (<20m Torr) at room temperature. The reaction was conducted twice to yield the required amount of 2-amino-2-methyl-1-propanol hydrogen sulfate for the next step. ^{1}H NMR (400.1 MHz, D_2O): δ (ppm) 1.30 (s), 3.94 (s). ^{13}C NMR (100.6 MHz, D_2O): δ (ppm) 72.00, 53.62, 21.64.

Next, 2-amino-2-methyl-1-propanol hydrogen sulfate (18.24 g) was dissolved with water (89.69 g) in a 100 mL round bottom flask. To start the reaction, 20.4 g of 50 wt% aqueous solution of NaOH was added to the flask and connected to a vacuum distillation apparatus. The mixture was stirred at room temperature for 2 h. Next, the temperature of the mixture was increased to 60 °C. Once this temperature was reached, vacuum was slowly introduced into the reaction vessel and crude 2,2-dimethylenimine was distilled as a clear liquid. Next, increments of 0.30 g NaOH were added and dissolved into a centrifuge tube containing 2,2-dimethylenimine until the solution was saturated with NaOH. Two layers were observed upon adding NaOH, and the top layer, consisting of 2,2-dimethylenimine (4.76 g, 0.81 g/mL at 25 °C), was removed by a pipette and stored in a freezer. ^{1}H NMR (400.1 MHz, $CDCl_3$): δ (ppm) 1.56 (s), 1.25 (s). ^{13}C NMR (100.6 MHz, $CDCl_3$): δ (ppm) 33.83, 31.56, 25.14.

In a 75 mL pressure tube, 2,2 dimethylethylenimine (2.9 mL), 2-methylpropane-1,2-diamine dihydrochloride (0.28 g), and DI water (2.9 g) was stirred for 60 h at 70 ℃. The mixture was brought to room temperature and was stirred with 25 mL of AMBERSEP 900 to remove chloride ions. The mixture was then filtered with deionized water and subsequently purified by rotary evaporation to produce poly(2,2-dimethylenimine) (PDMEI), in the form of a light-yellow viscous liquid. Elemental analysis confirmed that no chloride ions remained.

Polymer/silica composites were prepared by wet impregnation. First, SBA-15 was dried in a round bottom flask overnight on a Schlenk line at 100 ℃ under vacuum (<20 mTorr). Next, 10 mL of methanol was added into the round bottom flask containing SBA15, and the slurry was stirred for 30 min. In a separate vial, the required amount of polymer was dissolved in 5 mL of methanol. The methanolic polymer solution was added into the round bottom flask containing the SBA-15 slurry and was stirred at room temperature for 4 h. Afterwards, the methanol was removed by rotary evaporation at room temperature, and the resulting powder was dried overnight under vacuum (<20 mTorr) at room temperature.

4.2.3 Materials Characterization

^{1}H NMR and ^{13}C NMR experiments to characterize 2,2-dimethylenimine and the 2-amino-2-methyl-1-propanol hydrogen sulfate were conducted on a Bruker AVIII-400 spectrometer operating at 400.1 MHz and 100.6 MHz respectively.

Inverse-gated ^{13}C NMR and Distortionless Enhancement by Polarization Transfer (DEPT-135) experiments were conducted on the PDMEI sample using a Bruker Avance

III HD 500 MHz spectrometer operating at 125.7 MHz. The inverse-gated ^{13}C NMR experiment was run with 8000 scans at a recycle time of 5 times the spin lattice relaxation time of the slowest relaxing carbon on the aminopolymer (T_1=1.2 sec). Chromium (III) acetylacetonate (6 mg) was added to the NMR tube consisting of poly(2,2-dimethylenimine) (70 mg) and CD_3OD (0.75mL) to assist in reducing long spin lattice relaxation times (T_1) of the carbons on the aminopolymer for the inverse-gated ^{13}C NMR experiments. A relaxation study was conducted prior to the inverse-gated ^{13}C NMR experiment to find the relaxation times of all carbons on the aminopolymer. Proton NMR of PDMEI was conducted on a Bruker AVIII-400 spectrometer operating at 400.1 MHz with CD_3OD as the solvent.

Aqueous phase gel permeation chromatography (GPC) was performed using a Shimadzu HPLC system with a refractive index detector (RID-10A) and TSKgelG3000-G6000-PWxl-CP, G3000-PWxl-CP, and G5000-PWxl-CP columns. The eluent phase consisted of 0.4 M acetic acid and 0.3 M $NaNO_3$ and was flowed at 1 mL/min. Poly(ethylenimine) of known molecular weights were used as standards. Electrospray Ionization-Mass Spectrometry (ESI-MS) was conducted on a Waters Quattro LC system for PDMEI.

Nitrogen physisorption was performed on a Micromeritics Tristar II instrument at -196 ℃. The samples were activated under vacuum at 60 ℃ for 12 h before the measurement. Resulting N_2 adsorption isotherms were used to calculate surface area using the Brunauer-Emmett-Teller (BET) method.[33] The P/P_o range used to calculate BET surface areas was 0 – 0.3. Pore volumes were determined by total amount of N_2 adsorbed

at P/P_o=0.95 and pore size distributions were calculated using the NLDFT isothermal model with Quantachrome VersaWin software.[34]

Elemental analysis (Atlantic Microlabs, Norcross, GA) was used to determine amine loadings of the sorbents. Total organic loadings were estimated by thermogravimetric analysis (TGA) using a Netzsch STA409 instrument. The samples were analyzed by increasing the temperature to 900 ℃ from room temperature at a rate of 10 ℃/min under combined air (90 mL/min) and N_2 (30 mL/min) flow. The organic loadings were estimated by the mass loss between 120 and 900 ℃. The ratio of the amount of PEG to aminopolymer in the composites was estimated by the following equation.[35]

$$\frac{g\ C}{g\ N} = \frac{\frac{g\ C}{g\ aminopolymer} * g\ aminopolymer + \frac{g\ C}{g\ PEG} * g\ PEG}{\frac{g\ N}{g\ aminopolymer} * g\ aminopolymer} \qquad (4.1)$$

4.2.4 CO_2 and H_2O Adsorption Measurements

Water adsorption measurements were conducted at both 30 and 40 ℃ on a Micromeritics 3Flex, which measures single-component water vapor adsorption isotherms using the volumetric method. Samples were activated at 60 ℃ for 12 h before each run.

A TA Instruments Q500 thermogravimetric analyzer (TGA) was used to measure the dry CO_2 uptake capacity. About 10-15 mg of sample was used for each run. Each sample was activated in He flow at 60 ℃ for 3 h. The sample was then cooled to the desired adsorption temperature and the gas was switched to a 10% CO_2/He mixture at atmospheric

pressure for 2 h. The CO_2 capacity was calculated based on the weight change between the activated sample and after exposure to 10% CO_2/He for 2 h. The Q500 TGA was also used to estimate volatility of the samples. Each sample was ramped to the desired temperature (60 or 90 °C) and held at that temperature for 10 h.

A glass fixed bed (6 mm outer diameter x 4 mm inner diameter) was used to obtain CO_2 capacities under humid conditions. A schematic of the apparatus can be seen in Chapter 2.[36] The outlet gas was analyzed using an Omnistar GSD 320 mass spectrometer. The samples were pelletized using a carver press at a pressure of 1000 psi for 30 sec. A typical run used 70-100 mg of sample that was sieved to the size range of 300-500 μm. Before each humid CO_2 adsorption run, all samples were activated under dry N_2 flow (50 mL/min) at 60 °C for 2 h and were presaturated under humid N_2 flow (50 mL/min) at the desired adsorption temperature. Humidity was generated by flowing gases through a sparger containing DI H_2O at a controlled temperature of 18 °C. The sample was considered saturated when the outlet concentration of water matched the inlet concentration of water.

The CO_2 adsorption experiments employed a premixed gas cylinder, which was composed of 10% CO_2/ 10% He/ 80% N_2. The He gas was used as an inert tracer to calculate the dead-time of the fixed bed apparatus. Adsorption runs were stopped once the outlet CO_2 concentration reached 98% of the inlet stream CO_2 concentration. Pseudo-equilibrium CO_2 capacities were calculated by evaluating the area between the He and CO_2 outlet concentrations of the breakthrough curves generated from the adsorption run. The flow rate of the CO_2 containing gas was fixed at 20 mL/min. The accuracy of the instrument was verified by comparing CO_2 capacities calculated between the TGA and fixed bed using

SBA_PEI under dry 10% CO_2 flow at 30 °C, whereby it was determined that there was no difference in capacity.

4.2.5 In Situ FTIR Spectroscopy

A Thermo Nicolet iS10 with a mercury cadmium telluride **(**MCT) detector and a Harrick High Temperature Transmission Cell equipped with CaF_2 windows was used for *in situ* FTIR spectroscopy studies. The samples were pressed into self-supporting wafers at 1000 psig for 30 s using a Carver Press and a pellet die set. Each sample was activated at 60 ℃ for 3 h under He flow and was cooled to 30 ℃ subsequently. The flow rate for all gases was held constant at 50 mL/min at atmospheric pressure.

For dry CO_2 adsorption experiments, 10% CO_2/He was introduced into the cell after activation. The activated sample was used as the background spectrum for dry CO_2 adsorption experiments. For humid CO_2 adsorption experiments, humid helium was introduced into the cell for 2 h after activation to presaturate the sample with water. Humid CO_2 was then introduced into the cell, and spectra were recorded throughout this period using the presaturated sample as the background spectrum. To eliminate additional water vapor peaks for humid CO_2 adsorption experiments, a background spectrum containing water vapor and helium was also subtracted from the results. After CO_2 adsorption, dry or humid He was employed for desorption under dry and humid conditions, respectively.

All CO_2 adsorption spectra were collected for a duration of 65 min. Furthermore, spectra were collected between 0 and 5 min with 1 scan at a resolution of 4 cm^{-1} every 5 sec, and spectra between 5 and 65 min were collected with 64 scans at a resolution of 4 cm^{-1} every 2 min. Desorption spectra were collected with 64 scans at a resolution of 4 cm^{-1}

every 2 min for 60 minutes. After each experiment, the self-supporting wafer was cut with a circular stamp (6.35 mm in diameter) and was weighed to determine its mass. All spectra were normalized by the mass of the wafer (mg).

4.3 Results and Discussion

4.3.1 Synthesis of PDMEI

PDMEI was synthesized by ring opening polymerization of 2,2-dimethylenimine, which had a weight average molecular weight of 600 g/mol (8 repeat units) under the reaction conditions employed. PDMEI had a lower molecular weight and fewer repeat units than PEI samples typically used for CO_2 adsorption (M_w~800, 23 repeat units). The PDMEI polymer was analyzed using electrospray ionization mass spectrometry (ESI-MS), and the molecular weights found suggested that the polymerization was terminated by the diamine capping agent added to the reaction, a hydroxyl group through solvolysis, an unopened 2,2-dimethylenimine group, or cyclization (Figure 4.1). It was also determined by quantitative carbon NMR that the distribution of 1°/2°/3° amines (%) was 19/78/3 (Figure C.2 and Figure C.3). It should be noted that small quantities of unhindered secondary amines were observed (hindered 2°/unhindered 2°~92/8).

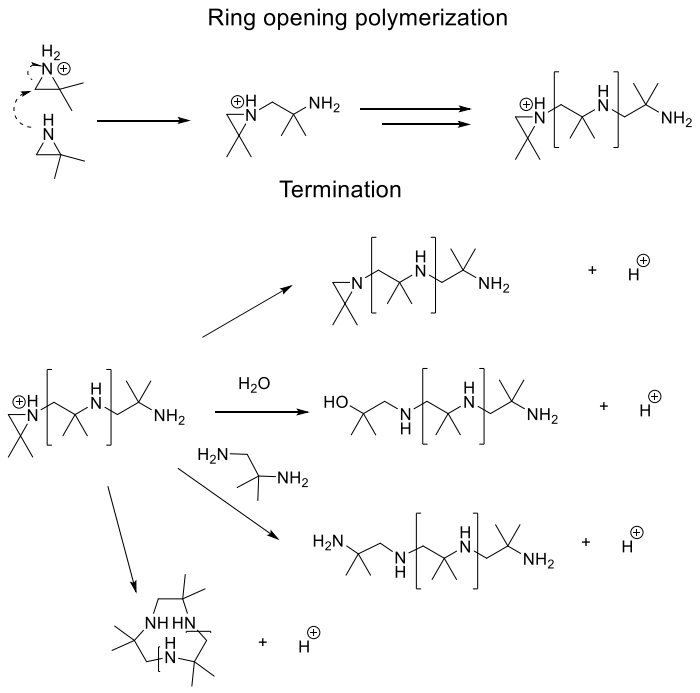

Figure 4.1. Reactions of 2,2-dimethylaziridine.[32,37–39]

4.3.2 Thermal Stability of Materials

A practical sorbent must be regenerable over multiple cycles. Furthermore, the aminopolymers must not readily volatilize at operational temperatures. The thermal stability of PDMEI (M_w 600) was compared to PEI (M_w 800), which exhibits good thermal stability.[13,40] Neat aminopolymers and aminopolymer/silica composites were held at 60 and 90 °C for 12 hours under N_2 flow and thermal stability was estimated from the slope of mass loss between 200 and 400 min (Figure 4.2). The neat PDMEI polymer exhibited poor thermal stability when compared to neat PEI at 60 and 90 °C. This result may be due in part to the comparatively lower molecular weight of PDMEI. However, the PDMEI polymer/silica composites exhibited low weight loss rates comparable to PEI polymer/silica composites, indicating suitable stability in composite form. It should be noted that both composites had similar amine loadings (Table 4.1). The increased thermal

stability of aminopolymer/silica composites is likely due to hydrogen bonding interactions between the aminopolymer and the hydroxyl groups on the walls of the silica support.[41] The low mass loss observed for SBA_PDMEI suggests that temperatures of 60 and 90 °C can be used to regenerate low molecular weight PDMEI/silica composites.

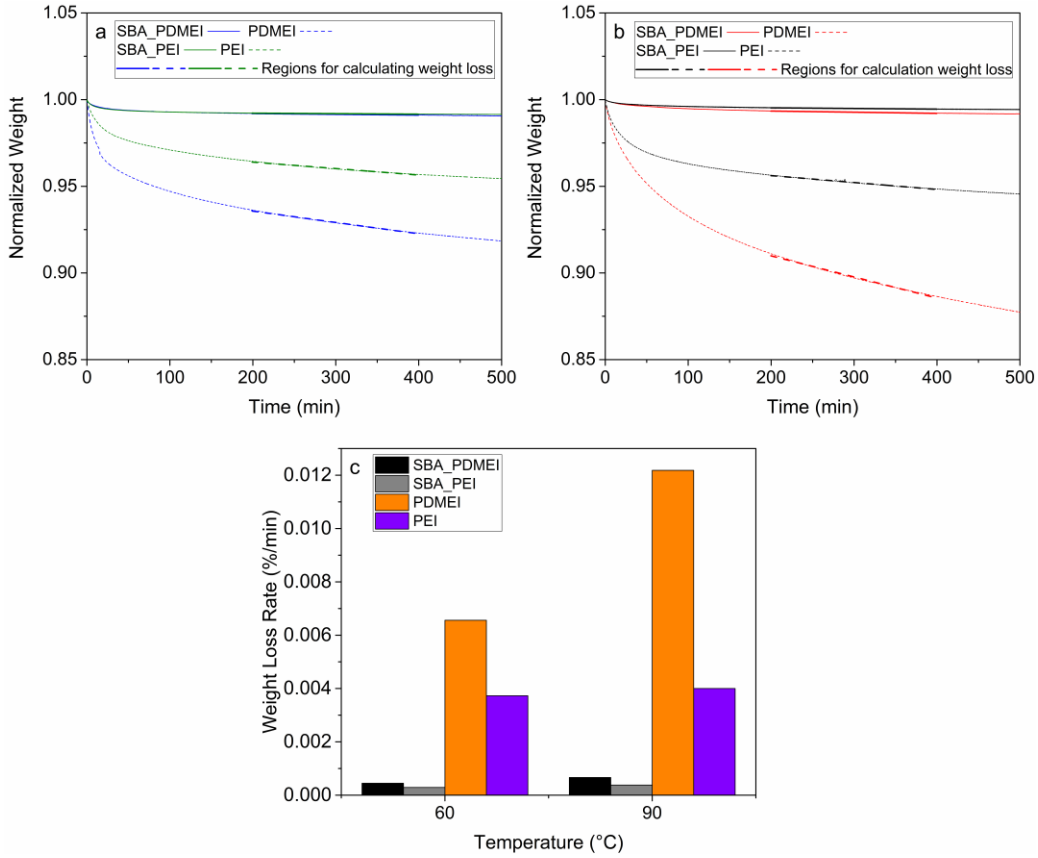

Figure 4.2. Thermogravimetric analysis of the stability of neat polymers and polymer/silica composites conducted at (a) 60 and (b) 90 °C. (c) Weight loss rates for neat polymers and polymer/silica composites.

Table 4.1. Physical and textural properties of aminopolymer/silica composites.

Material	BET Surface Area (m^2/g_{SiO2})	Pore Volume (cm^3/g_{SiO2})	Pore Volume Filled (%)	Amine Loading ($mmol_N/g_{SiO2}$)	Organic Loading (wt%)	PEG/ Aminopolymer Ratio(g/g)
SBA15	834	1.08	-	-		-
SBA_PDMEI	360	0.63	42	5.8	35	-
SBA_PDMEI_PEG	170	0.32	70	6.1	47	0.93
SBA_PEI	415	0.80	26	5.6	23	-
SBA_PEI_PEG	276	0.52	60	5.1	37	0.80

4.3.3 CO_2 and H_2O Adsorption of Aminopolymer/silica Composites

The amine efficiencies (mol CO_2 adsorbed/mol N) of the composite materials were evaluated for 10% CO_2 at 30 and 40 °C under dry and humid conditions (P_{H2O} = 21 mbar) (Figure 4.3a). All sorbents had similar amine loadings, and impregnation of polymers into the support mesopores was confirmed by reduction of pore volume (Table 4.1). All sorbents had an increase in amine efficiency when comparing humid to dry runs, as noted by the efficiency enhancement factor (humid CO_2 amine efficiency/dry CO_2 amine efficiency) (Figure 4.3b). Water can enhance the adsorption capacity by changing the species adsorbed from carbamates (1 CO_2/2 N) to bicarbonates (1 CO_2/1 N) in whole or in part, enhancing amine-CO_2 species formation through hydrogen bonding, by increasing accessible amine sites by enhancing the mobility of polymer chain, and/or freeing the chain from interactions with the silica surface.[42–44] The effect of humidity on adsorption performance was greatly diminished at 40 °C for all sorbents, which may be due to reduced amounts of water adsorbed (Figure 4.4).

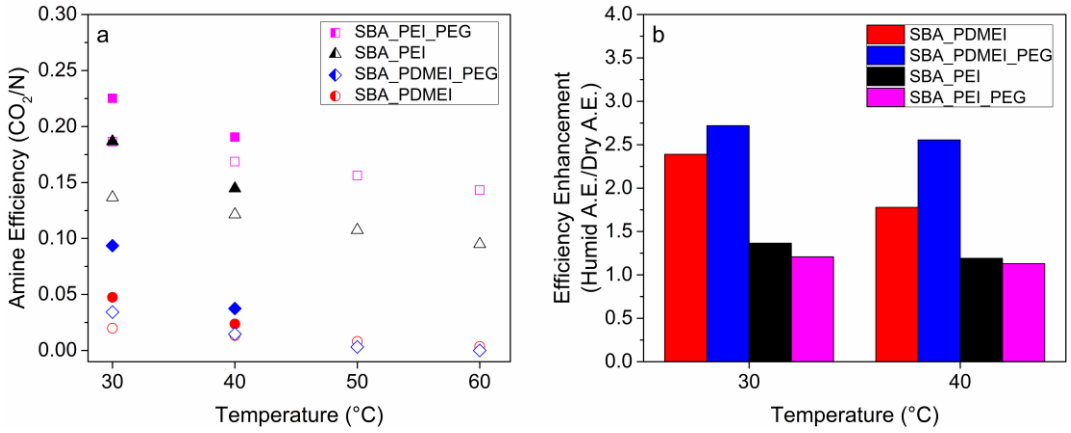

Figure 4.3. (a) Amine efficiencies of aminopolymer/silica composites at 10% CO_2 between 30 and 60 °C. Unfilled and filled shapes represent amine efficiencies under dry and humid conditions (P_{H2O} = 21 mbar) respectively. (b) Efficiency enhancement of aminopolymer/silica composites at 30 and 40 °C.

As expected, SBA_PDMEI was ineffective at capturing CO_2 under dry conditions because of the large quantities of severely hindered secondary amines (72%) found in the PDMEI polymer. Severely hindered secondary amines are unable to form a C-N covalent bond necessary to form amine-CO_2 species typically formed under dry conditions, such as alkylammonium carbamates. However, severely hindered amines, when in the presence of water, should theoretically be active for CO_2 capture by forming alkylammonium bicarbonates. While an increase in amine efficiency is observed for the SBA_PDMEI sample under humid conditions, the hindered aminopolymer sorbent had a lower amine efficiency than SBA_PEI at each condition studied here. In addition, the SBA_PDMEI material exhibited lower amine efficiencies than what was reported in Chapter 3 for sterically hindered aminosilanes (0.18-0.31 mol N/ mol CO_2), which used the same conditions as this study.[18]

One possible explanation for the poor amine efficiency exhibited by SBA_PDMEI when compared to SBA_PEI is that SBA_PDMEI has more mass transfer limitations; the

hindered polymer is expected to have poor polymer mobility due to the heavy monomer units of PDMEI, making it difficult for CO_2 to access the amine sites of PDMEI. Also, the additional methyl substituents in PDMEI makes the polymer more hydrophobic than PEI, resulting in lower water uptakes at the conditions studied here (<0.5 mol H_2O/mol N) (Figure 4.4). Theoretically, one mol H_2O/mol N is required for ammonium bicarbonate formation. Thus, inefficient water uptake may be a key contributor to the low amine efficiencies for SBA_PDMEI.

To improve CO_2 adsorption performance, poly (ethylene glycol) (PEG, M_w=200) was incorporated into the aminopolymer/silica composites. CO_2 uptakes on both hindered and unhindered polymer sorbents were enhanced with the PEG additive at the conditions studied. Like the enhancement effects of water, PEG can improve CO_2 adsorption performance by increasing chain mobility and amine site accessibility.[35,45] The addition of PEG can also make the adsorbents more hydrophilic, increasing the chances of bicarbonates to form on hindered aminopolymer sorbents. Also, the alcohol of the PEG molecule can hydrogen bond with amine-CO_2 species, making it more thermodynamically favourable for such species to form.[46,47]

The SBA_PDMEI_PEG material exhibited higher amine efficiencies and higher efficiency enhancements than SBA_PDMEI under dry and humid conditions. In addition, the SBA_PDMEI_PEG material adsorbed more than the theoretical amounts of water required for ammonium bicarbonate formation at 30 °C under the humid conditions studied here. The theoretical amine efficiency associated with ammonium bicarbonates, however, was not reached for the SBA_PDMEI_PEG sample. In fact, the SBA_PDMEI_PEG sample exhibited lower amine efficiencies than SBA_PEI and SBA_PEI_PEG composites.

Even though there is enough water per amine site, it is possible that some water molecules are not close enough to the amine site to be active for bicarbonate formation. Water is also theorized to enhance the formation of amine-CO_2 species through hydrogen bonding interactions.[48,49] Amine-CO_2 species such as bicarbonates may form more readily in solution due to the large availability of water with which such species may interact.

The PEG additive also increased the amine efficiency of the unhindered polymer sorbent under dry and humid conditions. Efficiency enhancements of the unhindered polymer sorbents were lower than what were found for their hindered counterparts, suggesting that there may be differences in how water improves CO_2 adsorption performance between the two aminopolymers. Both the SBA_PEI and SBA_PEI_PEG samples adsorbed water near or greater than the theoretical amounts for bicarbonate formation at 30 °C. Previous literature suggests that bicarbonate formation on unhindered amines is not likely to form in large quantities under the humid conditions studied here, indicating that an increase in amine efficiency by water is most likely due to reduced mass transfer limitations.[43,50]

A composite with PDMEI and PEI both incorporated into SBA-15 (SBA_PDMEI_PEI) was also studied. The SBA_PDMEI_PEI composite was compared to a PDMEI/silica composite with low amine loading (SBA_PDMEI_lo) and SBA_PEI. Furthermore, the SBA_PDMEI_lo and SBA_PEI composites had comparable amine loadings (mmol N/g_{SiO2}) to the PDMEI and PEI amine loadings respectively of the SBA_PDMEI_PEI composite (Table C.2). No synergistic effects for the SBA_PDMEI_PEI composite were observed as the sum of the amine efficiencies of the

SBA_PDMEI_lo and SBA_PEI were higher than what was observed for SBA_PDMEI_PEI at the conditions studied (Figure C.17).

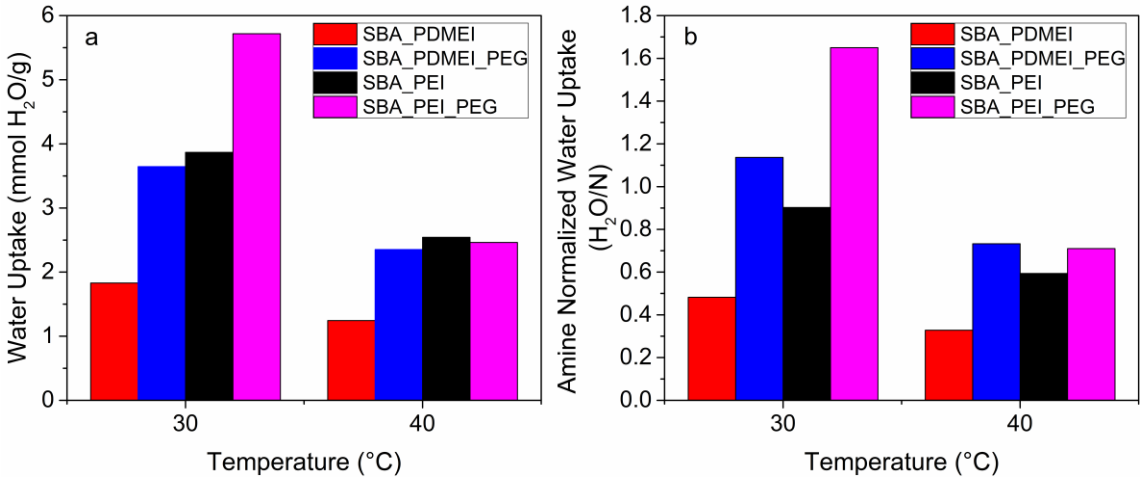

Figure 4.4. (a) Water uptake and (b) amine normalized water uptake of aminopolymer/silica composites at 30 and 40 °C and P_{H2O} = 21 mbar.

4.3.4 FTIR Spectra of Adsorbed CO_2 on Aminopolymer/silica Composites

In situ FTIR spectroscopy experiments were conducted to elucidate the amine-CO_2 species formed on the aminopolymer/silica composites in the presence of dry and humid CO_2 (Figure 4.5). The region typically evaluated for chemisorbed CO_2 species is between 1800 and 1270 cm^{-1}. Peak assignments of amine-CO_2 species are listed in Figure 4.6. For all sorbents, the overall peak areas were larger for humid runs when compared to the dry runs, consistent with efficiency enhancements described in the previous section.

The peaks in the dry CO_2 adsorption spectrum of PEI containing sorbents are associated with carbamates and carbamic acids, as amines cannot form bicarbonates without the presence of water. The main difference between the dry CO_2 adsorption spectrum of SBA_PEI and SBA_PEI_PEG is that the overall peak area is larger for the

SBA_PEI_PEG spectrum. This is consistent with the fact that the SBA_PEI_PEG sample had a higher CO_2 capacity. Also consistent with the measured CO_2 adsorption capacities, there is little change in the overall peak area when comparing humid CO_2 adsorption spectra of SBA_PEI to that of SBA_PEI_PEG.

The peaks associated with bicarbonate modes overlap with peaks associated with the alkylammonium deformation mode and the skeletal vibration of carbamate. To probe if bicarbonates form in the presence of humid CO_2, the peaks associated with bicarbonate stretching vibrations (~1610 and ~1350 cm^{-1}) must increase relative to peaks associated with carbamate stretching modes (1566 and 1477 cm^{-1}) when comparing humid to dry CO_2 adsorption spectra. Peak intensities around 1610 and 1350 cm^{-1} did not increase relative to carbamate stretching mode peaks when comparing the humid and dry CO_2 adsorption spectra of each unhindered aminopolymer sorbent, indicating that bicarbonates did not readily form.

Ammonium carbamate formation was also observed in the dry CO_2 adsorption spectrum of PDMEI containing sorbents. Since severely hindered secondary amines are not able to form the C-N covalent bonds necessary for carbamate formation, the primary and unhindered secondary amines were likely responsible for adsorbing CO_2 in PDMEI sorbents under dry conditions.[16,51] There was an increase of peak intensity at 1614 and 1350 cm^{-1} relative to peaks associated with carbamate (1564 and 1397 cm^{-1}) when comparing the humid and dry CO_2 adsorption spectra of SBA_PDMEI, suggesting formation of ammonium bicarbonate on the hindered polymer sorbent under humid CO_2 flow. However, lower amounts of bicarbonates formed on SBA_PDMEI when compared to molecular amine analogues. In Chapter 3, which was conducted under the same

conditions used here, peaks associated with bicarbonates were more intense for the humid CO_2 adsorption spectra of silica supported hindered aminosilanes.

Consistent with CO_2 adsorption capacities, the overall peak area of the CO_2 adsorption spectrum was larger for SBA_PDMEI_PEG when compared to that of SBA_PDMEI under both dry and humid conditions (Figure C.12). However, the SBA_PDMEI_PEG sorbent appeared to form larger quantities of bicarbonates than SBA_PDMEI in the presence of humidity, as peaks associated with bicarbonate were more intense when comparing the humid CO_2 adsorption spectra of SBA_PDMEI_PEG and SBA_PDMEI. The increase in bicarbonate formation on the SBA_PDMEI_PEG sample may be due to its higher water content, increased polymer mobility, and additional interactions of the amine-CO_2 species with the alcohol group of the PEG molecule. The results here suggest that aminopolymers with hindered amine moieties can be active for CO_2 capture if they are designed to be in a chemical environment that is conducive for amine-CO_2 species to readily form.

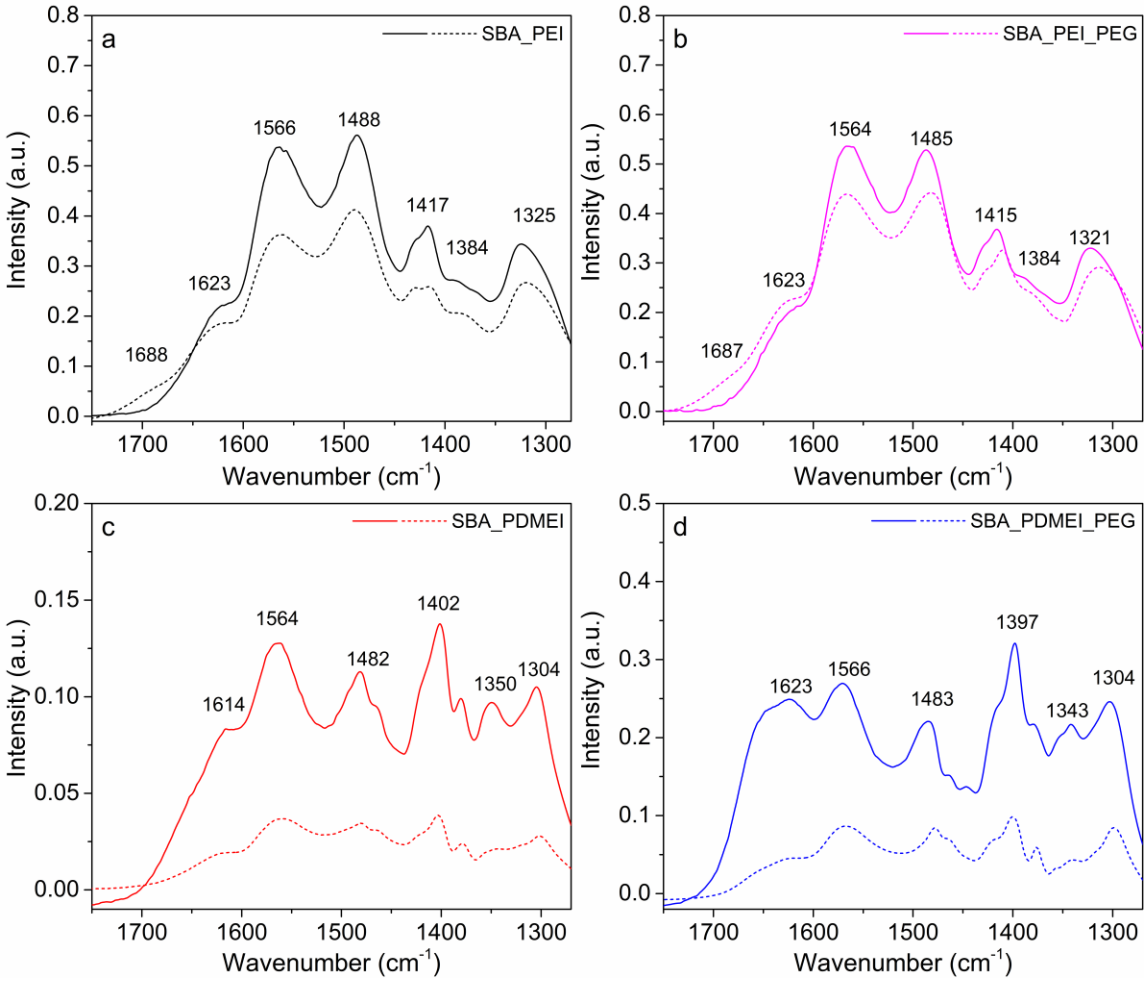

Figure 4.5. FTIR spectra for 10% CO_2 adsorption on (a) SBA_PDMEI, (b) SBA_PDMEI_PEG, (c) SBA_PEI, and (d) SBA_PEI_PEG under dry and humid conditions (P_{H2O} = 21 mbar) at 30 °C after 65 min of time on stream. Solid lines and dotted lines represent humid and dry runs respectively.

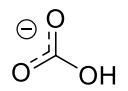

bicarbonate

Assignment	Position (cm^{-1})
CO_2^- asym str.	1650-1600
CO_2^- sym str.	1360-1300

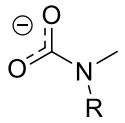

carbamate

Assignments	Position (cm^{-1})
CO_2^- asym str.	1570-1530
CN str.	1500-1470
CO_2^- sym str.	1440-1380
NCO_2^- skeletal vibrations	1350-1300

alkylammonium

Assignments	Position (cm^{-1})
NH_{2-3}^+ def.	1640-1600
NH_{2-3}^+ def.	1520-1470

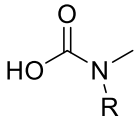

carbamic acid

Assignments	Position (cm^{-1})
C=O str.	1700-1650
CN str.	1500-1470

Figure 4.6. FTIR peaks assignments of vibrational modes of bicarbonate,[36,52] carbamate,[43,53,54] alkylammonium[43,55,56], and carbamic acid.[53] R denotes an alkyl group or a hydrogen atom.

4.3.5 CO_2 Adsorption/Desorption Kinetics

CO_2 adsorption kinetics were also probed using in-situ FTIR spectroscopy by evaluating the integrated peak area associated with amine-CO_2 species (1750-1270 cm^{-1}) during adsorption runs (Figure 4.7). As expected, both humidity and the incorporation of the PEG additive increased the rate of CO_2 adsorption for all sorbents studied. Furthermore, the kinetic data support the hypothesis that the increase in amine efficiency for aminopolymer/silica composites in the presence of water and/or PEG is in part associated with a reduction of mass transfer limitations.[35,45] Water enhanced the CO_2 adsorption kinetics the least on PEG containing samples. This result indicates that the PEG additive

may have sufficiently enhanced mobility of the aminopolymer chain, making the effects of water on CO_2 adsorption kinetics marginal.

The SBA_PDMEI sample under dry conditions had the slowest adsorption and desorption kinetics, which could be due to poor polymer mobility associated with the polymer's bulky monomeric units. However, the SBA_PDMEI_PEG sorbent had a CO_2 uptake rate comparable to PEI containing sorbents, indicating that the kinetics of hindered polymer sorbents can have adsorption rates comparable to unhindered polymer sorbents.

The PEG additive and water also enhance CO_2 desorption rates of the aminopolymer/silica sorbents studied here (Figure C.13 and Figure C.14). It is also apparent when looking at the unnormalized desorption curves (Figure C.15), that after an hour of desorption there are less quantities of CO_2 adsorbed on the hindered amine sorbents. This is the expected result, as hindered amines form weaker chemisorbed species than unhindered amines.

While water enhances CO_2 adsorption/desorption kinetics and amine efficiencies of aminopolymer/silica sorbents studied here, if too much water is present on such sorbents the regeneration energy required will increase, as some energy will go into heating of water.[15] The same argument can be made for any additional organic added into the aminopolymer/silica composite such as PEG.[35] Therefore, aminopolymer/silica composites that are practical CO_2 sorbents will contain limited amounts of excess organic content, adsorb the smallest quantity of water needed to form sufficient amounts of amine-CO_2 species, and have fast polymer dynamics.

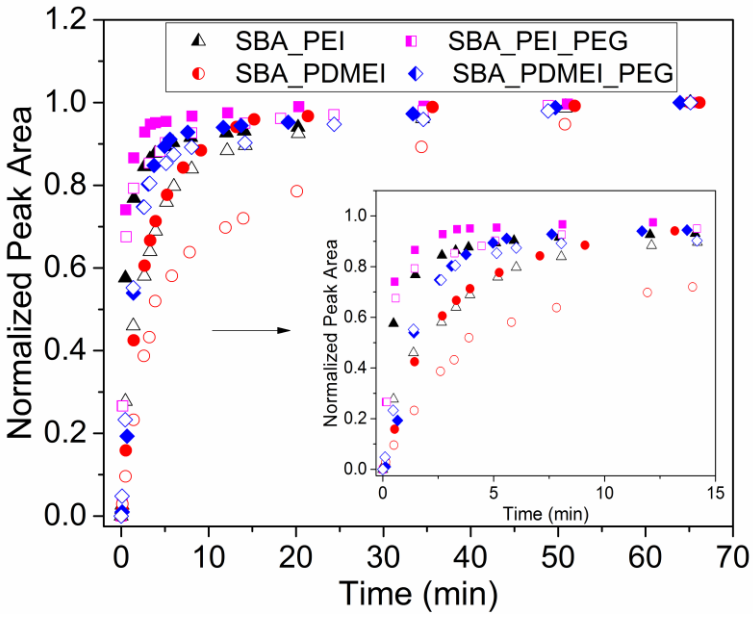

Figure 4.7. Normalized FTIR peak area between 1750 and 1270 cm^{-1} during adsorption of 10% CO_2 under dry and humid conditions (P_{H2O} = 21 mbar) at 30 °C. Unfilled shapes represent dry runs and filled shapes represent humid runs. The curves are normalized such that the end of the adsorption run (65 min) equals 1.

4.4 Conclusions

In this study, sterically hindered polymer PDMEI was synthesized, incorporated into the pores of mesoporous silica, and the CO_2 adsorption performance of the resulting hindered aminopolymer/silica composites were compared to their unhindered counterparts. The SBA_PDMEI and SBA_PDMEI_PEG materials exhibited poor amine efficiencies under dry and humid conditions when compared to SBA_PEI AND SBA_PEI_PEG and silica supported hindered aminosilane sorbents reported Chapter 3. It is posited that the poor performance of the hindered aminopolymer/silica composites is due to poor polymer mobility and hydrophobicity. Aminopolymer/silica composites with the PEG additive achieved faster CO_2 adsorption/desorption kinetics and higher amine efficiencies, indicating that the sorbents were mass transfer limited at the conditions studied. The PEG

additive enhanced formation of ammonium bicarbonate species on the hindered polymer sorbent under humid conditions due to a combination of more adsorbed water and a reduction of mass transfer limitations.

The results of this study suggest the CO_2 adsorption performance of an aminopolymer does not always translate well from its molecular amine derivative; furthermore, the amine type is only one factor to consider when designing aminopolymers. Characteristics such as polymer chain mobility and hydrophilicity must be considered when designing aminopolymers to be used in practical CO_2 sorbents. While the sterically hindered polymers had low amine efficiencies at the conditions studied here, it is posited that polymers with sterically hindered amines moieties can be designed to be active for CO_2 capture given that the chemical environment is favorable for amine-CO_2 species to form.

4.5 References

(1) Holewinski, A.; Sakwa-Novak, M. A.; Jones, C. W. Linking CO_2 Sorption Performance to Polymer Morphology in Aminopolymer/Silica Composites through Neutron Scattering. *J. Am. Chem. Soc.* **2015**, *137*, 11749–11759.

(2) Ma, X.; Wang, X.; Song, C. "Molecular Basket" Sorbents for Separation of CO_2 and H_2S from Various Gas Streams. *J. Am. Chem. Soc.* **2009**, *131*, 5777–5783.

(3) Alkhabbaz, M. A.; Khunsupat, R.; Jones, C. W. Guanidinylated Poly(Allylamine) Supported on Mesoporous Silica for CO_2 Capture from Flue Gas. *Fuel* **2014**, *121*, 79–85.

(4) Pang, S. H.; Lee, L.-C.; Sakwa-Novak, M. A.; Lively, R. P.; Jones, C. W. Design of Aminopolymer Structure to Enhance Performance and Stability of CO_2 Sorbents: Poly(Propylenimine) vs Poly(Ethylenimine). *J. Am. Chem. Soc.* **2017**, *139*, 3627–3630.

(5) Sarazen, M. L.; Jones, C. W. Insights into Azetidine Polymerization for the Preparation of Poly(Propylenimine)-Based CO_2 Adsorbents. *Macromolecules* **2017**,

50, 9135–9143.

(6) Didas, S. A.; Choi, S.; Chaikittisilp, W.; Jones, C. W. Amine–Oxide Hybrid Materials for CO_2 Capture from Ambient Air. *Acc. Chem. Res.* **2015**, *48*, 2680–2687.

(7) Choi, W.; Min, K.; Kim, C.; Ko, Y. S.; Jeon, J. W.; Seo, H.; Park, Y. K.; Choi, M. Epoxide-Functionalization of Polyethyleneimine for Synthesis of Stable Carbon Dioxide Adsorbent in Temperature Swing Adsorption. *Nat. Commun.* **2016**, *7*, 12640−12648.

(8) Xu, X.; Song, C.; Andresen, J. M.; Miller, B. G.; Scaroni, A. W. Novel Polyethylenimine-Modified Mesoporous Molecular Sieve of MCM-41 Type as High-Capacity Adsorbent for CO_2 Capture. *Energy and Fuels* **2002**, *16*, 1463–1469.

(9) Chaikittisilp, W.; Khunsupat, R.; Chen, T. T.; Jones, C. W. Poly(Allylamine)–Mesoporous Silica Composite Materials for CO_2 Capture from Simulated Flue Gas or Ambient Air. *Ind. Eng. Chem. Res.* **2011**, *50*, 14203–14210.

(10) Sarazen, M. L.; Jones, C. W. Insights into Azetidine Polymerization for the Preparation of Poly(Propylenimine)-Based CO2 Adsorbents. *Macromolecules* **2017**, *50*, 9135–9143.

(11) Sarazen, M. L.; Sakwa-Novak, M. A.; Ping, E. W.; Jones, C. W. Effect of Different Acid Initiators on Branched Poly(Propylenimine) Synthesis and CO_2 Sorption Performance. *ACS Sustain. Chem. Eng.* **2019**, *7*, 7338–7345.

(12) Pang, S. H.; Lively, R. P.; Jones, C. W. Oxidatively-Stable Linear Poly(Propylenimine)-Containing Adsorbents for CO_2 Capture from Ultradilute Streams. *ChemSusChem* **2018**, *11*, 2628–2637.

(13) Heydari-Gorji, A.; Sayari, A. Thermal, Oxidative, and CO_2-Induced Degradation of Supported Polyethylenimine Adsorbents. *Ind. Eng. Chem. Res.* **2012**, *51*, 6887–6894.

(14) Lively, R. P.; Realff, M. J. On Thermodynamic Separation Efficiency: Adsorption Processes. *AIChE J.* **2016**, *62*, 3699–3705.

(15) Min, K.; Choi, W.; Kim, C.; Choi, M. Rational Design of the Polymeric Amines in Solid Adsorbents for Postcombustion Carbon Dioxide Capture. *ACS Appl. Mater. Interfaces* **2018**, *10*, 23825–23833.

(16) Sartori, G.; Savage, D. W. Sterically Hindered Amines for Carbon Dioxide Removal from Gases. *Ind. Eng. Chem. Fundam.* **1983**, *22*, 239–249.

(17) Kortunov, P. V.; Siskin, M.; Paccagnini, M.; Thomann, H. CO_2 Reaction Mechanisms with Hindered Alkanolamines: Control and Promotion of Reaction Pathways. *Energy & Fuels* **2016**, *30*, 1223–1236.

(18) Lee, J. J.; Yoo, C. J.; Chen, C. H.; Hayes, S. E.; Sievers, C.; Jones, C. W. Silica-Supported Sterically Hindered Amines for CO_2 Capture. *Langmuir* **2018**, *34*, 12279–12292.

(19) Calleja, G.; Sanz, R.; Arencibia, A.; Sanz-Pérez, E. S. Influence of Drying Conditions on Amine-Functionalized SBA-15 as Adsorbent of CO_2. *Top. Catal.* **2011**, *54*, 135–145.

(20) Bollini, P.; Choi, S.; Drese, J. H.; Jones, C. W. Oxidative Degradation of Aminosilica Adsorbents Relevant to Postcombustion CO_2 Capture. *Energy & Fuels* **2011**, *25*, 2416–2425.

(21) Heydari-Gorji, A.; Belmabkhout, Y.; Sayari, A. Degradation of Amine-Supported CO_2 Adsorbents in the Presence of Oxygen-Containing Gases. *Microporous Mesoporous Mater.* **2011**, *145*, 146–149.

(22) Smith, D. R.; Quinn, J. A. The Prediction of Facilitation Factors for Reaction Augmented Membrane Transport. *AIChE J.* **1979**, *25*, 197–200.

(23) Abu-Zahra, M. R. M.; Sodiq, A.; Feron, P. H. M. Commercial Liquid Absorbent-Based PCC Processes. In *Absorption-Based Post-combustion Capture of Carbon Dioxide*; Paul Feron, Ed.; Woodhead Publishing, 2016; pp 757–778.

(24) Yamada, H.; Fujiki, J.; Chowdhury, F. A.; Yogo, K. Effect of Isopropyl-Substituent Introduction into Tetraethylenepentamine-Based Solid Sorbents for CO_2 Capture. *Fuel* **2018**, *214*, 14–19.

(25) Zhao, Y.; Winston Ho, W. S. Steric Hindrance Effect on Amine Demonstrated in Solid Polymer Membranes for CO_2 Transport. *J. Memb. Sci.* **2012**, *415–416*, 132–138.

(26) Lee, C. S.; Ong, Y. L.; Aroua, M. K.; Daud, W. M. A. W. Impregnation of Palm Shell-Based Activated Carbon with Sterically Hindered Amines for CO_2 Adsorption. *Chem. Eng. J.* **2013**, *219*, 558–564.

(27) Wang, X.; Schwartz, V.; Clark, J. C.; Ma, X.; Overbury, S. H.; Xu, X.; Song, C. Infrared Study of CO_2 Sorption over "Molecular Basket" Sorbent Consisting of Polyethylenimine-Modified Mesoporous Molecular Sieve. *J. Phys. Chem. C* **2009**, *113*, 7260–7268.

(28) Moschetta, E. G.; Sakwa-Novak, M. A.; Greenfield, J. L.; Jones, C. W. Post-Grafting Amination of Alkyl Halide-Functionalized Silica for Applications in Catalysis, Adsorption, and N-15 NMR Spectroscopy. *Langmuir* **2015**, *31*, 2218–2227.

(29) Li, X.; Chen, N.; Xu, J. An Improved and Mild Wenker Synthesis of Aziridines. *Synthesis (Stuttg).* **2010**, *2010*, 3423–3428.

(30) Wenker, H. The Preparation of Ethylene Imine from Monoethanolamine. *J. Am. Chem. Soc.* **1935**, *57*, 2328–2328.

(31) Buckley, B. R.; Patel, A. P.; Wijayantha, K. G. U. Observations on the Modified Wenker Synthesis of Aziridines and the Development of a Biphasic System. *J. Org. Chem.* **2013**, *78*, 1289–1292.

(32) Jones, G. D. The Polymerization of Homologs of Ethylenimine (1). *J. Org. Chem.* **1944**, *9*, 484–499.

(33) Brunauer, S.; Emmett, P. H.; Teller, E. Adsorption of Gases in Multimolecular Layers. *J. Am. Chem. Soc.* **1938**, *60*, 309–319.

(34) Ravikovitch, P. I.; Neimark, A. V. Characterization of Micro-and Mesoporosity in SBA-15 Materials from Adsorption Data by the NLDFT Method. *J. Phys. Chem. B* **2001**, *105*, 6817–6823.

(35) Sakwa-Novak, M. A.; Tan, S.; Jones, C. W. Role of Additives in Composite PEI/Oxide CO_2 Adsorbents: Enhancement in the Amine Efficiency of Supported PEI by PEG in CO_2 Capture from Simulated Ambient Air. *ACS Appl. Mater. Interfaces* **2015**, *7*, 24748–24759.

(36) Lee, J. J.; Chen, C.-H.; Shimon, D.; Hayes, S. E.; Sievers, C.; Jones, C. W. Effect of Humidity on the CO_2 Adsorption of Tertiary Amine Grafted SBA-15. *J. Phys. Chem. C* **2017**, *121*, 23480–23487.

(37) Schatz, V. B.; Clapp, L. B. Reactions of Ethylenimines. V. Hydrolysis. *J. Am. Chem. Soc.* **1955**, *77*, 5113–5116.

(38) Kostyanovskii, R. G.; Leshchinskaya, V. P.; Alekperov, R. K.; Kadorkina, G. K.; Shustova, L. L.; Él'natanov, Y. I.; Gromova, G. L.; Aliev, A. É.; Chervin, I. I. Oligomers of Aziridines and N-β-Aziridinoethylamides. *Bull. Acad. Sci. USSR Div. Chem. Sci.* **1988**, *37*, 2315–2323.

(39) Bunnett, J. F.; McDonald, R. L.; Olsen, F. P. Kinetics of Hydrolysis of Aziridines in Moderately Concentrated Mineral Acids. Relation of Φ Parameters to Reaction Mechanism. *J. Am. Chem. Soc.* **1974**, *96*, 2855–2861.

(40) Zhu, G.; Carrillo, J.-M. Y.; Sujan, A.; Okonkwo, C. N.; Park, S.; Sumpter, B. G.; Jones, C. W.; Lively, R. P. Molecular Blends of Methylated-Poly(Ethylenimine) and Amorphous Porous Organic Cages for SO_2 Adsorption. *J. Mater. Chem. A* **2018**, *6*, 22043–22052.

(41) Holewinski, A.; Sakwa-Novak, M. A.; Carrillo, J.-M. Y.; Potter, M. E.; Ellebracht, N.; Rother, G.; Sumpter, B. G.; Jones, C. W. Aminopolymer Mobility and Support Interactions in Silica-PEI Composites for CO_2 Capture Applications: A Quasielastic Neutron Scattering Study. *J. Phys. Chem. B* **2017**, *121*, 6721–6731.

(42) Mebane, D. S.; Kress, J. D.; Storlie, C. B.; Fauth, D. J.; Gray, M. L.; Li, K. Transport, Zwitterions, and the Role of Water for CO_2 Adsorption in Mesoporous Silica-Supported Amine Sorbents. *J. Phys. Chem. C* **2013**, *117*, 26617–26627.

(43) Didas, S. A.; Sakwa-Novak, M. A.; Foo, G. S.; Sievers, C.; Jones, C. W. Effect of Amine Surface Coverage on the Co-Adsorption of CO_2 and Water: Spectral Deconvolution of Adsorbed Species. *J. Phys. Chem. Lett.* **2014**, *5*, 4194–4200.

(44) Fan, Y.; Labreche, Y.; Lively, R. P.; Jones, C. W.; Koros, W. J. Dynamic CO_2 Adsorption Performance of Internally Cooled Silica-Supported Poly(Ethylenimine) Hollow Fiber Sorbents. *AIChE J.* **2014**, *60*, 3878–3887.

(45) Zhang, L.; Wang, X.; Fujii, M.; Yang, L.; Song, C. CO_2 Capture over Molecular Basket Sorbents: Effects of SiO_2 Supports and PEG Additive. *J. Energy Chem.* **2017**, *26*, 1030–1038.

(46) Miller, D. D.; Chuang, S. S. C. Control of CO_2 Adsorption and Desorption Using Polyethylene Glycol in a Tetraethylenepentamine Thin Film: An in Situ ATR and Theoretical Study. *J. Phys. Chem. C* **2016**, *120*, 25489–25504.

(47) Tanthana, J.; Chuang, S. S. C. In Situ Infrared Study of the Role of PEG in Stabilizing Silica-Supported Amines for CO_2 Capture. *ChemSusChem* **2010**, *3*, 957–964.

(48) Sumon, K. Z.; Bains, C. H.; Markewich, D. J.; Henni, A.; East, A. L. L. Semicontinuum Solvation Modeling Improves Predictions of Carbamate Stability in the CO_2 + Aqueous Amine Reaction. *J. Phys. Chem. B* **2015**, *119*, 12556–12264.

(49) Cho, M.; Park, J.; Yavuz, C. T.; Jung, Y. A Catalytic Role of Surface Silanol Groups in CO_2 Capture on the Amine-Anchored Silica Support. *Phys. Chem. Chem. Phys.* **2018**, *20*, 12149–12156.

(50) Bacsik, Z.; Ahlsten, N.; Ziadi, A.; Zhao, G. Y.; Garcia-Bennett, A. E.; Martín-Matute, B.; Hedin, N. Mechanisms and Kinetics for Sorption of CO_2 on Bicontinuous Mesoporous Silica Modified with n-Propylamine. *Langmuir* **2011**, *27*, 11118–11128.

(51) Xie, H.-B.; Wei, X.; Wang, P.; He, N.; Chen, J. CO_2 Absorption in an Alcoholic Solution of Heavily Hindered Alkanolamine: Reaction Mechanism of 2-(Tert-Butylamino)Ethanol with CO_2 Revisited. *J. Phys. Chem. A* **2015**, *119*, 6346–6353.

(52) Garand, E.; Wende, T.; Goebbert, D. J.; Bergmann, R.; Meijer, G.; Neumark, D. M.; Asmis, K. R. Infrared Spectroscopy of Hydrated Bicarbonate Anion Clusters: $HCO_3^-(H_2O)_{1-10}$. *J. Am. Chem. Soc.* **2010**, *132*, 849–856.

(53) Foo, G. S.; Lee, J. J.; Chen, C.-H.; Hayes, S. E.; Sievers, C.; Jones, C. W. Elucidation of Surface Species through in Situ FTIR Spectroscopy of Carbon Dioxide Adsorption on Amine-Grafted SBA-15. *ChemSusChem* **2017**, *10*, 266–276.

(54) Bossa, J. B.; Theule, P.; Duvernay, F.; Borget, F.; Chiavassa, T. Carbamic Acid and Carbamate Formation in NH_3:CO_2 Ices-UV Irradiation versus Thermal Processes. *Astron. Astrophys.* **2008**, *492*, 719–724.

(55) Socrates, G. *Infrared and Raman Characteristic Group Frequencies*, Third.; John Wiley & Sons LTD, 2001.

(56) Danon, A.; Stair, P. C.; Weitz, E. FTIR Study of CO_2 Adsorption on Amine-Grafted SBA-15: Elucidation of Adsorbed Species. *J. Phys. Chem. C* **2011**, *115*, 11540–11549.

CHAPTER 5. SUMMARY & FUTURE DIRECTIONS

5.1 Summary

This dissertation provides direct spectroscopic evidence (NMR and FTIR) that ammonium bicarbonates can form on solid supported amines. Furthermore, the supported tertiary and sterically hindered amine materials that were studied in this dissertation formed ammonium bicarbonates in the presence of water and dilute concentrations of CO_2. It should be noted that the formation of ammonium bicarbonates on these materials were modest when compared to their solution counterparts under the conditions employed here. It is posited that ammonium bicarbonates are less likely to form on solid supports than in solution due to smaller quantities of water found on solid supports. The results from this dissertation also suggest that tertiary amine-based sorbents are not likely to become practical CO_2 sorbents under direct air capture (DAC) and flue gas conditions due to their low CO_2 capacities.

Upon exposure to concentrations of CO_2 typically seen in flue gas (10 vol%) and water vapor, sterically hindered aminosilane grafted sorbents were found to have similar amine efficiencies (mol CO_2 adsorbed/mol N) and form weakly bound amine-CO_2 species when compared to their unhindered counterparts; furthermore, the CO_2 adsorption performance of these materials was promising and suggested that supported sterically hindered amines could be used in a practical separations process. However, only modest CO_2 capacities (CO_2 adsorbed per gram sorbent) associated with low amine densities were achieved on sterically hindered aminosilane grafted sorbents.

With the hopes of achieving high CO_2 capacities, an aminopolymer with large densities of sterically hindered amine moieties was synthesized and incorporated into the pores of a silica support. Unfortunately, the CO_2 adsorption performance of the resulting sterically hindered aminopolymer/silica composites was poor when compared to unhindered aminopolymer/silica composites and sterically hindered aminosilane grafted sorbents. Furthermore, the sterically hindered aminopolymer/silica composites were posited to have poor CO_2 adsorption performance due to (i) mass transfer limitations associated with poor polymer chain mobility and (ii) the hydrophobic nature of the composite materials. While the sterically hindered aminopolymer/silica composites studied here had poor amine efficiencies, it is predicted that polymers with sterically hindered amines moieties can be designed to be active for CO_2 capture given that the chemical environment is favorable for amine-CO_2 species to form.

The results from these studies suggest that the CO_2 adsorption performance of an aminopolymer does not always translate well from its molecular amine derivative and indicates that amine type is only one factor to consider when designing aminopolymer-based materials for practical CO_2 capture. Factors such as polymer chain mobility and hydrophilicity must also be taken into consideration when designing an effective CO_2 sorbent.

5.2 Future Directions

Potential future research directions on supported amine materials that build directly from this dissertation are proposed below:

5.2.1 Determination of the Quantity of Water Required for the Formation of Amine-CO_2 Species

A computation-based study on the amount of water molecules required to form practical amounts of amine-CO_2 species such as alkylammonium bicarbonates would be particularly useful. Water is thought to enhance the formation of amine-CO_2 species through hydrogen bonding interactions.[1–3] The findings of this dissertation infer that alkylammonium bicarbonates may not form readily on supported materials due the small quantities of water present. Furthermore, tertiary and sterically hindered amines in aqueous solutions have been found to reach the theoretical amine efficiency associated with alkylammonium bicarbonate, implying that water has a significant effect on the formation of such species.[4] In addition, the amount of water adsorbed will also affect the regeneration energy required.[5] Finding a theoretical minimum amount of water required for the formation of large quantities of ammonium bicarbonates would help researchers know if supported amines could form such species with quantities of adsorbed water that are achievable for a practical separations process.

5.2.2 Effect of Amine-CO_2 Species on Aminopolymer Chain Mobility

Aminopolymer/metal-oxide composites are often diffusion limited.[6,7] The rate of diffusion of CO_2 is expected to change over time throughout the CO_2 adsorption process in aminopolymer/metal-oxide composites and is expected to be the fastest when CO_2 is first introduced to the sorbent. Over time, CO_2 will react with amine sites forming ammonium carbamates, carbamic acids, and/or ammonium bicarbonates. The ammonium carbamate species requires two amines to capture one molecule of CO_2 and can cross-link

aminopolymer chains. This crosslinking effect is theorized to decrease the diffusion rate of CO_2.[8] In addition, it is also likely that species such as ammonium bicarbonates and carbamic acids can make aminopolymer chains more rigid, thus increasing mass transfer limitations. It is unknown how each species will affect the chain mobility of aminopolymers. Studying how aminopolymer chain mobility is affected by the formation of each amine-CO_2 species via neutron scattering or NMR spectroscopy could add fundamental insights on the mass transport of CO_2 molecules on supported amine sorbents.

5.2.3 Evaluation of Supported Piperazines for CO_2 Capture

Piperazines are commonly used in aqueous media.[9,10] Piperazines are cyclic compounds that contain 2 amines per molecule. They are observed to have fast CO_2 adsorption kinetics in part because there are always 2 amines adjacent to each other to form alkylammonium carbamates in the presence of CO_2.[9] In addition, piperazines in solution are resistant to oxidative degradation at process conditions.[9] Like sterically hindered amines, piperazines have not been studied in detail for CO_2 adsorption.

5.3 References

(1) Sumon, K. Z.; Bains, C. H.; Markewich, D. J.; Henni, A.; East, A. L. L. Semicontinuum Solvation Modeling Improves Predictions of Carbamate Stability in the CO_2 + Aqueous Amine Reaction. *J. Phys. Chem. B* **2015**, *119*, 12556–12264.

(2) Mebane, D. S.; Kress, J. D.; Storlie, C. B.; Fauth, D. J.; Gray, M. L.; Li, K. Transport, Zwitterions, and the Role of Water for CO_2 Adsorption in Mesoporous Silica-Supported Amine Sorbents. *J. Phys. Chem. C* **2013**, *117*, 26617–26627.

(3) Cho, M.; Park, J.; Yavuz, C. T.; Jung, Y. A Catalytic Role of Surface Silanol Groups in CO_2 Capture on the Amine-Anchored Silica Support. *Phys. Chem. Chem. Phys.* **2018**, *20*, 12149–12156.

(4) Kortunov, P. V.; Siskin, M.; Baugh, L. S.; Calabro, D. C. *In Situ* Nuclear Magnetic

Resonance Mechanistic Studies of Carbon Dioxide Reactions with Liquid Amines in Aqueous Systems: New Insights on Carbon Capture Reaction Pathways. *Energy & Fuels* **2015**, *29*, 5919–5939.

(5) Min, K.; Choi, W.; Kim, C.; Choi, M. Rational Design of the Polymeric Amines in Solid Adsorbents for Postcombustion Carbon Dioxide Capture. *ACS Appl. Mater. Interfaces* **2018**, *10*, 23825–23833.

(6) Xu, X.; Song, C.; Andresen, J. M.; Miller, B. G.; Scaroni, A. W. Novel Polyethylenimine-Modified Mesoporous Molecular Sieve of MCM-41 Type as High-Capacity Adsorbent for CO_2 Capture. *Energy and Fuels* **2002**, *16*, 1463–1469.

(7) Holewinski, A.; Sakwa-Novak, M. A.; Jones, C. W. Linking CO_2 Sorption Performance to Polymer Morphology in Aminopolymer/Silica Composites through Neutron Scattering. *J. Am. Chem. Soc.* **2015**, *137*, 11749–11759.

(8) Wilfong, W. C.; Srikanth, C. S.; Chuang, S. S. C. In Situ ATR and DRIFTS Studies of the Nature of Adsorbed CO_2 on Tetraethylenepentamine Films. *ACS Appl. Mater. Interfaces* **2014**, *6*, 13617–13626.

(9) Rochelle, G.; Chen, E.; Freeman, S.; Van Wagener, D.; Xu, Q.; Voice, A. Aqueous Piperazine as the New Standard for CO_2 Capture Technology. *Chem. Eng. J.* **2011**, *171*, 725–733.

(10) Freeman, S. A.; Dugas, R.; Van Wagener, D. H.; Nguyen, T.; Rochelle, G. T. Carbon Dioxide Capture with Concentrated, Aqueous Piperazine. *Int. J. Greenh. Gas Control* **2010**, *4*, 119–124.

APPENDIX A. SUPPLEMENT TO CHAPTER 2

A.1 Fixed Bed Setup and Discussion on Breakthrough Analysis

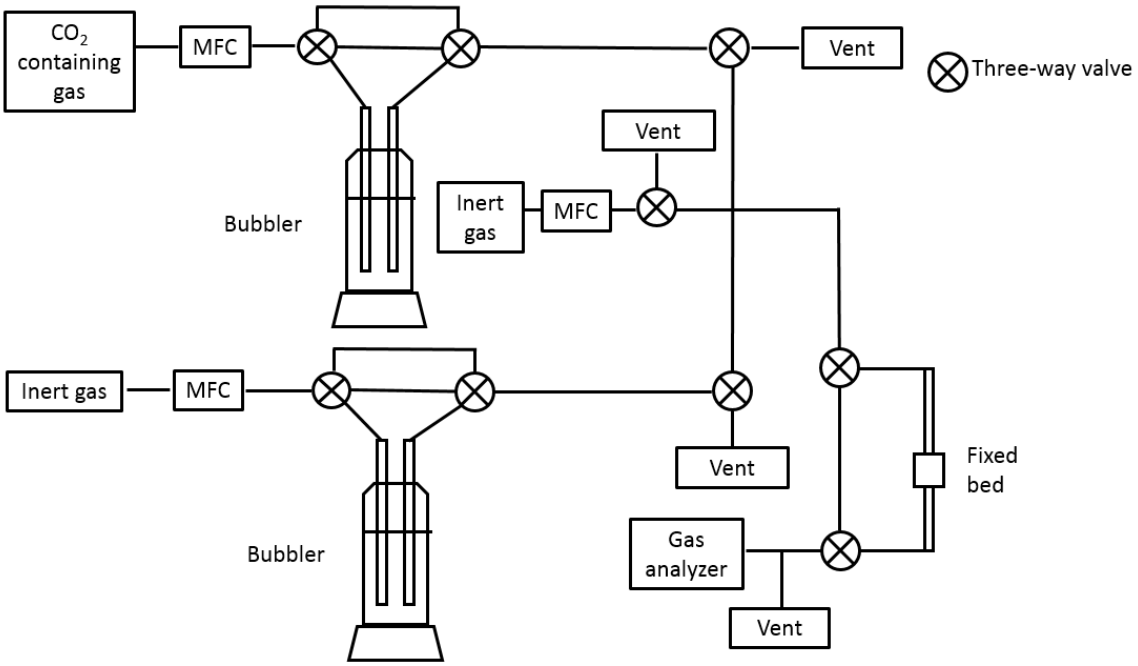

Figure A.1. Fixed bed adsorption testing apparatus.

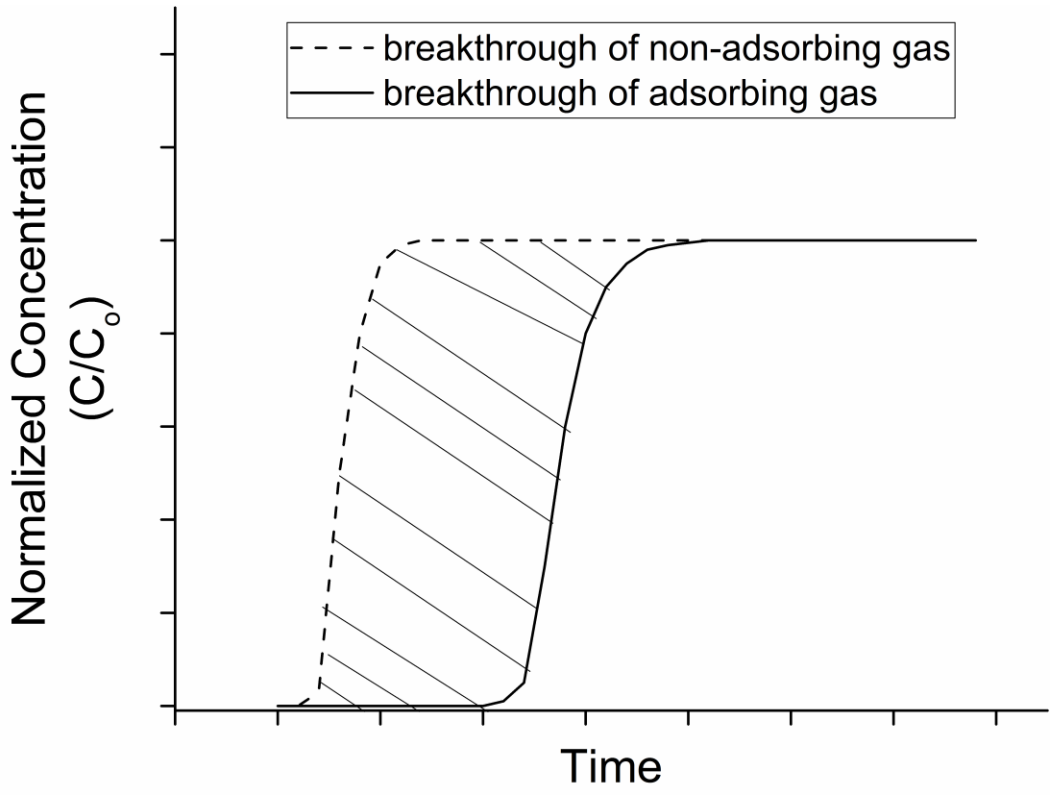

Figure A.2. Examples of breakthrough curves. C and C_o refers to the outlet and inlet concentration of the analyte respectively.

Figure A.2 displays examples of breakthrough curves. The breakthrough curve is a measure of outlet concentration of an analyte versus time on stream. Mean residence time of the system must be taken into account in order to produce accurate sorption capacities. Mean residence time (also known as dead-time) can be accounted for by collecting a breakthrough curve of a non-adsorbing tracer gas in an entirely separate experiment or in the same breakthrough run of the adsorbing species. It should be noted that the IR analyzer used in Chapter 2 can only measure CO_2 and H_2O making it impossible to measure the dead-time of the system using a non-adsorbing tracer gas. In this case, the dead-time can be estimated by collecting a breakthrough curve of the adsorbing species through a bed containing non-adsorbing materials such as glass wool.

The area between the breakthrough curve associated with the dead-time of the system and the breakthrough curve of an adsorbing gas for a sorbent yields the quantity of gas adsorbed on the sorbent. Equation A.1 yields the CO_2 capacity (Q, mmol/g) generated from a breakthrough experiment. In this equation $\dot{n}$ is the molar flow rate of CO_2 at the inlet of the fixed bed (mmol/min), t_q (min) is the integrated area calculated from a breakthrough experiment, and W (g) is the mass of the activated sample used. Desorption capacities can also be calculated by integrating the area below the desorption curves.

$$Q = \frac{\dot{n} * t_q}{W} \tag{A.1}$$

A.2 CO_2 Breakthrough Curves and Humid CO_2 Capacities over Cycles

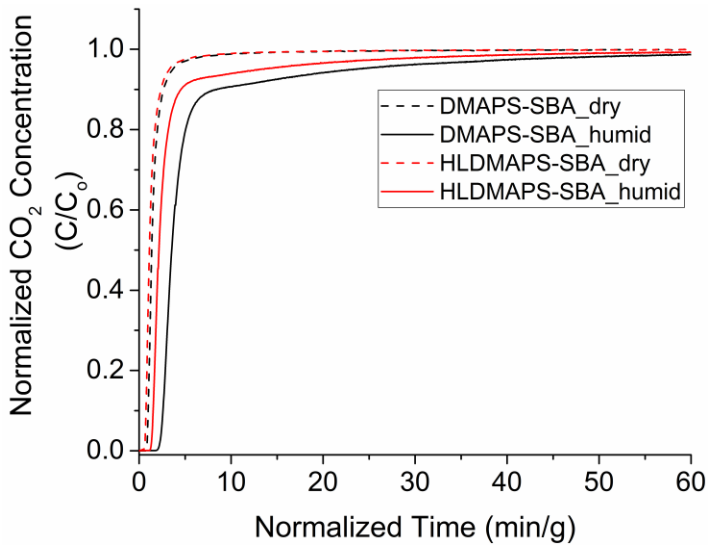

Figure A.3. 1% CO_2/He breakthrough curves at 30 °C for DMAPS-SBA and HLDMAPS-SBA under dry and humid conditions (P_{H2O} = 21 mbar).

Table A.1. Humid fixed bed cycles. CO_2 uptake in mmol/g.

	Cycle 1		Cycle 2	
	Adsorption	Desorption	Adsorption	Desorption
DMAPS-SBA	0.11	0.04	0.11	0.04
HLDMAPS-SBA	0.06	0.02	0.06	0.02

A.3 In Situ FTIR Spectroscopy

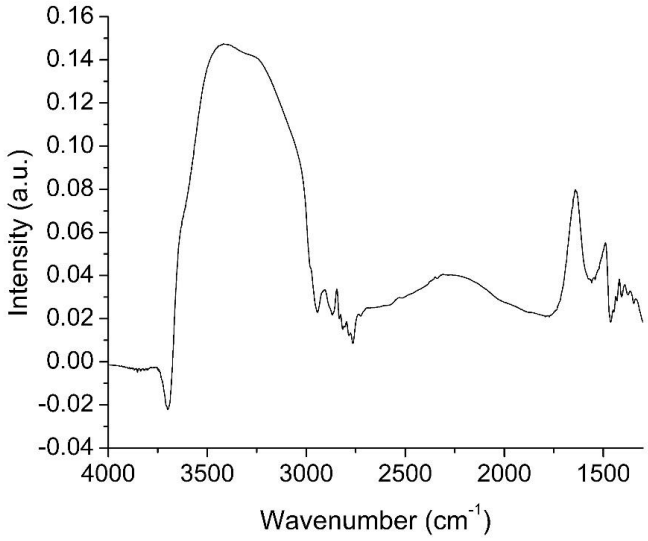

Figure A.4. FTIR spectra of DMAPS-SBA after humid He exposure with the activated sample as the background.

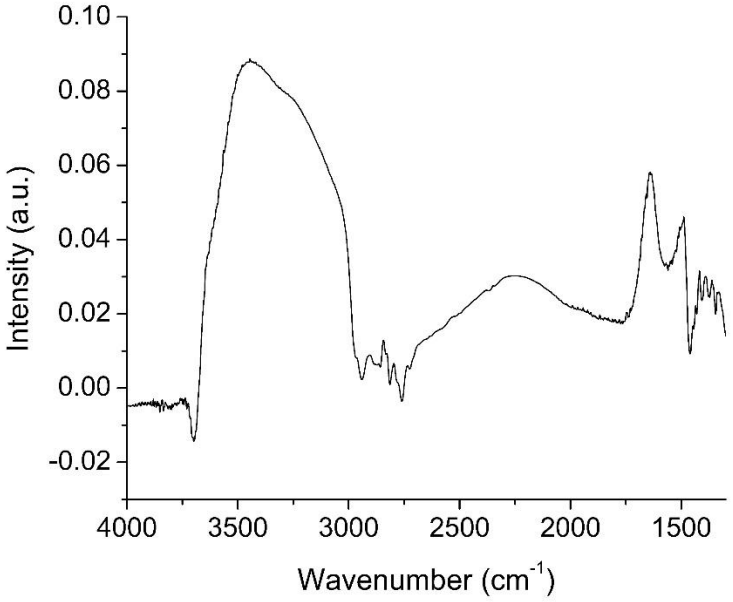

Figure A.5. FTIR spectra of HLDMAPS-SBA after humid He exposure with the activated sample as the background.

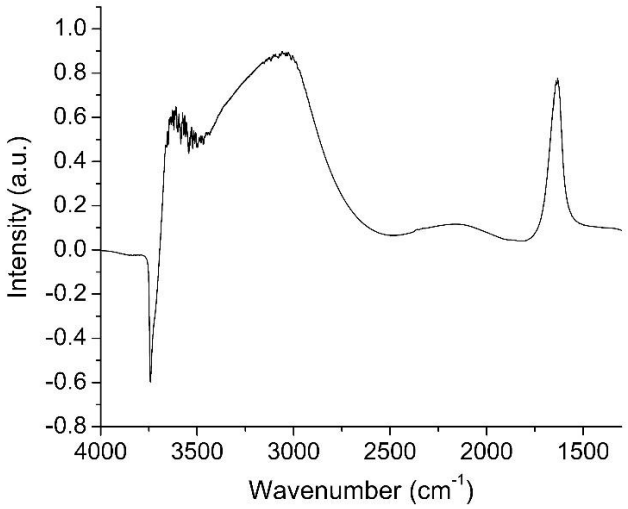

Figure A.6. FTIR spectra of SBA-15 after humid presaturation with the activated sample as the background.

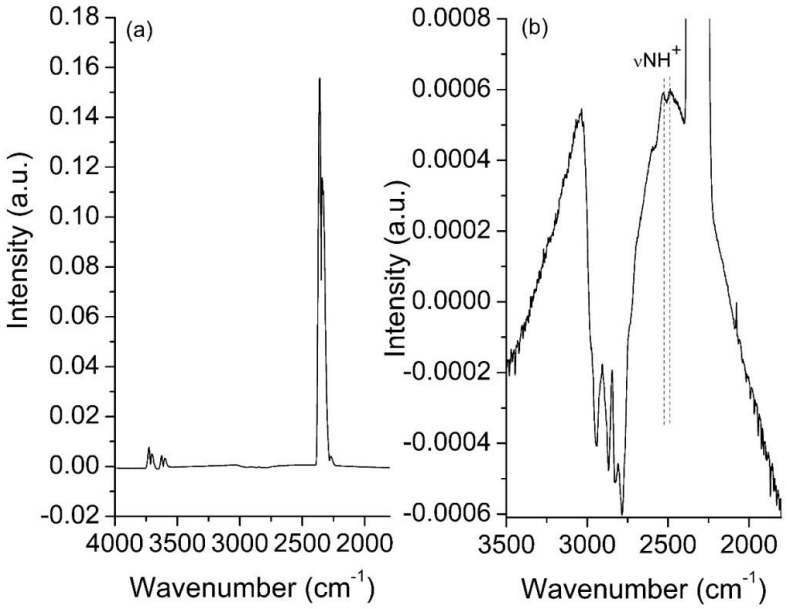

Figure A.7. FTIR spectra of DMAPS-SBA after humid CO_2 exposure with the presaturated sample as the background from (a) 4000-1800 wavenumbers and (b) 3500-1800 wavenumbers.

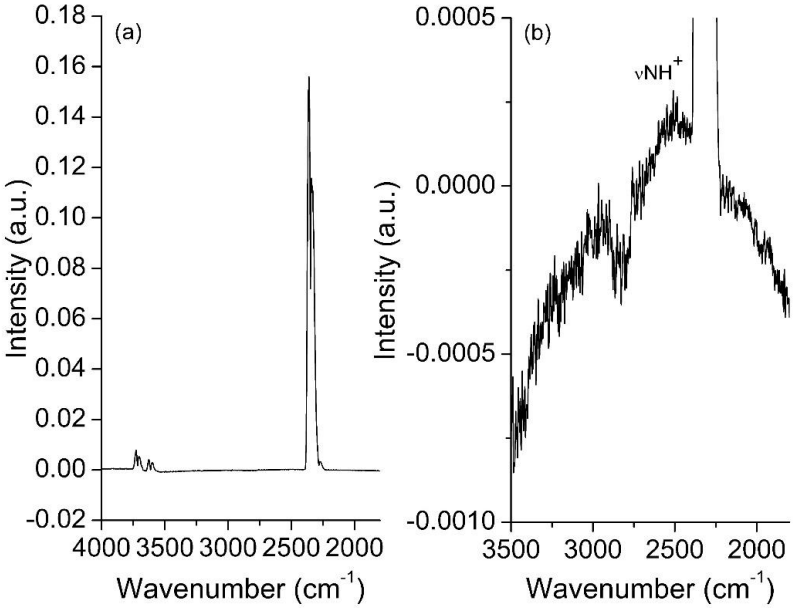

Figure A.8. FTIR spectra of HLDMAPS-SBA after humid CO_2 exposure with the presaturated sample as the background from (a) 4000-1800 wavenumbers and (b) 3500-1800 wavenumbers.

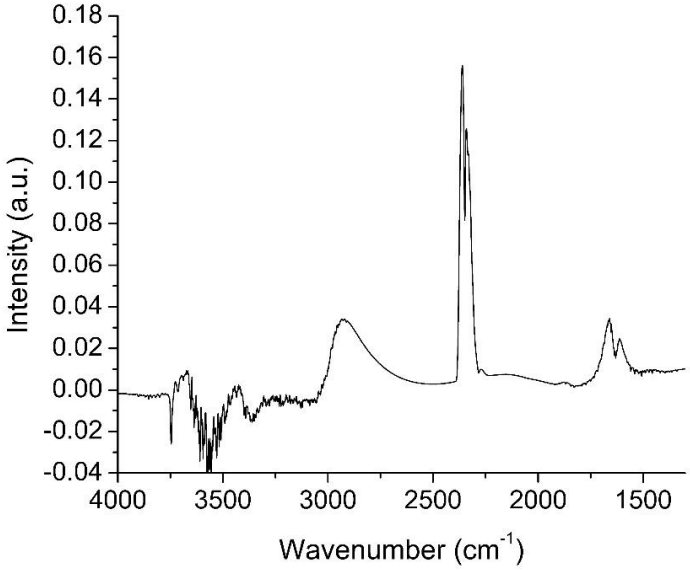

Figure A.9. FTIR spectra of SBA-15 after humid CO_2 exposure with the presaturated sample as the background.

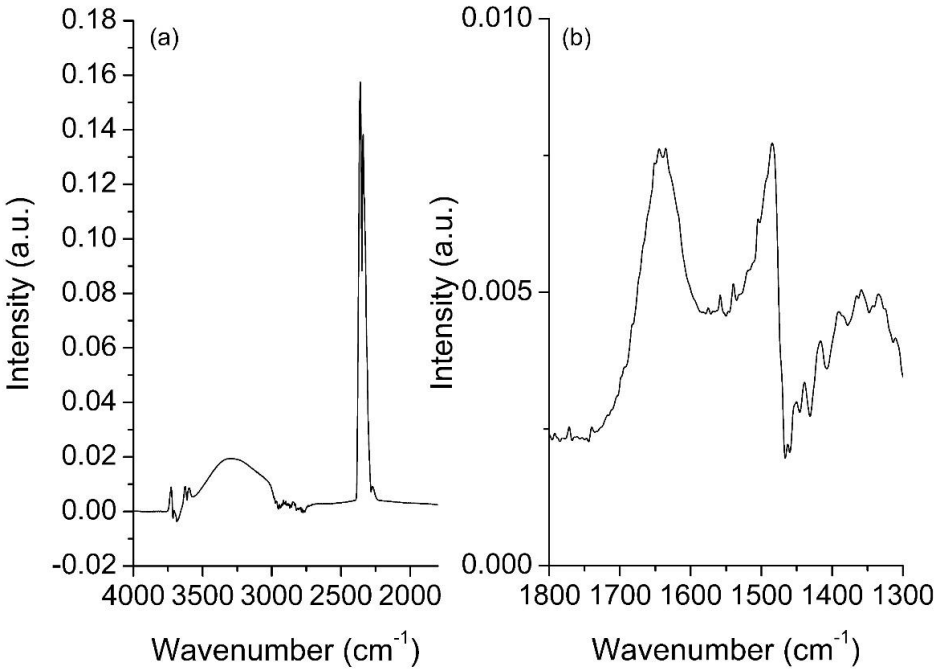

Figure A.10. FTIR spectra of DMAPS-SBA after dry CO_2 exposure with the presaturated sample as the background from (a) 4000-1800 wavenumbers and (b) 1800-1300 wavenumbers.

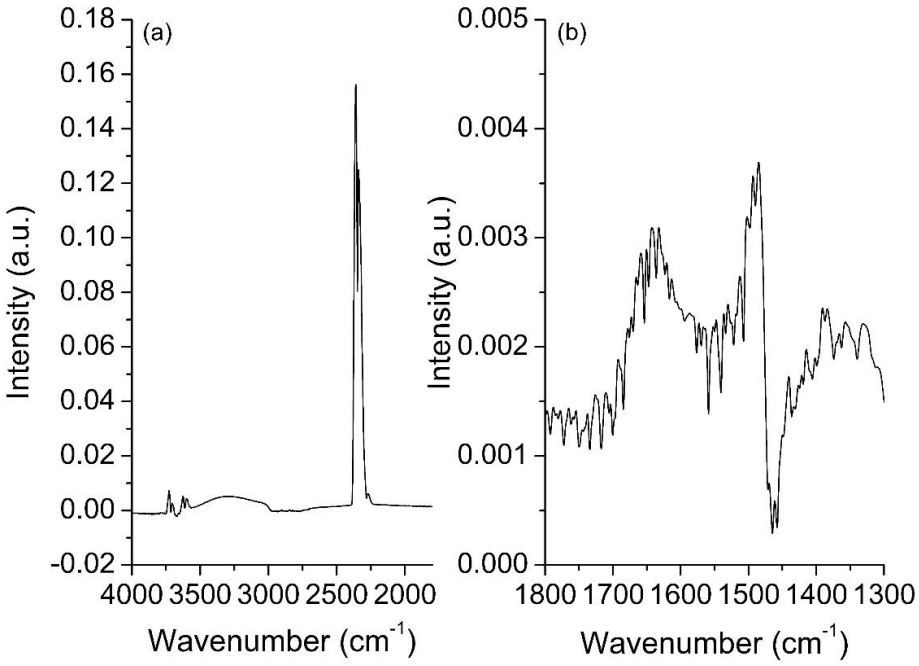

Figure A.11. FTIR spectra of HLDMAPS-SBA after dry CO_2 exposure with the activated sample as the background from (a) 4000-1800 wavenumbers and (b) 1800-1300 wavenumbers.

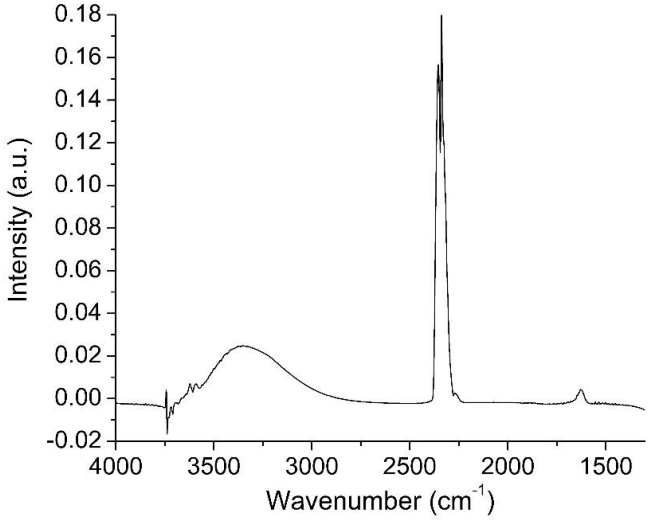

Figure A.12. FTIR spectra of SBA-15 after dry CO_2 exposure using the activated sample as the background.

APPENDIX B. SUPPLEMENT TO CHAPTER 3

B.1 N_2 Adsorption/Desorption Isotherms and Pore Size Distributions

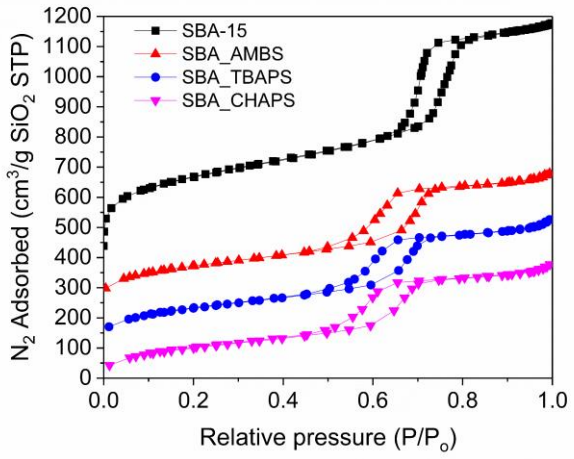

Figure B.1. Nitrogen adsorption/desorption isotherms for bare and functionalized silica. Isotherms are offset by 130 cm^3/g SiO_2 STP.

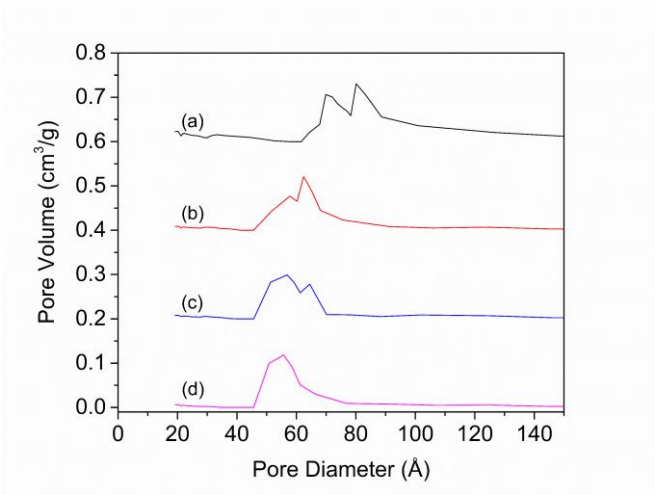

Figure B.2. Pore size distributions of (a) SBA-15, (b) SBA_AMBS, (c) SBA_TBAPS, and (d) SBA_CHAPS calculated from the N_2 physisorption isotherms (BdB-FHH). Pore size distributions are offset by 0.2 cm^3/g.

B.2 CO_2 Breakthrough Curves and Capacities

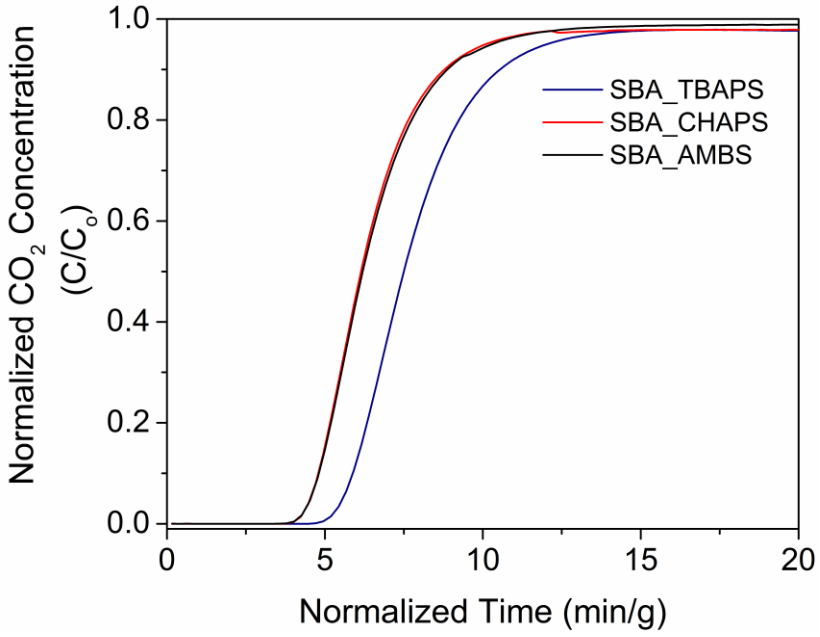

Figure B.3. 10% CO_2/He breakthrough curves at 30 ℃ for the first run of each hindered amine sorbents under humid conditions (P_{H2O} = 21 mbar).

Table B.1. CO_2 adsorption capacities (mmol/g) for each hindered amine sorbent at 30 ℃ under 10% CO_2/He flow under dry and humid conditions (P_{H2O} = 21 mbar).

Run Type	SBA_AMBS	SBA_CHAPS	SBA_TBAPS	DMAPS-SBA
dry run (TGA)	0.12	0.10	0.05	–
dry run (fixed bed)	0.11	0.08	0.06	–
humid run 1 (fixed bed)	0.35	0.35	0.59	0.31
humid run 2 (fixed bed)	0.43	0.34	0.55	–
humid run 3 (fixed bed)	0.41	0.32	0.59	–

The CO_2 adsorption capacity of the DMAPS-SBA sample from Chapter 2 was also re-evaluated at the conditions studied in Chapter 3 (10% CO_2/He, P_{H2O} = 21 mbar). The

humid CO_2 capacity of DMAPS-SBA was lower than that of the hindered amine sorbents (Table B.1.).

B.3 Water Adsorption Isotherms

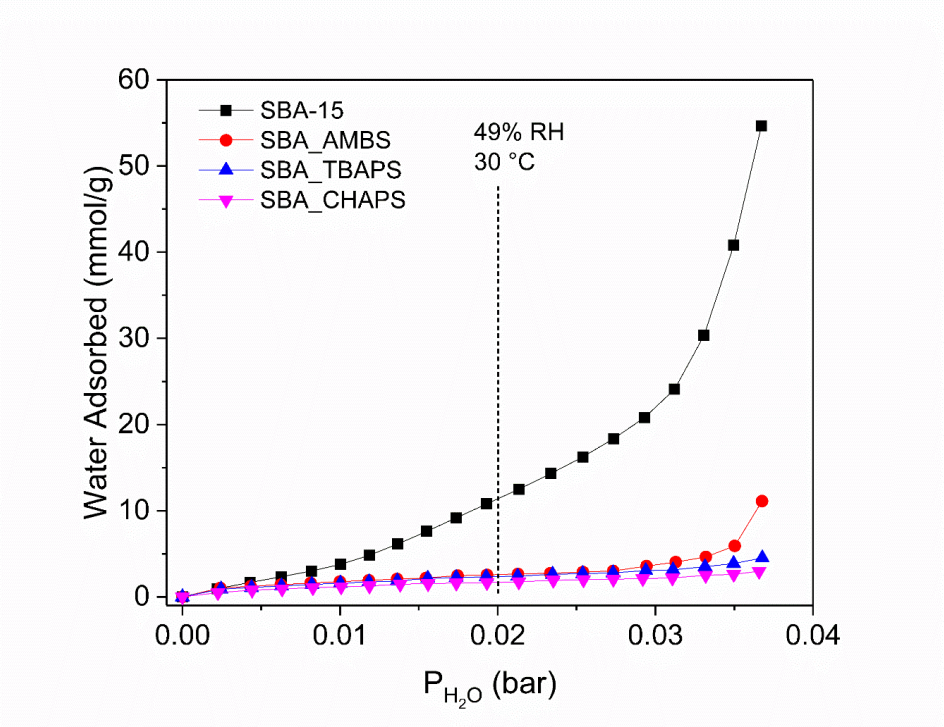

Figure B.4. Water adsorption isotherms for all sorbents. All measurements conducted at 30 °C.

B.4 In Situ FTIR Spectroscopy

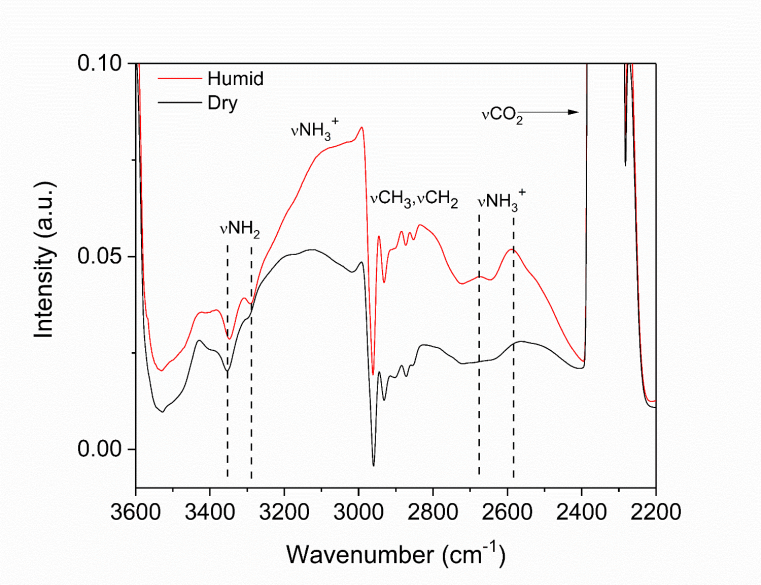

Figure B.5. FTIR spectra for 10% $^{12}CO_2$ adsorption on SBA_AMBS at 30 °C under dry conditions and humid conditions (P_{H2O} = 21 mbar).

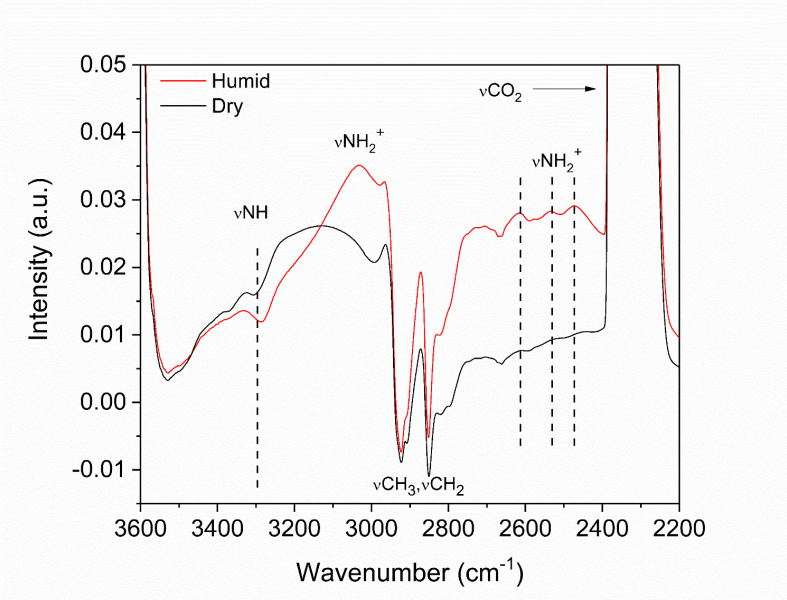

Figure B.6. FTIR spectra for 10% $^{12}CO_2$ adsorption on SBA_CHAPS at 30 °C under dry conditions and humid conditions (P_{H2O} = 21 mbar).

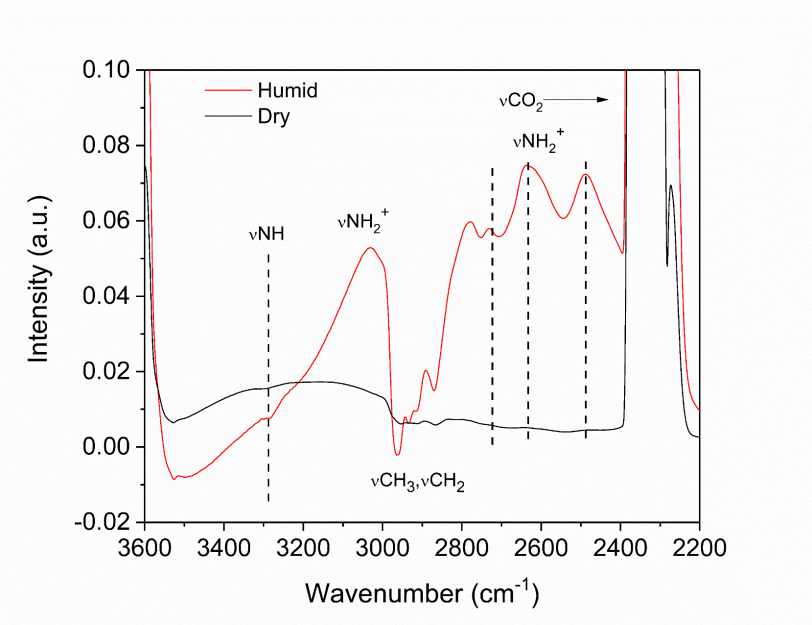

Figure B.7. FTIR spectra for 10% $^{12}CO_2$ adsorption on SBA_TBAPS at 30 °C under dry conditions and humid conditions (P_{H2O} = 21 mbar).

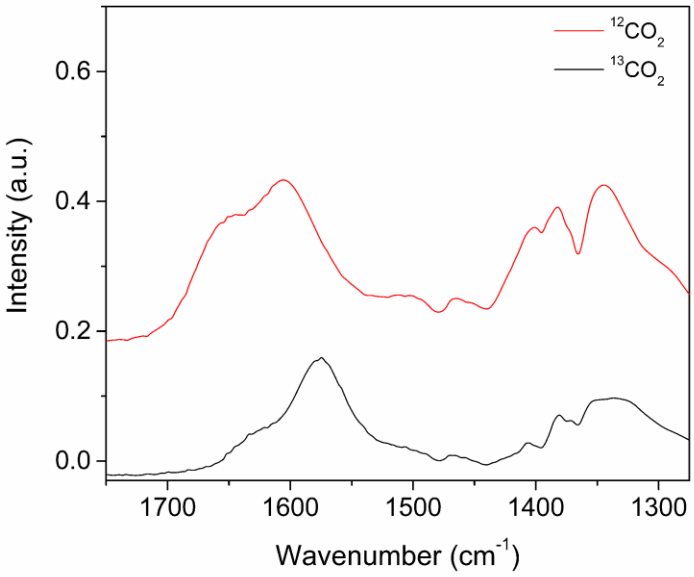

Figure B.8. FTIR spectra of the residual of humid-minus-dry conditions for 10% $^{12}CO_2$ and $^{13}CO_2$ adsorption on SBA_TBAPS at 30 ℃ after 65 min.

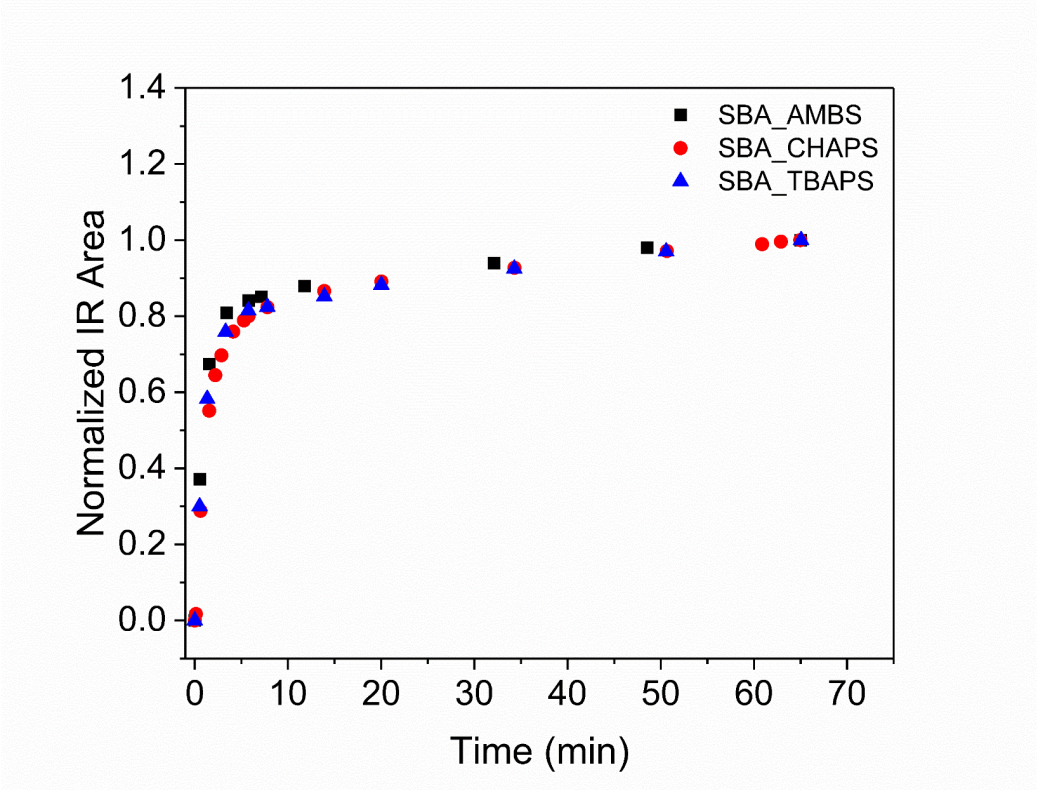

Figure B.9. Normalized integrated FTIR peak area between 1750 and 1275 cm^{-1} during adsorption of 10 % CO_2 under humid conditions (P_{H2O} = 21 mbar) at 30 °C. The curves are normalized such that the end of the adsorption run (65 min) equals 1.

Table B.2. IR assignments of bands formed during CO_2 adsorption on amine sorbents.

Wavenumber (cm^{-1})	Assignment	Species	Reference
3200 – 3000	NH_x^+ stretch	ammonium ion	2
2800 – 2400	NH_x^+ combination	ammonium ion	3,4
2360 – 2349	CO asym stretch	gas phase CO_2	2
1700 – 1650	CO stretch	carbamic acid	5
1700 – 1600	COO^- asym stretch	bicarbonate ion	6,7
1635 – 1610	NH_x^+ asym def	ammonium ion	2,8,9
1570 – 1530	COO^- asym stretch	carbamate ion	5,8,9
1500 – 1470	NH_x^+ sym def	ammonium ion	2,8,9
1500 – 1470	CN stretch + NH def	carbamate ion/carbamic acid	5,10,11
1440 – 1380	COO^- sym stretch	carbamate ion	5,8,9
1350 – 1300	$NCOO^-$ skeletal vibration	carbamate ion	4
1340 – 1300	COO^- sym stretch	bicarbonate ion	6,7

B.5 Isosteric Heats of CO_2 Adsorption and CO_2 Adsorption Isotherms

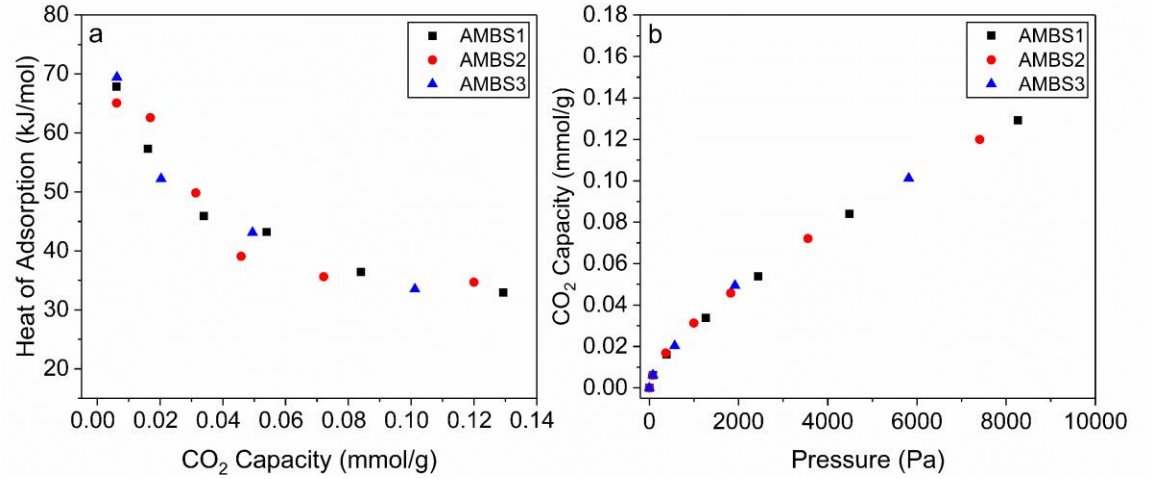

Figure B.10. (a) Isosteric heats of adsorption and (b) isotherms for multiple runs of SBA_AMBS at 30 ℃.

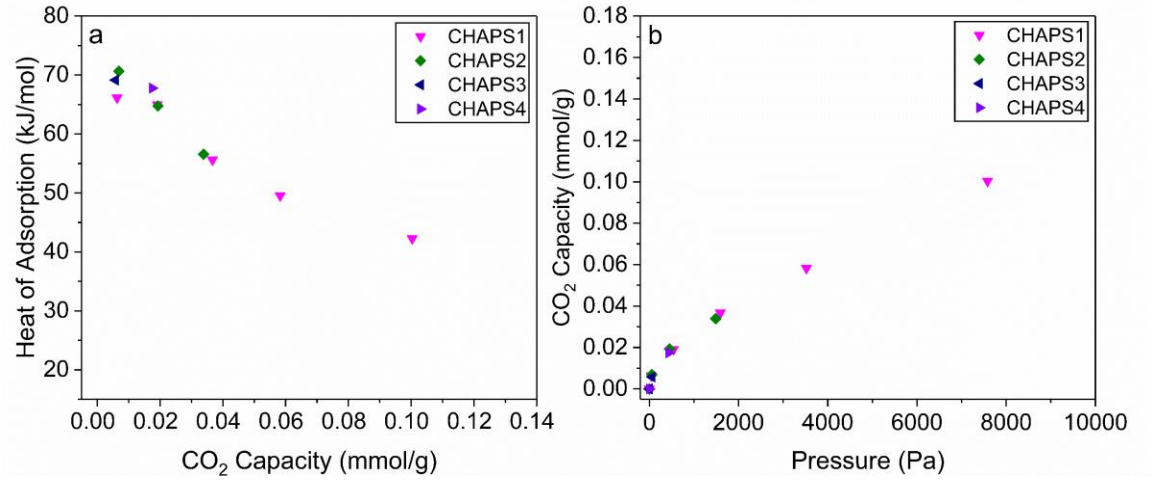

Figure B.11. (a) Isosteric heats of adsorption and (b) isotherms for multiple runs of SBA_CHAPS at 30 ℃.

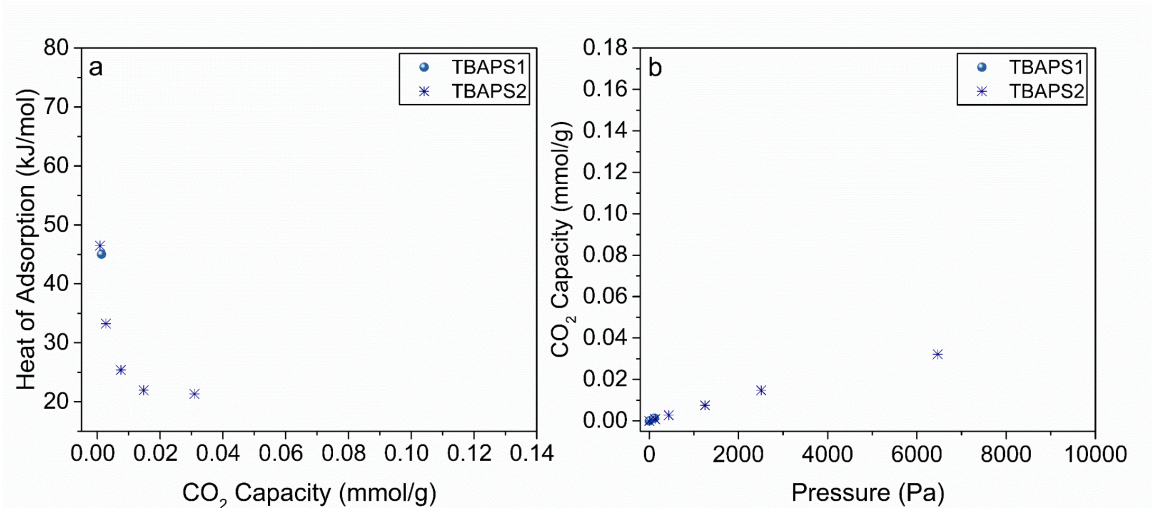

Figure B.12. (a) Isosteric heats of adsorption and (b) isotherms for multiple runs of SBA_TBAPS at 30 ℃.

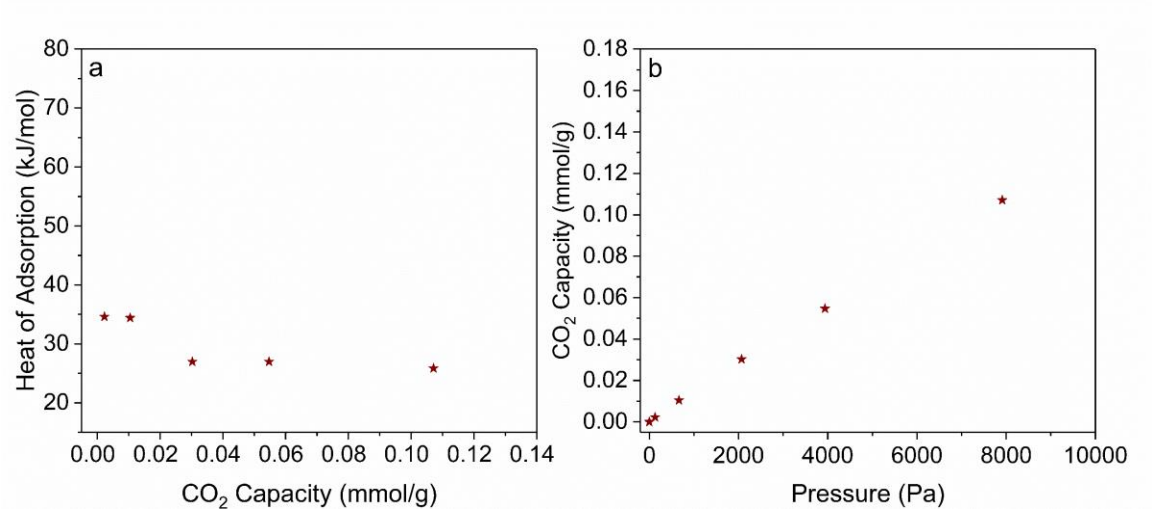

Figure B.13. (a) Isosteric heats of adsorption and (b) isotherm of SBA-15 at 30 ℃.

B.6 Isosteric Heat of CO_2 Adsorption of CHAPS_SBA Compared to Literature Values

The values of isosteric heat of adsorption of CHAPS functionalized SBA15 reported in this study are significantly higher than previously reported isosteric heat of adsorption values.[1] A possible difference in isosteric heat of adsorption values between the

two studies may be due to differences in local amine densities of the sorbents used. Furthermore, while the average amine densities in the two studies are similar to each other, the samples used in the previous study may have had less "amine clustering", leading to little or no cooperative amine-CO_2-amine chemisorption. In addition, a previously unpublished isosteric heat of adsorption run for the CHAPS material used for the previous study, which was thought to be an outlier and was thus discarded, is observed to match closely with isosteric heat of adsorption values reported here (Figure B.14). There may have also been variabilities in local amine densities of the CHAPS material used in each run in that study.

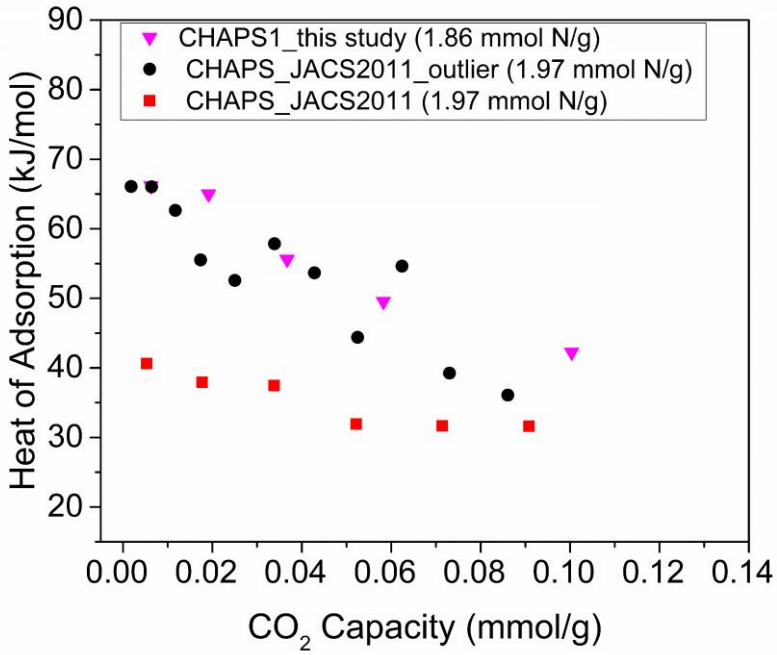

Figure B.14. Comparison of the isosteric heat of adsorption of CHAPS functionalized SBA15 to previously reported literature values at 30 °C.[1]

B.7 Amine Content and FTIR Spectra of Sorbents after Oxidative and Thermal Treatment

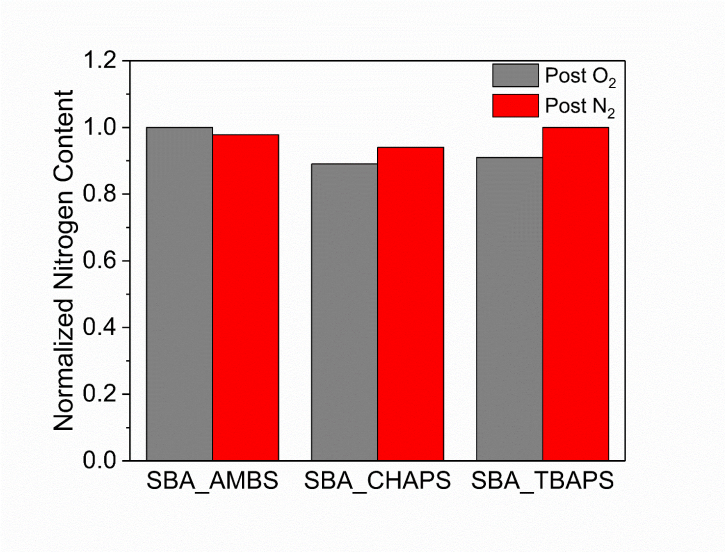

Figure B.15. Nitrogen content of amine sorbents determined from elemental analysis. Values are normalized to amine content of a fresh sorbent.

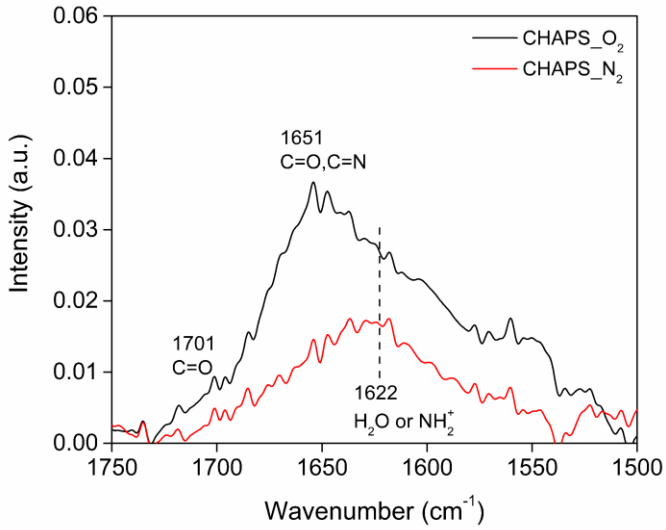

Figure B.16. FTIR spectra of oxidatively and thermally treated SBA_CHAPS.

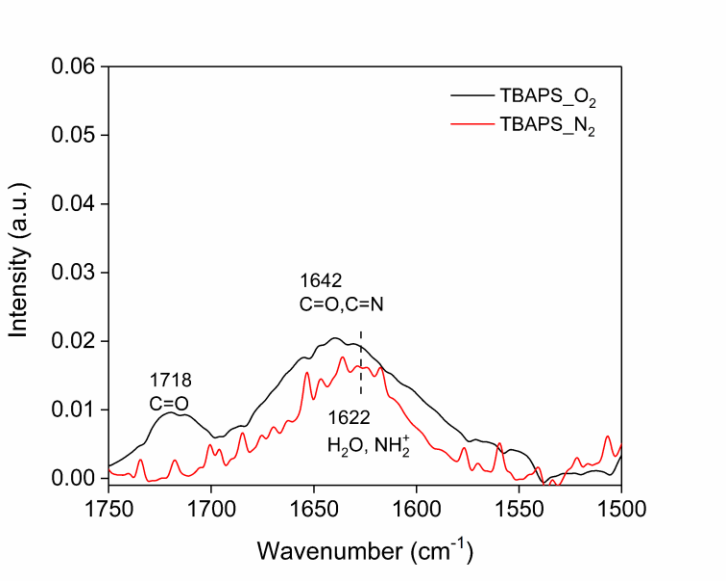

Figure B.17. FTIR spectra of oxidatively and thermally treated SBA_TBAPS.

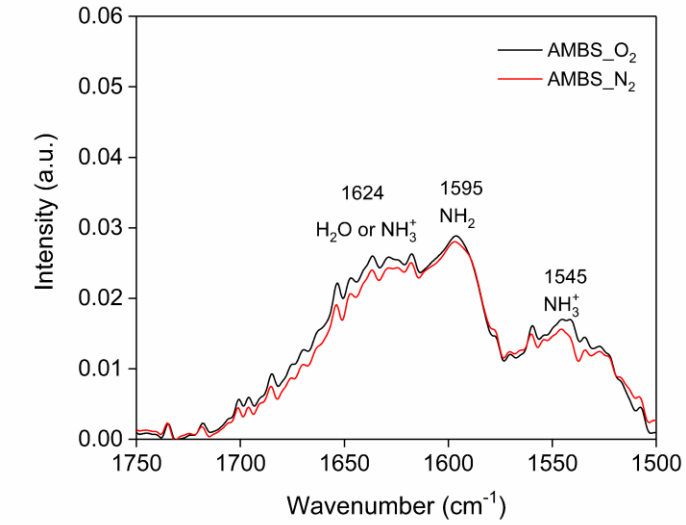

Figure B.18. FTIR spectra of oxidatively and thermally treated SBA_AMBS.

B.8 References

(1) Alkhabbaz, M. A.; Bollini, P.; Foo, G. S.; Sievers, C.; Jones, C. W. Important Roles of Enthalpic and Entropic Contributions to CO_2 Capture from Simulated Flue Gas and Ambient Air Using Mesoporous Silica Grafted Amines. *J. Am. Chem. Soc.*

2014, *136*, 13170–13173.

(2) Socrates, G. *Infrared and Raman Characteristic Group Frequencies*, Third.; John Wiley & Sons LTD, 2001.

(3) Miller, D. D.; Chuang, S. S. C. Control of CO_2 Adsorption and Desorption Using Polyethylene Glycol in a Tetraethylenepentamine Thin Film: An in Situ ATR and Theoretical Study. *J. Phys. Chem. C* **2016**, *120*, 25489–25504.

(4) Bacsik, Z.; Ahlsten, N.; Ziadi, A.; Zhao, G. Y.; Garcia-Bennett, A. E.; Martín-Matute, B.; Hedin, N. Mechanisms and Kinetics for Sorption of CO_2 on Bicontinuous Mesoporous Silica Modified with N-Propylamine. *Langmuir* **2011**, *27*, 11118–11128.

(5) Foo, G. S.; Lee, J. J.; Chen, C.-H.; Hayes, S. E.; Sievers, C.; Jones, C. W. Elucidation of Surface Species through in Situ FTIR Spectroscopy of Carbon Dioxide Adsorption on Amine-Grafted SBA-15. *ChemSusChem* **2017**, *10*, 266–276.

(6) Garand, E.; Wende, T.; Goebbert, D. J.; Bergmann, R.; Meijer, G.; Neumark, D. M.; Asmis, K. R. Infrared Spectroscopy of Hydrated Bicarbonate Anion Clusters: $HCO_3^-(H_2O)_{1-10}$. *J. Am. Chem. Soc.* **2010**, *132*, 849–856.

(7) Lee, J. J.; Chen, C.-H.; Shimon, D.; Hayes, S. E.; Sievers, C.; Jones, C. W. Effect of Humidity on the CO_2 Adsorption of Tertiary Amine Grafted SBA-15. *J. Phys. Chem. C* **2017**, *121*, 23480–23487.

(8) Didas, S. A.; Sakwa-Novak, M. A.; Foo, G. S.; Sievers, C.; Jones, C. W. Effect of Amine Surface Coverage on the Co-Adsorption of CO_2 and Water: Spectral Deconvolution of Adsorbed Species. *J. Phys. Chem. Lett.* **2014**, *5*, 4194–4200.

(9) Danon, A.; Stair, P. C.; Weitz, E. FTIR Study of CO_2 Adsorption on Amine-Grafted SBA-15: Elucidation of Adsorbed Species. *J. Phys. Chem. C* **2011**, *115*, 11540–11549.

(10) Bossa, J.-B.; Borget, F.; Duvernay, F.; Theulé, P.; Chiavassa, T. Formation of Neutral Methylcarbamic Acid ($CH_3NHCOOH$) and Methylammonium Methylcarbamate $[CH_3NH_3^+][CH_3NHCO_2^-]$ at Low Temperature. *J. Phys. Chem. A* **2008**, *112*, 5113–5120.

(11) Mafra, L.; Čendak, T.; Schneider, S.; Wiper, P. V.; Pires, J.; Gomes, J. R. B.; Pinto, M. L. The Structure of Chemisorbed CO_2 Species in Amine-Functionalized Mesoporous Silicas Studied by Solid-State NMR and Computer Modeling. *J. Am. Chem. Soc.* **2017**, *139*, 389–408.

APPENDIX C. SUPPLEMENT TO CHAPTER 4

C.1 ESI-MS and NMR Spectra of PDMEI

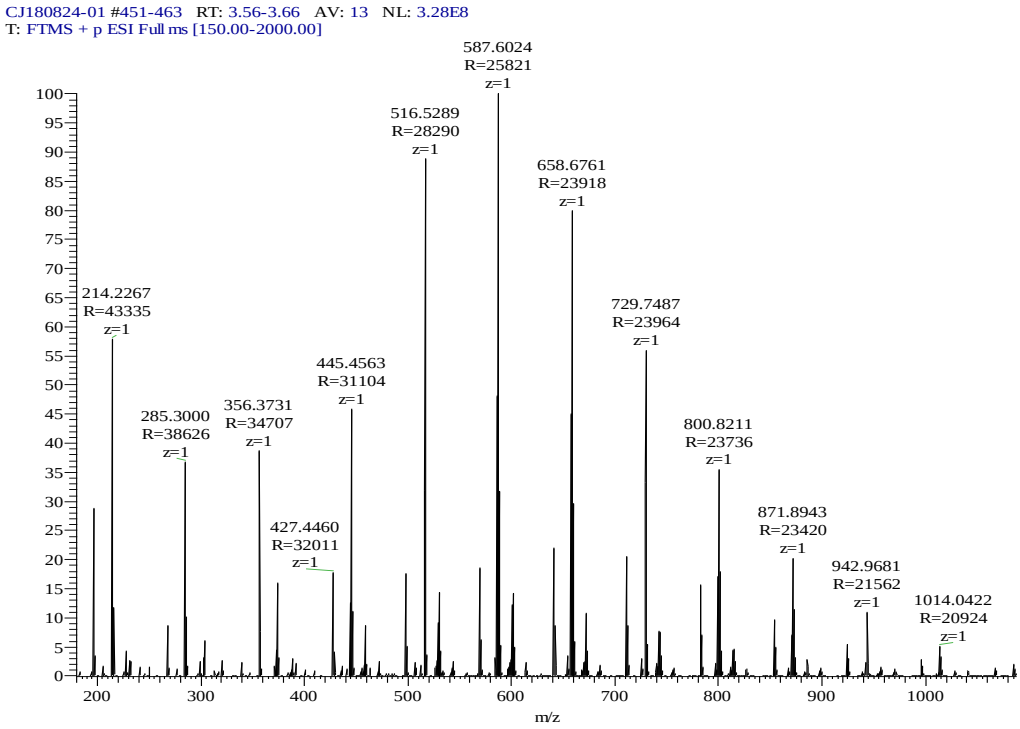

Figure C.1. ESI-MS spectrum of PDMEI.

Table C.1. Estimated m/z at z=1 of aminopolymer species.

Species	Estimated m/z, where z=1 or $[M+H]^+$
cyclized/aziridine terminated	71 + (71*monomer units) + 1
hydroxyl terminated	89 + (71*monomer units) + 1
diamine terminated	88 + (71*monomer units) + 1

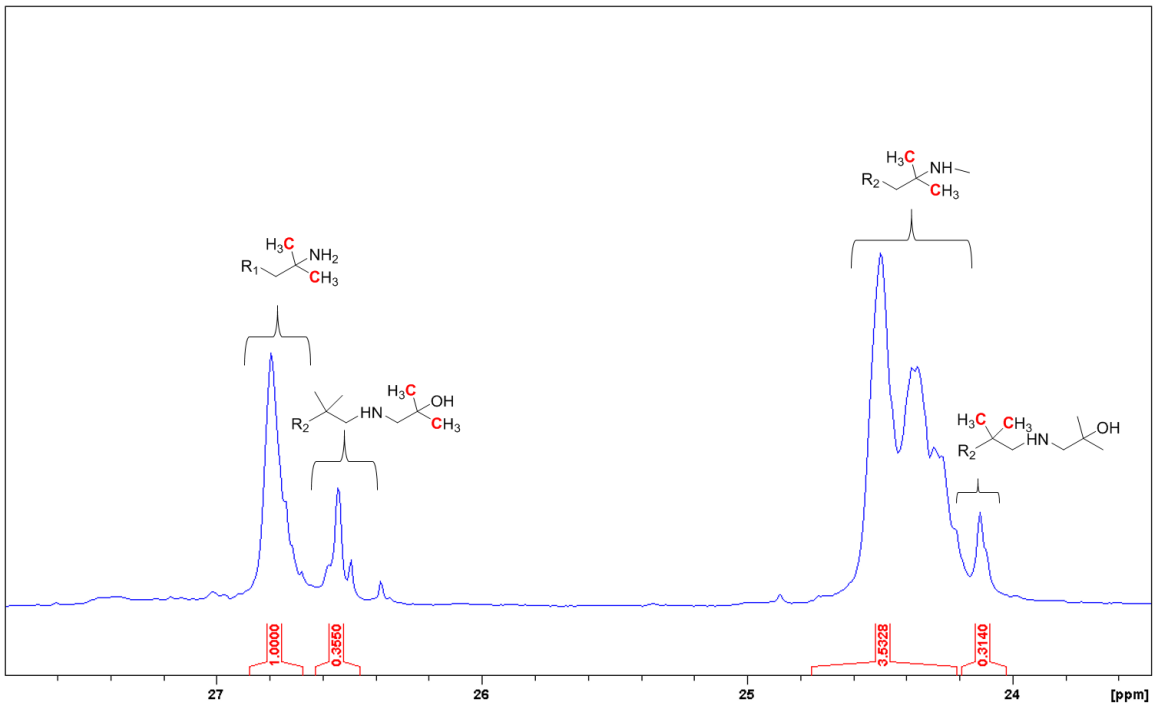

Figure C.2. ^{13}C NMR of PDMEI between 28-23 ppm. R_1 denotes a secondary or tertiary amine and R_2 denotes a primary, secondary, or tertiary amine.

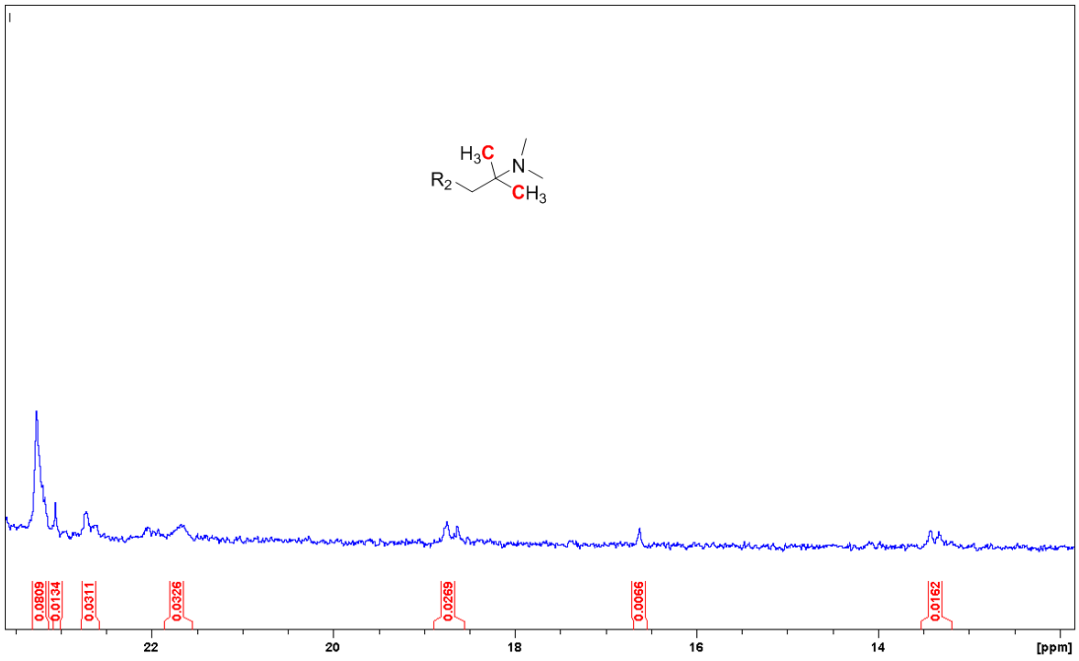

Figure C.3. ^{13}C NMR of PDMEI between 23-13 ppm. All peaks observed in this region are associated with methyl carbons of a hindered tertiary amine. R_2 denotes a primary, secondary, or tertiary amine.

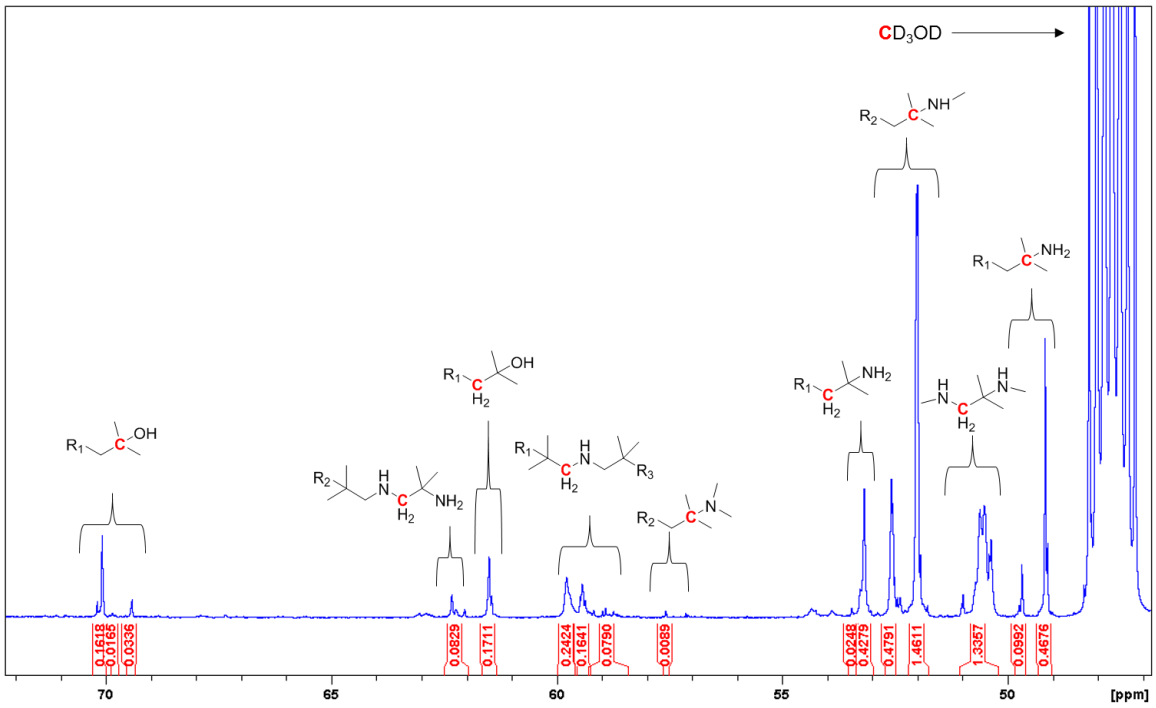

Figure C.4. ^{13}C NMR of PDMEI between 72-47 ppm. R_1 denotes a secondary or tertiary amine and R_2 denotes a primary, secondary, or tertiary amine.

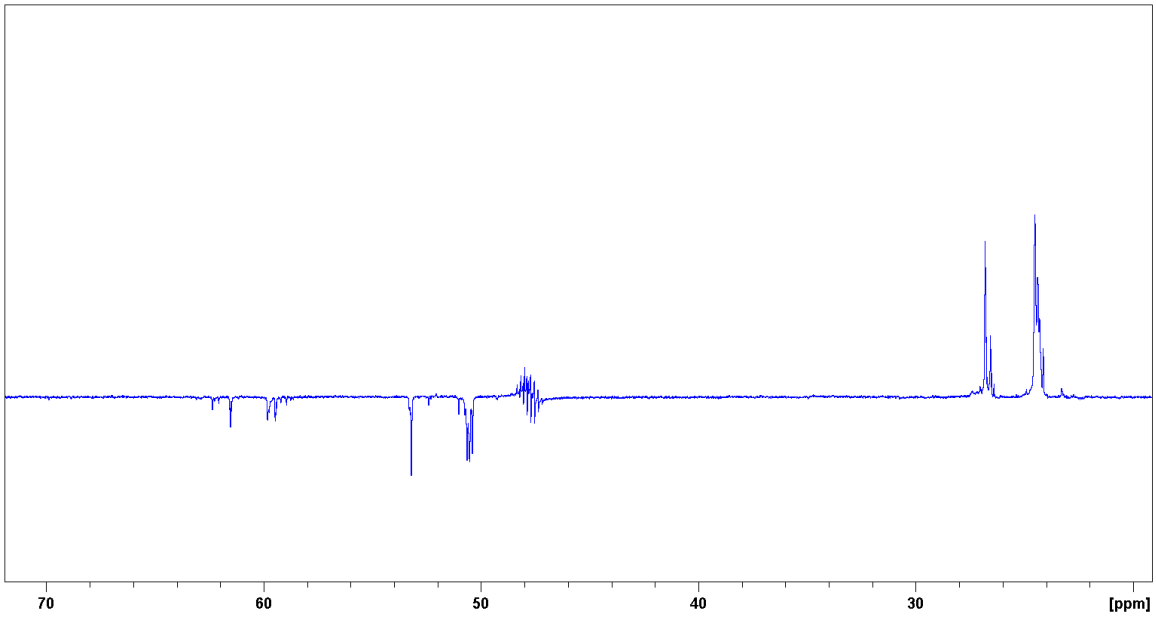

Figure C.5. DEPT-135 spectrum of PDMEI. CH_3 peaks have positive intensity, CH_2 peaks have negative intensity, and C peaks are not observed.

Carbon peaks of the aminopolymer were assigned with the help of predictive NMR software and by a Distortionless Enhancement by Polarization Transfer (DEPT-135) experiment. The peak at 70 ppm found in the ^{13}C spectrum is associated with a carbon adjacent to the alcohol group. When running a DEPT experiment on the aminopolymer, the peak at 70 ppm was absent, indicating that the carbon was not covalently bonded to a hydrogen atom. This result implies that the reaction mechanism of solvolysis (SN_1) was different than that of ring opening polymerization (SN_2), consistent with previous literature.[1,2]

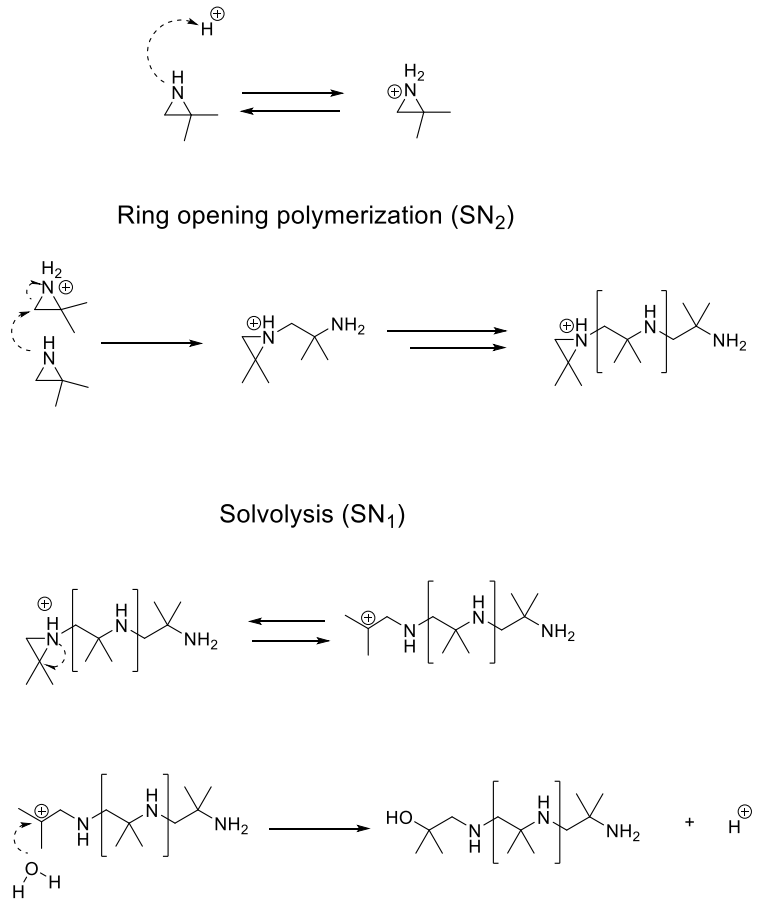

Figure C.6. Ring opening polymerization[1] and solvolysis[2] reaction mechanisms.

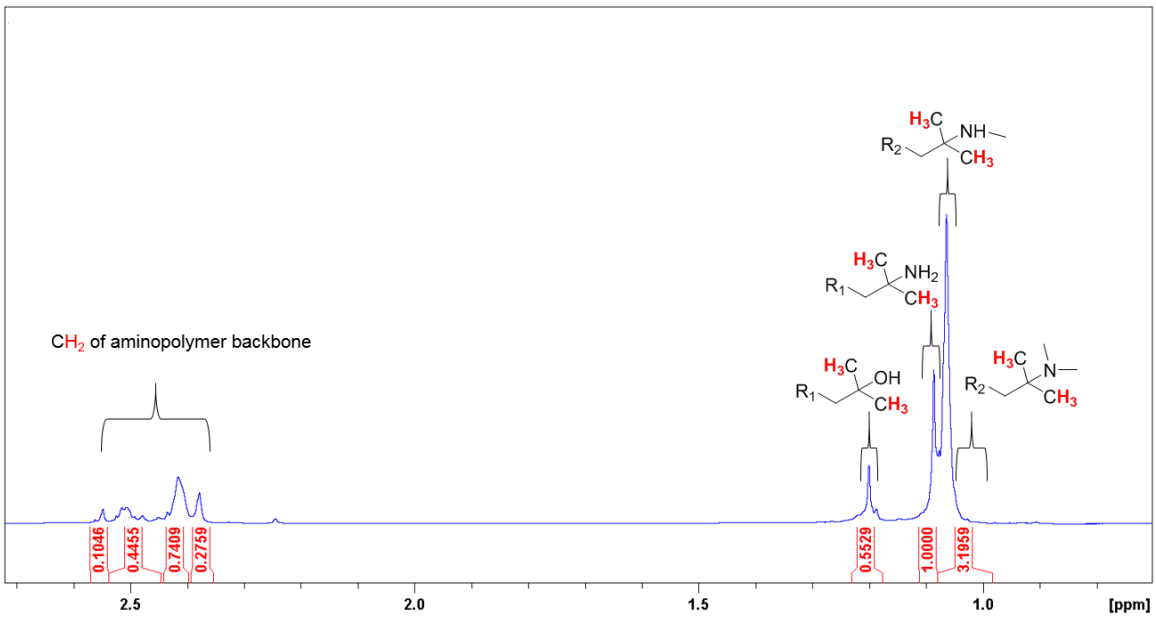

Figure C.7. ^{1}H NMR of PDMEI. R_1 denotes a secondary or tertiary amine and R_2 denotes a primary, secondary, or tertiary amine.

C.2 N_2 Adsorption/Desorption Curves and Pore Size Distributions

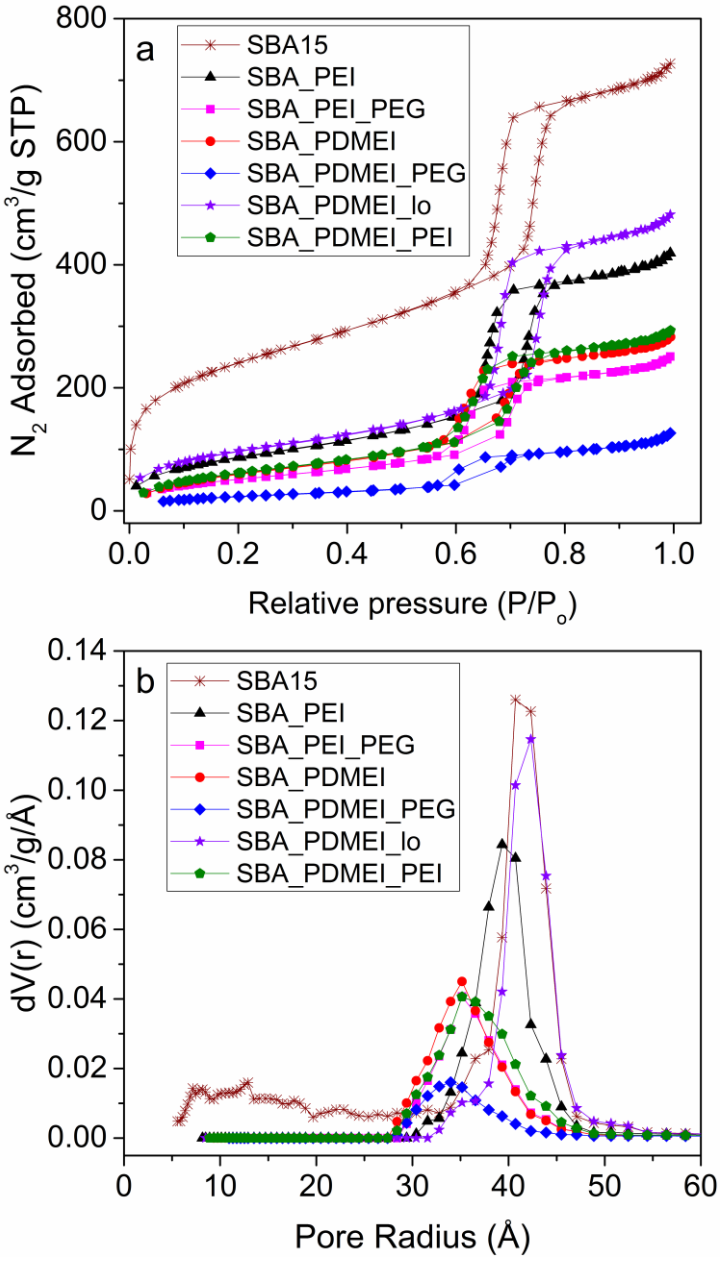

Figure C.8. N_2 adsorption/desorption curves and pore size distribution.

C.3 FTIR Spectra of Amine/Silica Composites after Activation

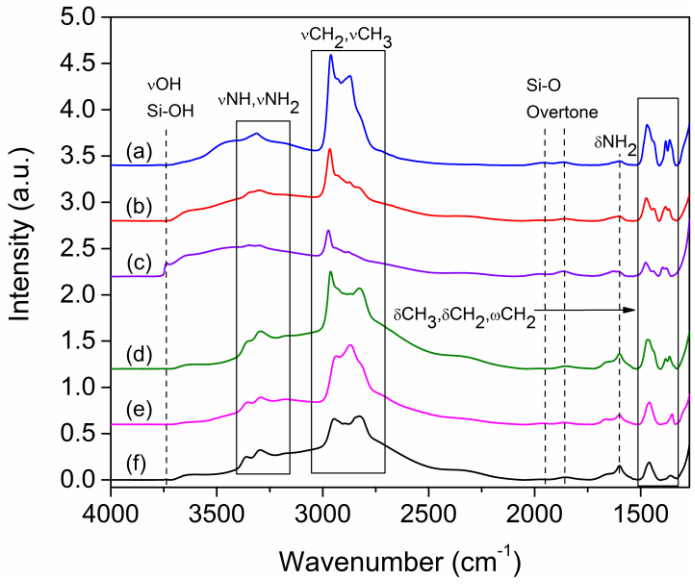

Figure C.9. FTIR spectra of activated sorbents: (a) SBA_PDMEI_PEG, (b) SBA_PDMEI, (c) SBA_PDMEI_lo, (d) SBA_PDMEI_PEI, (e) SBA_PEI_PEG, and (f) SBA_PEI. All spectra are baseline corrected and taken under He flow at 30 °C.

C.4 In Situ FTIR Spectroscopy of SBA_PEI, SBA_PDMEI, SBA_PDMEI_PEG, and SBA_PDMEI_PEG

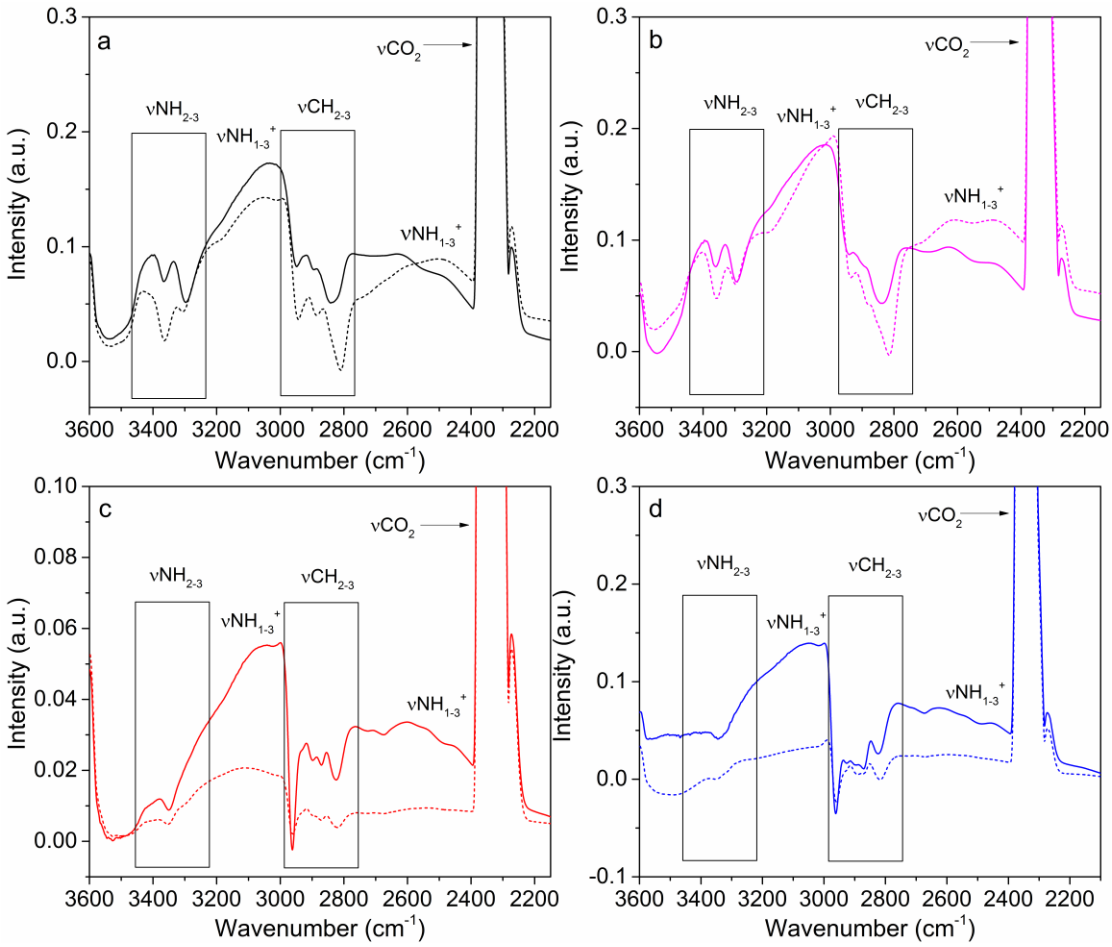

Figure C.10. FTIR spectra of 10% CO_2 adsorption on (a)SBA_PEI (b) SBA_PEI_PEG (c) SBA_PDMEI (d) SBA_PDMEI_PEG at 30 °C under dry and humid conditions (P_{H2O} = 21 mbar) after 65 min of time on stream. Dotted lines represent dry and humid runs respectively.

C.5 Water Adsorption Isotherms

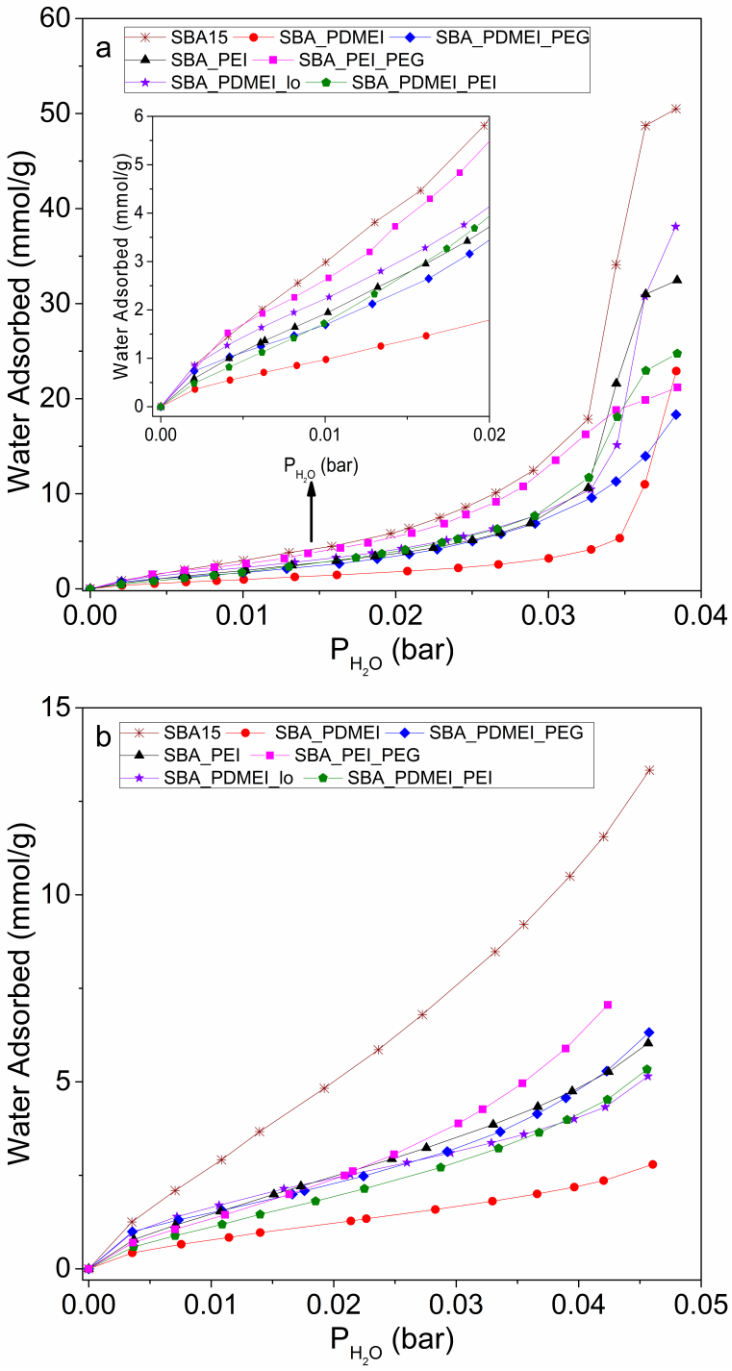

Figure C.11. Water adsorption isotherms for all sorbents. Measurements conducted at (a) 30 and (b) 40 °C.

C.6 CO_2 Adsorption Capacities and CO_2 Adsorption/Desorption Curves of SBA_PEI, SBA_PDMEI, SBA_PDMEI_PEG, and SBA_PDMEI_PEG

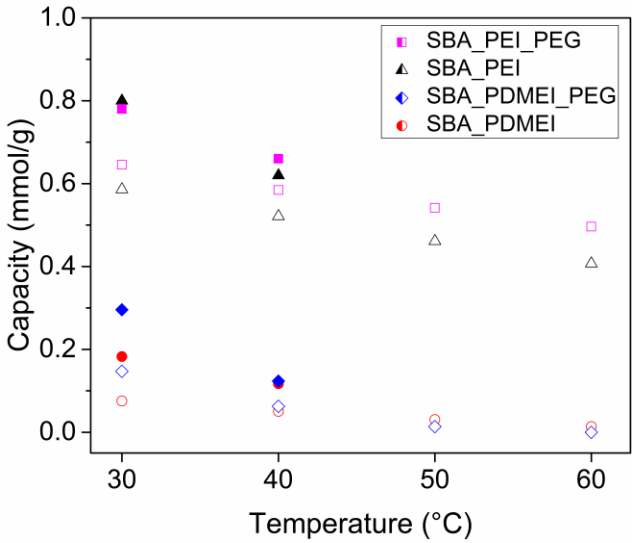

Figure C.12. CO_2 adsorption capacities of sorbents at 10% CO_2 between 30 and 60 °C. Unfilled and filled shapes represent amine efficiencies under dry and humid conditions (P_{H2O} = 21 mbar) respectively.

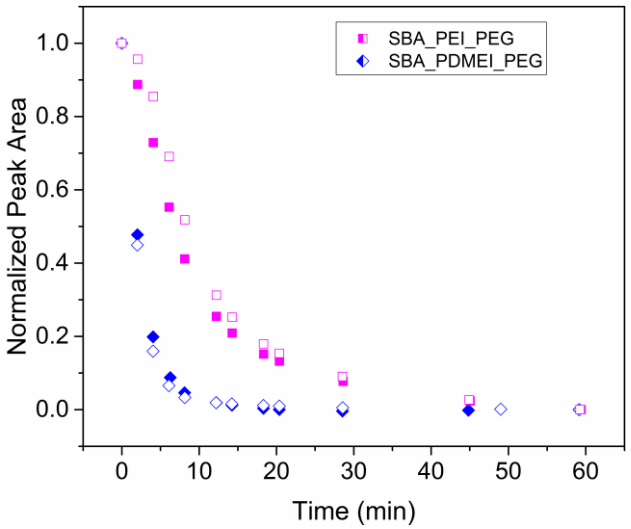

Figure C.13. Normalized FTIR peak area between 1750 and 1270 cm^{-1} during desorption of 10% CO_2 under dry and humid conditions (P_{H2O} = 21 mbar) at 30 °C. Unfilled shapes represent dry runs and filled shapes represent humid runs. The curves are normalized such that the start of the desorption run equals 1 and the end of the run (60 min) equals 0.

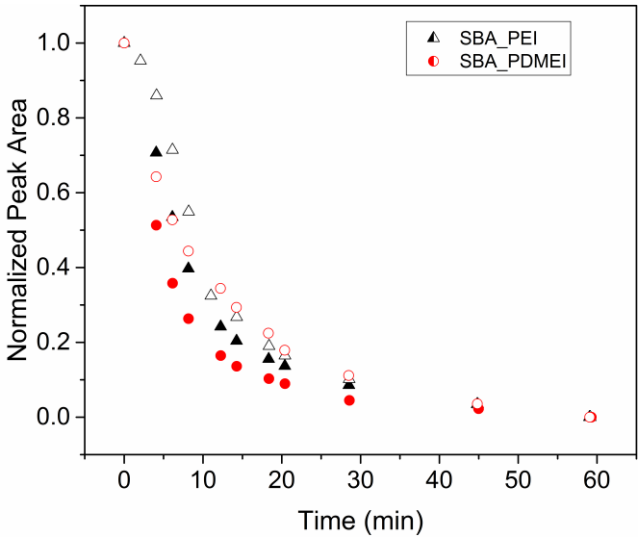

Figure C.14. Normalized FTIR peak area between 1750 and 1270 cm^{-1} during desorption of 10% CO_2 under dry and humid conditions (P_{H2O} = 21 mbar) at 30 °C. Unfilled shapes represent dry runs and filled shapes represent humid runs. The curves are normalized such that the start of desorption run equals 1 and end of desorption run (60 min) equals 0.

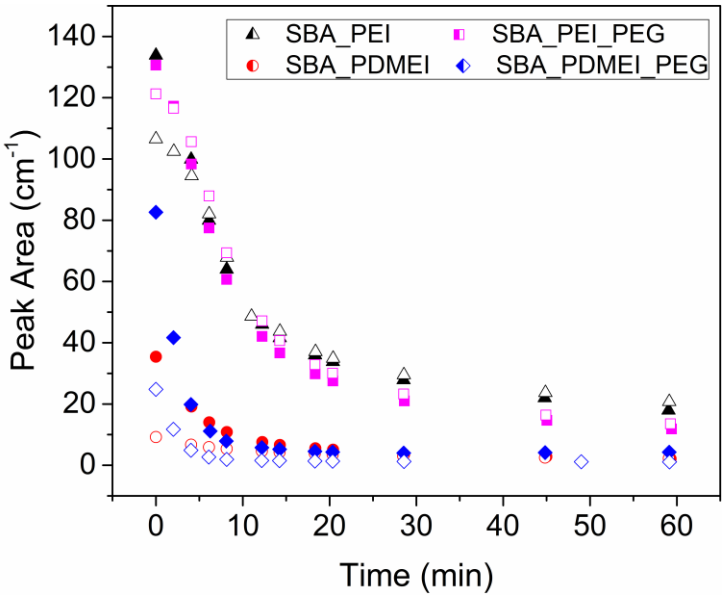

Figure C.15. FTIR peak area between 1750 and 1270 cm^{-1} during desorption of 10% CO_2 under dry and humid conditions (P_{H2O} = 21 mbar) at 30 ℃. Unfilled shapes represent dry runs and filled shapes represent humid runs.

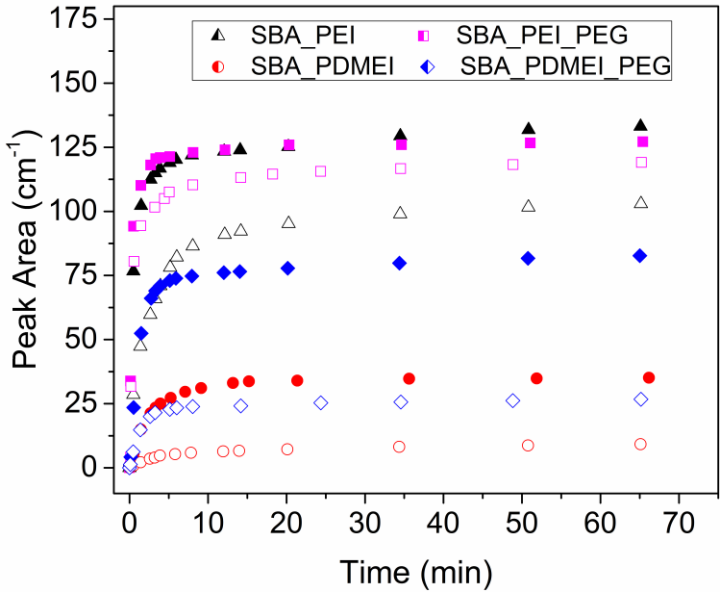

Figure C.16. FTIR peak area between 1750 and 1270 cm^{-1} during adsorption of 10% CO_2 under dry and humid conditions (P_{H2O} = 21 mbar) at 30 ℃. Unfilled shapes represent dry runs and filled shapes represent humid runs.

C.7 Physical and Textural Properties of SBA_PDMEI_lo and SBA_PDMEI_PEI

Table C.2. Textural and physical properties of additional aminopolymer/silica composites.

Material	BET Surface Area (m^2/g_{SiO2})	Pore Volume (cm^3/g_{SiO2})	Pore Volume Filled (%)	Amine Loading ($mmol_N/g_{SiO2}$)	Organic Loading (wt%)	Amine Loading Ratio (PEI/PDMEI)
SBA_PEI	415	0.80	26	5.6	23	-
SBA_PDMEI_lo	404	0.82	24	1.7	13	-
SBA_PDMEI_PEI	346	0.63	42	7.4	32	5.6/1.8

C.8 CO_2 and H_2O Adsorption Performance of SBA_PDMEI_lo and SBA_PDMEI_PEI

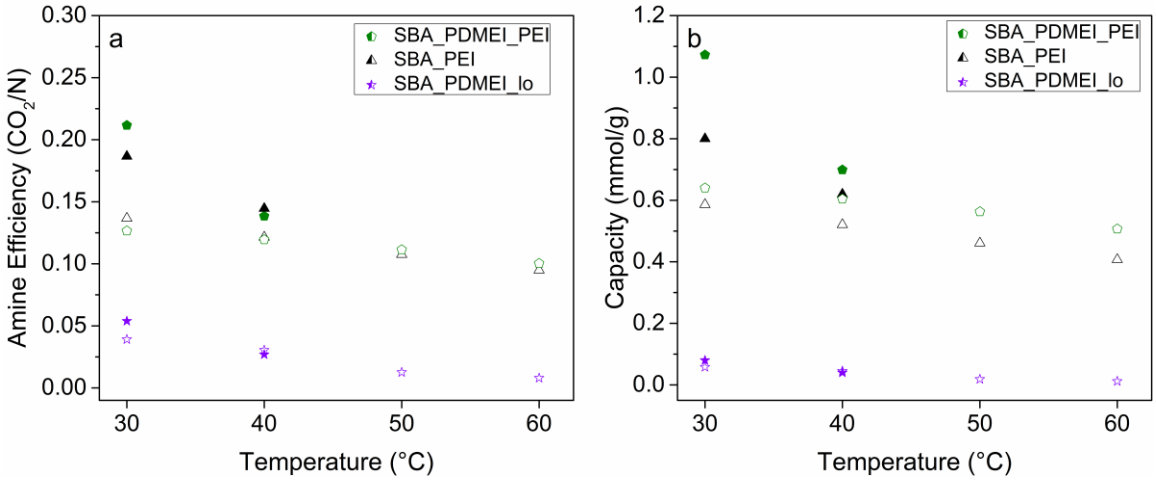

Figure C.17. (a) Amine efficiencies and (b) CO_2 capacities of aminopolymer/silica composites at 10% CO_2 between 30 and 60 °C. Unfilled and filled shapes represent amine efficiencies under dry and humid conditions (P_{H2O} = 21 mbar) respectively.

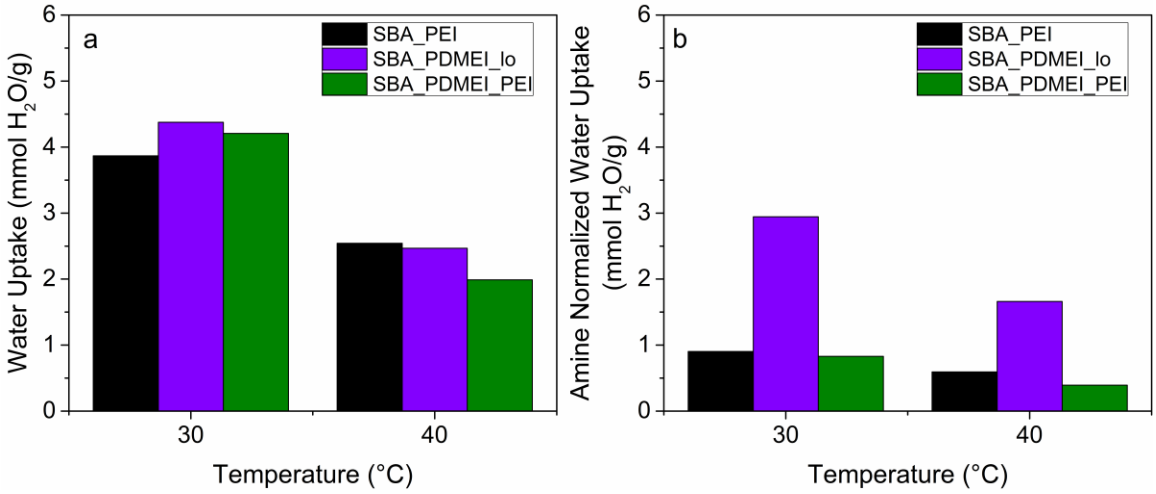

Figure C.18. (a) Water uptake and (b) amine normalized water uptake of aminopolymer/silica composites at 30 and 40 °C and P_{H2O} = 21 mbar.

C.9 In Situ FTIR Spectra and CO_2 Adsorption/Desorption Curves of SBA_PDMEI_lo and SBA_PMDEI_PEI

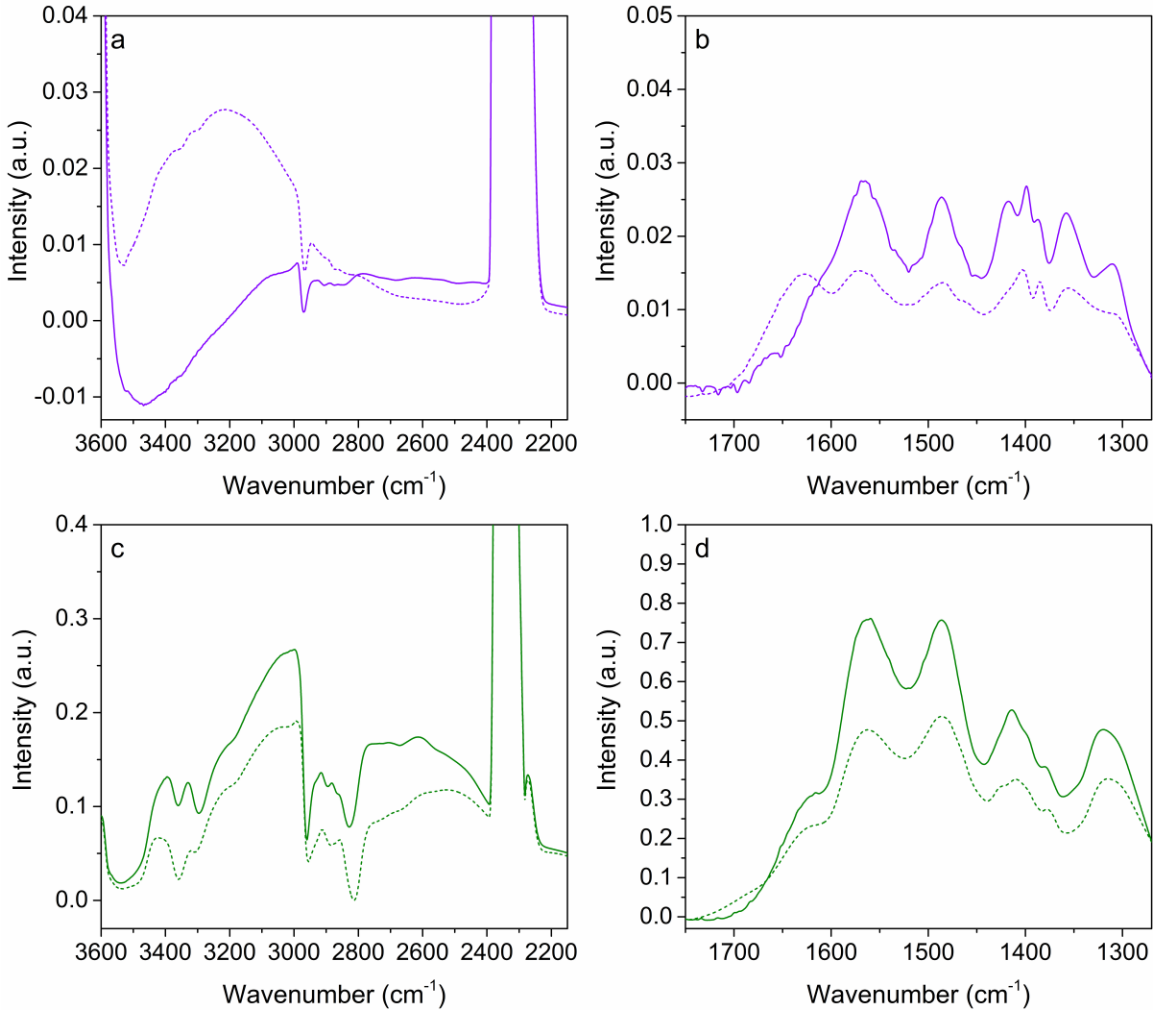

Figure C.19. FTIR spectra of 10% CO_2 adsorption on (a, b) SBA_PDMEI and (c, d) SBA_PDMEI_PEI under dry and humid conditions (P_{H2O} = 21 mbar) at 30 °C after 65 min of time on stream. Dotted lines and solid lines represent dry and humid runs respectively.

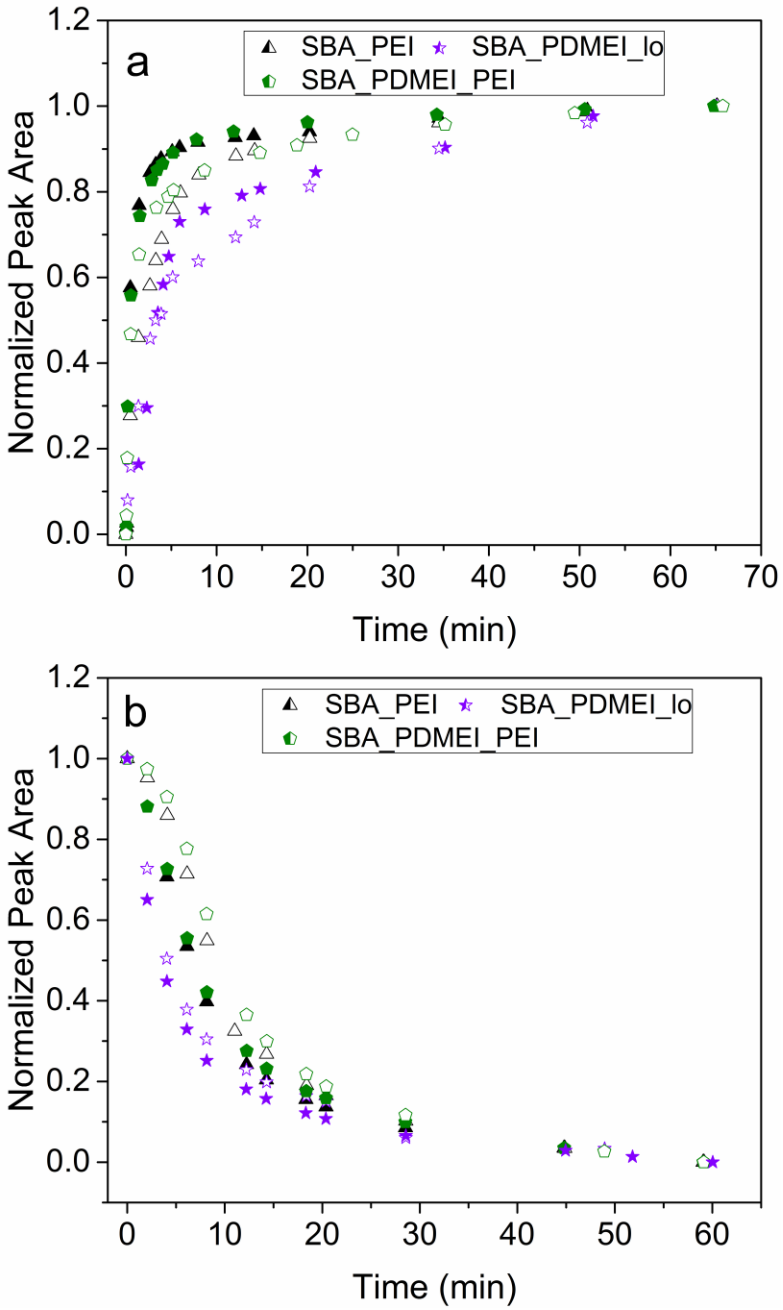

Figure C.20. Normalized FTIR peak area integrated between 1750 and 1275 cm^{-1} during (a) adsorption and (b) desorption of 10% CO_2 under dry and humid conditions (P_{H2O} = 21 mbar) at 30 °C. Unfilled shapes represent dry runs and filled shapes represent humid runs. The curves are normalized such that the end of the adsorption run (65 min) equals 1 and the desorption curves are normalized such that the start of desorption run equals 1 and end of desorption run (60 min) equals 0.

C.10 CO_2 Breakthrough Curves

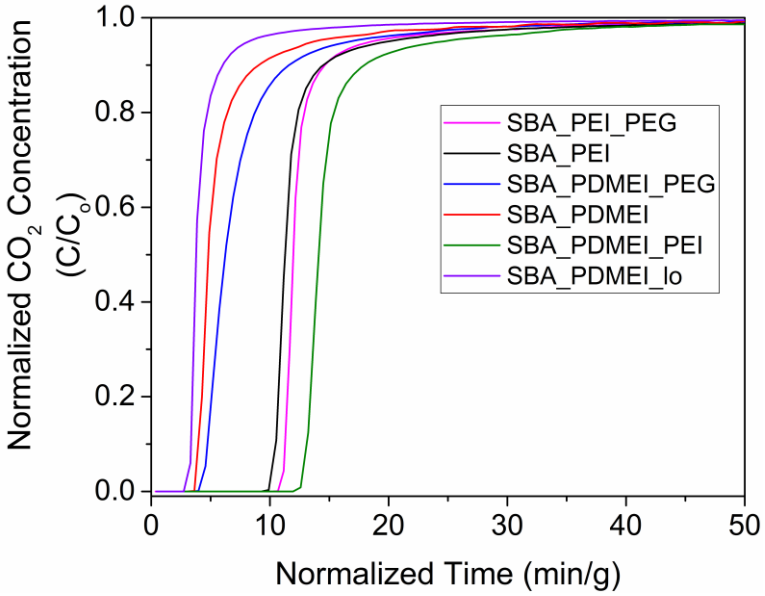

Figure C.21. 10% CO_2 breakthrough curves at 30 ℃ for all sorbents under humid conditions (P_{H2O} = 21 mbar).

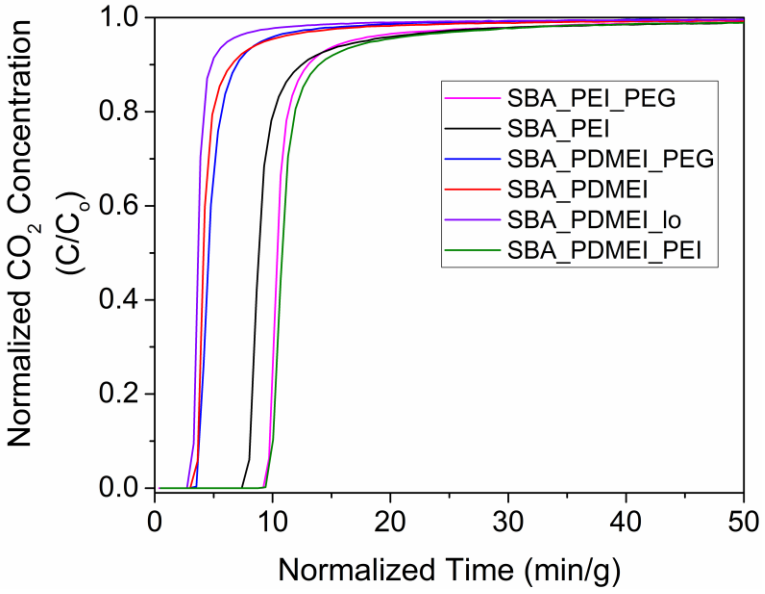

Figure C.22. 10% CO_2 breakthrough curves at 40 ℃ for all sorbents under humid conditions (P_{H2O} = 21 mbar).

C.11 References

(1) Jones, G. D. The Polymerization of Homologs of Ethylenimine (1). *J. Org. Chem.* **1944**, *9*, 484–499.

(2) Bunnett, J. F.; McDonald, R. L.; Olsen, F. P. Kinetics of Hydrolysis of Aziridines in Moderately Concentrated Mineral Acids. Relation of Φ Parameters to Reaction Mechanism. *J. Am. Chem. Soc.* **1974**, *96*, 2855–2861.